NUEJ

NARESUAN UNIVERSITY ENGINEERING JOURNAL

January - June 2022 Vol.17, No.1
ISSN : 2651-1568

NUEJ

Naresuan University Engineering Journal

Editorial Team

NUEJ

Naresuan University
Engineering Journal

Editorial Board

NUEJ
Naresuan University
Engineering Journal

Editorial Board

NUEJ
Naresuan University
Engineering Journal

Research Articles

NUEJ
Naresuan University
Engineering Journal

Aims and Objectives

The primary objective of the *Naresuan University Engineering Journal (NUEJ)* is to publish high quality research articles presenting contemporary developments in theory, design, and applications in all areas of Engineering, Science and Technology, including research in Civil and Environmental Engineering, Mechanical Engineering, Electrical and Computer Engineering, Industrial, Chemical, and Material Engineering. NUEJ covers all multidisciplinary research in associated areas**,** such as Mechatronics, Energy, Industrial and Engineering Design, Manufacturing Technology, Engineering Management and Medical Engineering.

Journal Policies

Naresuan University Engineering Journal (NUEJ) is a peer reviewed journal, regularly published with 2 issues per year (January – June, and July – December). Submissions must be original, unpublished works, and not currently under review by other journals. NUEJ will consider only submitted works which respect research ethics, including confidentiality, consent, and the special requirements for human and animal research. All research articles dealing with human or animal subjects must attach an approval certificate from the appropriate Ethics Committee. Additionally, the research articles dealing with human subjects must provide evidence of informed consent.

Editorial board of NUEJ reserves the right to decide whether the submitted manuscript should be accepted for publication. The final decision of the editorial board cannot be appealed.

The submitted manuscript has to be written in English only, and can be in Microsoft Word (doc or docx) or PDF file format. The corresponding author is required to register and submit the manuscript at https://ph01.tci-thaijo.org/index.php/nuej

Editorial board of Naresuan University Engineering Journal

Faculty of Engineering, Naresuan University,

Phitsanulok, 65000, Thailand

Tel. +66 (0) 55 964092

Fax +66 (0) 55 964000

Email: nuej@nu.ac.th

NUEJ
Naresuan University
Engineering Journal

Editor's Note

Naresuan University Engineering Journal (NUEJ) provides a resource and platform for sharing new knowledge and information in all areas of engineering. The journal has the following procedures. The journal receives articles, then reviews the articles using a strict peer review process to ensure the publication maintains high standards. Articles are accepted for publication only if at least two out of three independent reviewers provide approval, followed by Editors permission; the Editor-in-Chief makes the final decision in any case. NUEJ is approved to be in the first tier of the Thai-Journal Citation Index (TCI 1) and the Asean Citation Index (ACI).

As part of the journal's efforts to continue to grow and improve, and aligned with the goal of becoming a worldwide reference, all manuscripts must be submitted in English as of October 1, 2020. This issue, Vol. 17 No. 1 (2022), is the first English publication and there are seven fascinating engineering articles. As always, sincere appreciation is extended to the authors and reviewers for their contributions.

Dr. Phisut Apichayakul

Editor

Naresuan University Engineering Journal

NUEJ
Naresuan University
Engineering Journal

Determination of Suitable Solvent and Extraction Conditions for Lycopene Isolation from Gac Fruit (*Momordica Cochinchinensis Spreng.*)

Kittapat Sooknuan, Suppakiet Saksuntor, Sornchai Thongsri, Panatpong Boonnoun and Noppawan Motong*

Chemical Engineering Program, Faculty of Engineering, Naresuan university, Phitsanulok, Thailand

* Corresponding author e-mail: noppawanm@nu.ac.th

(Received: 18 August 2021, Revised: 25 February 2022, Accepted: 10 March 2022)

Abstract

This study investigated the extraction of lycopene from the Gac arils. The selection of suitable extraction solvent was firstly predicted using Hansen solubility parameters prediction. The suitable extraction conditions including Gac aril size powder, solvent to solid ratio, and extraction time were then determined. The prediction results revealed that the most suitable extraction solvent was ethyl acetate following by methyl acetate, ethanol, and methanol, respectively. The validation results also confirmed that ethyl acetate gave the highest lycopene yield (0.272 mg/g dried aril powder) compared with the others (0.250, 0.235, and 0.069 mg/g dried aril powder for methyl acetate, ethanol, and methanol, respectively.). The suitable extraction conditions were found to be 40 mesh of Gac aril size powder, 30:1(ml/g) of solvent to solid ratio, and 120 minutes of extraction time, giving lycopene content of 0.448 mg/g dried aril powder.

Keywords: Suitable Extraction Condition, Gac Fruit, Hansen Solubility Parameters, Lycopene.

1. INTRODUCTION

Nowadays, food supplementary or nutraceutical products from natural sources are increasing interested, making the continuing growth in market share. The products normally contain some bioactive compounds that have specific health-beneficial effects. Ones of the most important bioactive compounds are carotenoids which have many health benefits such as anti-inflammatory activity, antioxidants, including sun protection, improved heart health, and a lower risk of certain types of cancer (Do et al., 2019; Le et al., 2018).

Lycopene classified as carotenoids has been widely focused on by many groups of researchers (Saini et al., 2020; Costa-Rodrigues et al., 2017; Gerster, 1997). The well-known source of lycopene in tomatoes. However, Gac fruit (*Momordica cochinchinensis* Spreng.) is the plant that originates in Vietnam (United States Department of Agriculture, 2019) and is found in other countries in South East Asia including Thailand, was found to contain an 8 times higher amount of lycopene compared to those amounts found in tomato (Chuyen et al., 2014). The Gac fruit composes of peel, fruit, aril, and seed but has the highest amount of lycopene in aril (seed membrane) (Shida et al., 2004). Therefore, there were many studies about lycopene extraction from Gac aril using various solid-liquid extraction techniques such as supercritical CO_2 and maceration with an organic solvent (Akkarachaneeyakorn et al., 2016; Kubola et al., 2013)

To achieve the highest efficiency of solid-liquid extraction, the screening of suitable extraction solvent is the crucial step. Hansen solubility parameters (HSPs), the parameters describing the solubility behavior by three parameters of dispersion energy or London force (δ_D), polar interaction energy (δ_P), and hydrogen-bond break energy (δ_H) are recently used as the prediction method for screening the suitable extraction solvent. The three parameters can be used to estimate the relative energy difference between any solvents and target solute. The HSPs were reported as a good prediction for the selection of the solvent for solid-liquid extraction. For example, M. Aissou et al. (2017) reported the good agreement with prediction results and HSPs and experimental results in which D-limonene was reported as the most suitable solvent for β-carotene extraction from dried carrot. Yara-Varón et al. (2016) also reported the good agreement between experimental data and HSPs prediction of the screening suitable solvent (cyclopentyl methyl ether) for carotenoids extraction from dried carrot.

This work, therefore, aimed to study the extraction of lycopene from Gac aril. The HSPs were firstly used to predict the suitable extraction solvent. Ethyl acetate, methyl acetate, ethanol, and methanol were selected for this study due to their availability and low toxicity. The prediction result was validated with the experiment result by Soxhlet extraction. The effects of extraction conditions including the size of aril powder, solvent to solid ratio (ml/g), and extraction time on the amount of lycopene were then investigated. The statistically analyzed use t-test: paired two sample for means method.

2. MATERIALS AND METHOD

2.1 Materials and Chemicals

Fresh Gac fruits were purchased from entrepreneurs of Ban Chok Na Sam Sub-District, Prasat District, Surin Province, which were separated arils from Gac seeds. The arils were dried in the hot air oven at 60 ° C for 5 hours. The dried arils with less than 10 percent moisture were obtained and then grounded at the desired particle size (5, 10, and 40 mesh or 4, 2, and 0.4 mm, respectively). The dried aril powder was kept in an incubator to obtain the sample with <5% moisture. Solvents used for extraction including ethanol (99.8%), methanol (99.8%), ethyl acetate (99.8%), and methyl acetate (99.8%) were purchased from Sigma Aldrich, Singapore.

2.2 Screening of suitable extraction solvent

2.2.1 Hansen solubility parameters prediction

The Hansen solubility parameters (HSPs) (Charles, 2007) is starting from the basic theory is "like dissolves like". Values for describing a substance "like" or "unlike" consist of three components from the total energy of vaporization nonpolar or dispersion (atomic) forces (E_D), the permanent dipole–permanent dipole (molecular) forces (E_P), and hydrogen bonding (molecular) forces (E_H).

$$E = E_D + E_P + E_H \quad (1)$$

Dividing the individual cohesive energy terms by the molar volume (V) gives Equation (2)

$$\frac{E}{V} = \frac{E_D}{V} + \frac{E_P}{V} + \frac{E_H}{V} \quad (2)$$

$$\delta_T^2 = \delta_D^2 + \delta_P^2 + \delta_H^2 \quad (3)$$

δ_D, δ_P, and δ_H are the HSP for the dispersion, polar, and hydrogen bonding interactions, respectively. δ_T is the Hildebrand solubility parameter, $(E/V)^{1/2}$. It might be noted that the value of a solubility parameter in $MPa^{1/2}$ is 2.0455 times larger than in the often used $(cal/cm^3)^{1/2}$ units.

These 3 parameters will used calculated the distance of substances properties as shown in Equation (4).

$$R_a = \sqrt{4(\delta_{D1} - \delta_{D2})^2 + (\delta_{P1} - \delta_{P2})^2 + (\delta_{H1} - \delta_{H2})^2} \quad (4)$$

Subscript 1 refers to HSPs of solvent, 2 refers to HSPs of solute and R_a is the energy distance between two molecules, lower R_a means substances more soluble.

However, the values of HSPs of a number of bioactive compounds were not reported, but they could be estimate by contribution method as shown in Equations (5)-(7).

$$\delta_D = \frac{\sum F_{Di}}{Vm} \quad (5)$$

$$\delta_P = \frac{\sqrt{\sum F_{Pi}^2}}{Vm} \quad (6)$$

$$\delta_H = \sqrt{\frac{\sum E_{Hi}}{Vm}} \quad (7)$$

where F_{Di}, F_{Pi}, and E_{Hi} are the group contributions of type i to the dispersion component, polar component and hydrogen-bonding energy per structural group, respectively and these terms can be taken from the Hansen Handbook by (Charles, 2007). The molar volume values (Vm) were obtained from Van Krevelen and Hoftyzer (1976).

2.2.2 Validation method

10 grams of Gac aril powder (particle size = 10 mesh) was placed into a cellulose extraction thimble which then placed in Soxhlet apparatus. The exact amount of 200 ml of extraction solvent (ethyl acetate, methyl acetate, ethanol, and methanol) was then added to Soxhlet apparatus. The extraction was carried out at solvent to solid (dried Gac aril powder) ratio 20:1 (ml/g) for 60 minutes.

2.3 Study of suitable extraction conditions

To study suitable extraction conditions, the extraction was carried out using Soxhlet apparatus which the detail was described in section 2.2.2. In this section, Gac aril powder size, solvent to solid ratio and extraction time were varied from 5 to 40 mesh, 20:1 to 40:1 (ml/g) and 60 to 180 minutes, respectively.

2.4 Lycopene analysis

The lycopene in the extracts was analyzed by a UV-visible spectrophotometer at wavelength 470 nm. The absorbance obtained (A) was used to calculate the lycopene concentration (C_{st}) in the extract by substituting it into the Equation (8).

$$C_{st} = \frac{A \times 10{,}000}{3.450} \quad (8)$$

where C_{st} is the concentration of lycopene in the spectrophotometer (mg/ml), A is the absorbance value, 3.450 is the specific absorbance of all lycopene in hexane and 10,000 is the conversion factor to get the concentration in milligrams per liter (Akkarachaneeyakorn et al., 2016).

The results were reported as total lycopene content (mg lycopene to g of dried Gac aril powder) which can be calculated by multiply the concentration of lycopene obtained from Equation (8) with dilution volume and then divide by dilution weight as shown in Equation (9).

$$Total\ lycopene\ content = \frac{C_{st} \times v}{w} \times 10 \quad (9)$$

where w is milligram of dilution extract weight (5-10 mg), v is dilution volume in lycopene analysis (5 ml), and 10 is gram of dried Gac aril powder.

2.5 Statistical analysis

The experiments were carried out in triplicate. The results were expressed as mean ± SD and assessed for statistical significance using t-test: paired two sample for means method (using Microsoft Excel 2016). The differences between means, correlations and regressions were considered statistically significant at $\alpha < 0.05$.

3. RESULTS AND DISCUSSION

3.1 Screening of suitable extraction solvent

3.1.1 Prediction suitable solvent by HSPs

As shown in Figure 1, lycopene structure consists of CH_3, CH_2, =C< and -CH= groups which frequency of the groups are 10, 4 ,8, 18, respectively. The frequency of group contribution was used to calculate ΣF_{Di}, $\Sigma F_{Pi,}$ and ΣE_{Hi} which the values are shown in Table 1. The Hansen solubility parameters (δ_D, δ_P, and δ_H) of lycopene were then estimated by using Equations (5)-(7).

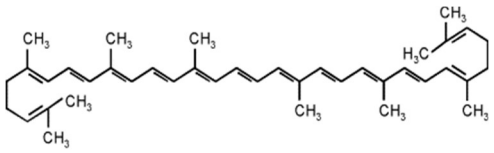

Figure 1 Lycopene structure

Table 1 List of group contributions of lycopene

Group	Freq.	ΣF_{Di} $(MJ/m^3)^{1/2}$ /mol	ΣF_{Pi} $(MJ/m^3)^{1/2}$ /mol	ΣE_{Hi} (J/mol)	V_m (cm^3/mol)
-CH3	10	4200	0	0	335
-CH2-	4	1080	0	0	64.4
=C<	8	560	0	0	-44
-CH=	18	3600	0	0	243
Sum	-	9440	0	0	598.4

Table 2 Energy distance (R_a) of lycopene and any solvent

Substances		δ_D	δ_P	δ_H	R_a
Solute	Lycopene	15.78	0.00	0.00	-
Solvent	Methanol	15.10	12.30	22.30	25.50
	Ethanol	15.80	8.80	19.40	21.30
	Methyl acetate	15.50	7.20	7.60	10.48
	Ethyl acetate	15.80	5.30	7.20	8.94

The Hansen solubility parameters prediction results are shown in Table 2. Hansen solubility parameters of methanol, ethanol. Methyl acetate, and ethyl acetate were obtained from Hansen's handbook. The results suggested that ethyl acetate was the most suitable solvent for extraction of lycopene, indicated by the lowest value of Ra (8.94). Compared to other solvents, the dispersion term (δ_D) of ethyl acetate was comparable to methanol, ethanol, and methyl acetate. However, the differences were showed in values of polarity term (δ_P) and H-bonding term (δ_H). The lowest δ_P and δ_H of ethyl acetate implied that the low polarity of the solvent which is described the good solubility for lycopene (non-polar substance (Zuorro, 2017)). It is worth to be noted that the using of lower polarity solvent such as propyl acetate might give the lower value of Ra compared with ethyl acetate. However, ethyl acetate was more attractive solvent in term of its availability and lower toxicity.

3.1.2 Validation of HSPs prediction by experiments.

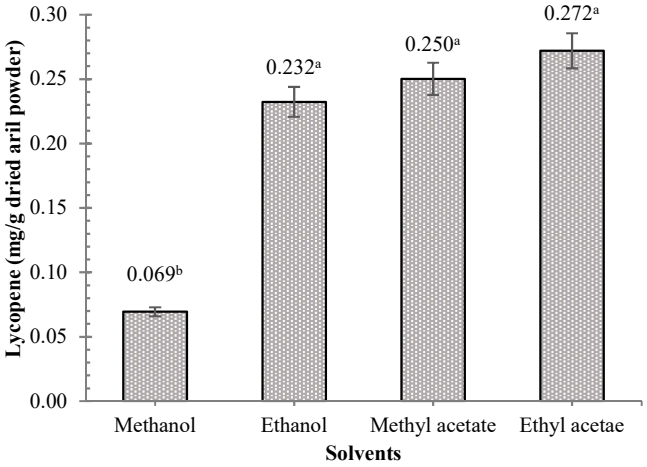

Figure 2 Extraction yield of lycopene using 4 different solvents: methanol, ethanol, methyl acetate, and ethyl acetate.

The validation results were shown in Figure 2 which the experimental results were in good agreement with HSPs prediction. Ethyl acetate was the most suitable solvent for lycopene extraction from Gac arils in this study based on the highest lycopene yield (0.272 mg/g dried Gac aril powder). The slightly lower of lycopene yields were observed by using methyl acetate and ethanol as solvent (0.250 and 0.232 mg/g dried Gac aril powder). Methanol was found to be the lowest performance for lycopene extraction since it gave the significantly lower of lycopene yield (0.069 mg/g dried Gac aril powder).

3.2 Study of suitable extraction conditions

3.2.1 Effect of size of Gac aril powder

For this experiment, ethyl acetate as the most suitable solvent was used in extraction at the solvent to solid ratio (mL/g) of 20:1 for 60 minutes. The Gac aril powder size was varied from 5 to 40 mesh. As shown in Figure 3, the results indicated that the decrease in Gac aril powder size from 5 to 10 mesh resulted in the significantly increase in lycopene yield from 0.039 to 0.272 mg/g dried Gac aril powder. The lycopene yield was found to be slightly increased from 0.272 to 0.311 mg/g dried Gac aril powder by decrease in Gac aril powder size from 10 to 40 mesh. These results might be explained by the increased in contact surface area of the powder and solvent when

decreasing powder size. The 40 mesh of Gac aril powder size was therefore selected as the most suitable condition for the next study. These results were also observed by Yuliani et al. (2019) who studied effect of particle size on daidzein yield extracted from tempeh. The results showed that the decrease in sample particle size from 1.7 to 1.2 mm resulted in higher yield of daidzein from 8.13 to 8.64 mg.

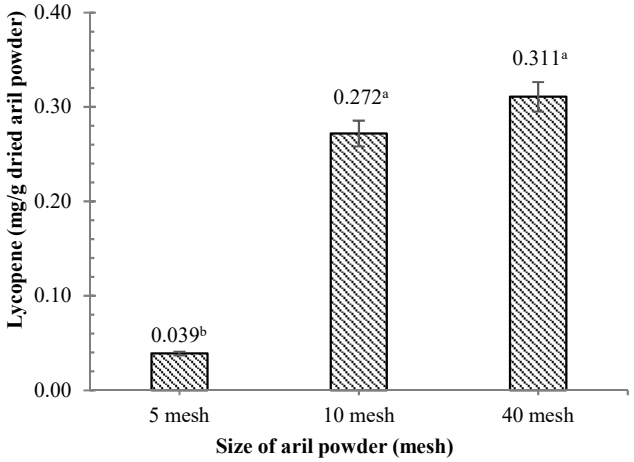

Figure 3 Extraction yield of lycopene with any size of aril powder at 5, 10, and 40 mesh

3.2.2 Effect of solvent to aril powder ratio

The extraction in this section was carried out using 40 mesh Gac aril powder for 60 minutes of extraction time. The solvent to solid ratio was varied from 20:1 to 40:1 (mL/g). From Figure 4, the increase in solvent to solid ratio from 20:1 to 30:1 (ml/g) resulted in the significantly increased lycopene yield from 0.311 to 0.412 mg/g dried Gac aril powder. However, lycopene yield was found to be insignificant different at the solvent to solid ratio higher than 30:1 (ml/g). In general, increased amounts of solvent can increase the extraction yield but the extraction was limited by the solubility of the solute in the solvent (Machmudah et al., 2012), causing the constant extraction yield at the higher solvent to solid ratios.

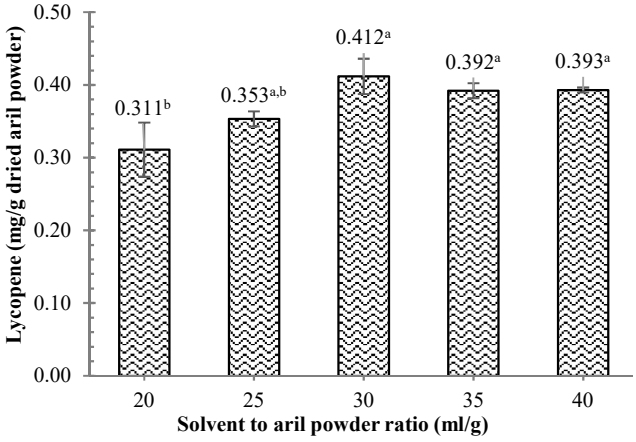

Figure 4 Extraction of lycopene yield with any solvent to aril powder ratio at 20:1, 25:1, 30:1, and 40:1

3.2.3 Effect of extraction time

In this section, the extraction was conducted using 40 mesh of Gac aril powder at solvent to solid ratio of 30:1 (mL/g). The extraction time was varied from 60 to 180 minutes as shown in Figure 5, the increase in extraction time from 60 to 120 minutes caused the increase in lycopene yield from 0.412 to 0.448 mg/g dried Gac aril powder. However, the insignificant different results can be observed at the extraction time higher than 120 minutes. The results could also be explained by extraction equilibrium. In addition, the amount of highest lycopene content obtained in this study (0.448 mg/g dried Gac aril powder) were in the range that reported by other research groups (0.38 – 0.45 mg/g of dried Gac seed aril powder) (Aoki et al., 2002; Tran et al., 2016). The differences of lycopene content might be related to the variety of species, harvesting methods, and cultivation regions.

Moreover, it is worth to be noted that lycopene has high thermal stability at the temperature of 90 °C for 3 hours (Xianquan et al., 2005). In our study, the extractions were carried out for 1 hr with extraction temperature lower than 90 °C, relating to the boiling point temperature of solvents (56.9, 64.6, 77, and 78.5 °C for ethanol, methanol, ethyl acetate, and methyl acetate, respectively). Therefore, the degradation of lycopene might be neglectable at these extraction conditions.

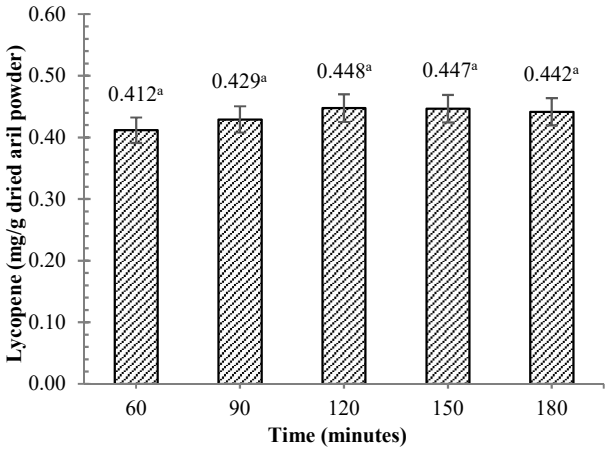

Figure 5 Extraction yield of lycopene with any extraction time at 60, 90, 120, 150, and 180 minutes

4. CONCLUSION

In this study, Hansen solubility parameters (HSPs) showed the reasonable prediction results of suitable solvent for lycopene extraction from Gac aril powder. The prediction suggested that ethyl acetate was the most suitable solvent following by methyl acetate, ethanol, and methanol, respectively. The prediction was in good agreement with validation results which ethyl acetate gave highest lycopene yield. These results confirmed that HSPs prediction might help decrease experiment number, time, and cost. The most suitable extraction conditions were then study using ethyl acetate as solvent and the

results revealed that 40 mesh of aril size powder, 30:1 (mL/g) of solvent to solid ratio and 120 minutes of extraction time were the suitable extraction conditions, giving 0.448 mg/g dried Gac aril powder.

5. REFERENCES

Aissou, M., Chemat-Djenni, Z., Varón, E.Y., Fabiano, A.S., & Chemat, F. (2017). Limonene as an agro-chemical building block for the synthesis and extraction of bioactive compounds. Comptes Rendus Chimie, 20, 346-358. https://doi.org/10.1016/j.crci.2016.05.018

Akkarachaneeyakorn, S., Boonrattanakom, A., Pukpin, P., Rattanawaraha, S., & Mattaweewong, N. (2016). Extraction of aril oil from Gac (*Momordica cochinchinensis* spreng) using supercritical carbon dioxide. Journal of Food Processing and Preservation, 2, 1745-4549. http://doi:10.1111/jfpp.13122

Aoki, H., Kieu, N. T. M., Kuze, N., Tomisaka, K., & Chuyen, N. V. (2002). Carotenoid pigments in GAC fruit (Momordica cochinchinensis SPRENG). Bioscience, biotechnology, and biochemistry, 66(11), 2479-2482. https://doi.org/10.1271/bbb.66.2479.

Charles, H. (2007). Hansen solubility parameters a User's Handbook. 2nd ed., Taylor & Francis Group, LLC.

Chuyen, H.V., Nguyen, M., Roach, P.D., Golding, J.B., & Parks, S. (2014). Gac fruit (*Momordica cochinchinensis* Spreng.): a rich source of bioactive compounds and its potential health benefits. International Journal of Food Science and Technology. http://doi:10.1111/ijfs.12721

Costa-Rodrigues, J., Pinho, O., & Monteiro, P.R.R. (2017). Can lycopene be considered an effective protection against cardiovascular disease? Food Chemistry. https://doi.org/10.1016/j.foodchem.2017.11.055

Do, T.V.T., Fan, L., Suhartini, W., & Girmatsion, M. (2019). Gac (*Momordica cochinchinensis* Spreng) fruit: A functional food and medicinal resource. Journal of Functional Foods, 62, 1756-4646. https://doi.org/10.1016/j.jff.2019.103512

Gerster, H. (1997). The potential role of lycopene for human health. Journal of the American College of Nutrition, 2, 109-126. http://10.1080/07315724.1997.10718661

Kubola, J., Meeso, N., & Siriamornpun, S. (2013). Lycopene and beta carotene concentration in aril oil of Gac (*Momordica cochinchinensis* Spreng) as influenced by aril-drying process and solvents extraction. Food Research International, 50, 664-669. http://dx.doi.org/10.1016/j.foodres.2011.07.004

Le, A.V., Huynh, T. T., Parks, S.E., Nguyen, M.H., & Roach, P.D. (2018). Bioactive composition, antioxidant activity, and anticancer potential of freeze-dried extracts from defatted Gac (*Momordica cochinchinensis* Spreng) seeds. Medicines, 5, 104. http://dx.doi.org/10.3390/medicines5030104

Machmudah, S., Zakaria, Winardi, S., Sasaki, M., Goto, M., Kusumoto, N., & Hayakawa, K. (2012). Lycopene extraction from tomato peel by-product containing tomato seed using supercritical carbon dioxide. Journal of Food Engineering, 108, 290-296. http://dx.doi.org/10.1016/j.jfoodeng.2011.08.012

Saini, R.K., Rengasamya, K., Mahomoodally, F., & Keumc, Y.S. (2020). Protective effects of lycopene in cancer, cardiovascular, and neurodegenerative diseases: An update on epidemiological and mechanistic perspectives. Pharmacological Research, 155, 1043-6618. https://doi.org/10.1016/j.phrs.2020.104730

Shida, B.K., Turner, C., Charpman, M.H., & Mckeon, T.A. (2004). Fatty acid and carotenoid composition of Gac (*Momordica cochinchinensis* Spreng) fruit. Journal of agricultural and food chemistry, 2, 274-279. http://10.1021/jf030616i

Tran, X. T., Parks, S. E., Roach, P. D., Golding, J. B., & Nguyen, M. H. (2016). Effects of maturity on physicochemical properties of Gac fruit (M omordica cochinchinensis S preng.). Food science & nutrition, 4(2), 305-314. https://doi.org/10.1002/fsn3.291

United States Department of Agriculture; USDA. (2019). Taxon:Momordica cochinchinensis (Lour.) Spreng. U.S. National Plant Germplasm System. Agricultural Research Service, Germplasm Resources Information Network (GRIN-Taxonomy).

Van Krevelen, D. W., & Hoftyzer, P. J. J. (1976). Properties of polymers: their estimation and correlation with chemical structure. 2nd ed., Elsevier, Amsterdam.

Xianquan, S., Shi, J., Kakuda, Y., and Yueming, J. (2005) Stability of lycopene during food processing and storage. Journal of medicinal food. 4, 413–422. https://doi.org/10.1089/jmf.2005.8.413

Yara-Varón, E., Fabiano-Tixier, A.D., Balcells, M., Canela-Garayoa, R., & Bily, A. (2016). Is it possible to substitute hexane with green solvents for extraction of carotenoids A theoretical versus experimental solubility study? The Royal Society of Chemistry, 6, 27750-27759. https://doi.org/10.1039/C6RA03016E

Yuliani, S.H., Sandrapitaloka, A.S., Restiana, F.R., Aji, P.D.T., Gani, M.R., & Riswanto, F.D.O. (2019). Effects of particle size, extraction time, and solvent on daidzein yield extracted from tempeh. Jurnal Farmasi Sains dan Komunitas, 1, 44-49. https://doi.org/10.24071/jpsc.001794

Zuorro, A. (2020). Enhanced lycopene extraction from tomato peels by optimized mixed-polarity solvent mixtures. Molecules, 25, 2038. http://dx.doi.org/10.3390/molecules25092038

NUEJ
Naresuan University
Engineering Journal

Maximum-Power-Point Tracking for Photovoltaic Arrays with Partial-Shading Detection

Peeradech Lousuwankun and Niphat Jantharamin*

Department of Electrical and Computer Engineering, Faculty of Engineering, Naresuan University, Phitsanulok, Thailand

*Corresponding author e-mail: niphatj@nu.ac.th

(Received: 14 December 2021, Revised: 18 February 2022, Accepted: 4 March 2022)

Abstract

In this paper, an approach to maximum-power-point tracking (MPPT) for photovoltaic (PV) arrays with partial-shading detection is demonstrated. The proposed MPPT algorithm consists of the incremental conductance (IncCond) technique with step-size variation, the partial-shading detection, and the scan for global maximum power point (GMPP) with search area restriction. The variable step size for MPPT relied on the change in array power and current. Inspection of irradiance condition was performed, so that the scan for GMPP over a voltage range occurred only if the partial shading was detected. Two partial-shading detection criteria were developed: the array was assumed to be partially shaded if just either of these two criteria was satisfied. Then, the array short-circuit current and open-circuit voltage under the present weather condition were also used for the search area restriction. After one side of the search area boundaries had been reached and the necessity of scan towards the other side was confirmed, the array operating point was then moved directly to its initial position to avoid retracing the route of search. Following the completion of scan, the array operating point was moved directly to the recorded GMPP without steady-state oscillation. In comparison to the two previously published algorithms, simulation results of the proposed MPPT technique indicated that the search area of GMPP could be narrowed by at least 20% under partial-shading conditions, and the tracking could be accelerated by about 90% under uniform irradiance.

Keywords: Maximum Power Point, Photovoltaic, Partial Shading, Incremental Conductance

1. INTRODUCTION

Solar energy has recently been a promising energy source for rural electrification. Direct conversion of solar energy into electricity is made possible by using a photovoltaic (PV) module. To increase the output electrical power, several PV modules are interconnected to form a PV array. However, the PV array power is strongly affected by weather variations. To maximize the PV array power related to each weather condition, the array operating point is placed at the maximum power point (MPP). This approach is called maximum-power-point tracking (MPPT), which can be achieved by regulating the PV array voltage, typically by means of a power converter. Partial shading, which can be caused by neighboring construction, trees, clouds or dirt on the array, results in uneven irradiance and has consequently negative effects on power-voltage characteristics of the array. According to the power-voltage curves in Fig. 1, a sole MPP exists under even irradiance condition. Apart from reduction in output power, the partial shading causes multiple peaks on the power-voltage curve. Among those peaks, the highest one is termed a global MPP (GMPP), and the others are called a local MPP (LMPP). The well-known MPPT methods, such as the perturb and observe (P&O) and the incremental conductance (IncCond), cannot effectively handle those multiple MPPs single-handed since their algorithms halt the tracking after a peak on the power-voltage characteristic curve, either a GMPP or an LMPP, is reached. If the operating point is stuck at the LMPP, the optimum power cannot be extracted from the array, which can be considered as a loss of array power. Therefore, an additional approach to track the GMPP is usually incorporated into the MPPT algorithm to obtain the optimum power output of the PV array under partial shading condition.

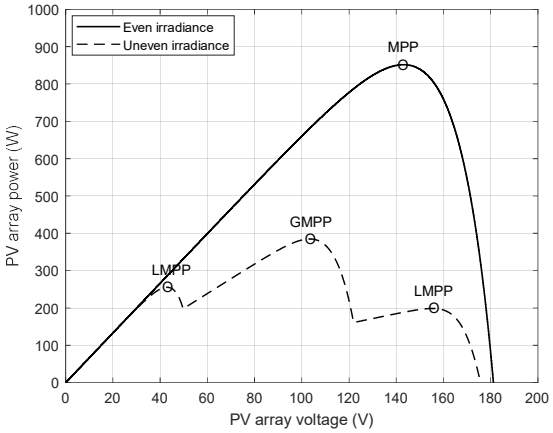

Figure 1 Effect of partial shading on a PV array power-voltage curve

Many GMPP tracking (GMPPT) techniques have been introduced in the literature. PV module rearrangement under each weather condition is presented by Elserougi et al. (2015), by which two certain configurations of modules are specified so that highest array power is investigated. Nonetheless, more strings of modules require more switches for the rearrangement, and tracking time is approximately doubled since two configurations are always implemented under each weather condition. As proposed by Ghasemi et al. (2018), speculation of the array current-voltage characteristics to specify the search area for the GMPP depends on the present operating point, the array open-circuit voltage under standard test conditions (STC: 1000 W/m^2, 25˚C) and the MPP of one module under the present weather condition. However, parameter determination for the speculation is complicated, and the operating point must be moved throughout the array voltage range. Based on the assumption that power at the peaks is increased or decreased consecutively, power observation at each peak of the array power-voltage curve contributes to knowledge of GMPP location without scanning the whole voltage range of the array (Tey & Mekhilef, 2014). The scheme is unfeasible for all partial-shading cases yet and causes the whole voltage-range search under uniform irradiance unnecessarily. Rough specification of the GMPP search area by using a linear mathematical equation derived from the short-circuit current and the open-circuit voltage of the array under present weather condition is presented by Ji et al. (2011). Consequently, the operating point is moved directly to a position assumed to be near the GMPP, and then moved towards the GMPP by means of the IncCond algorithm. Again, this approach is unfeasible for all partial-shading cases.

Furtado et al. (2018) and Ramana et al. (2019) present the P&O algorithm along with search area restriction for GMPPT, which is applicable to all characteristics of PV power-voltage curves under partial-shading conditions. The left boundary of the search area is specified by a minimum voltage which is derived from the ratio of the MPP current under STC. The right boundary used by Furtado et al. (2018) is fixed at 90% of the array open-circuit voltage under STC. On the other hand, the right boundary used by Ramana et al. (2019) is determined by a minimum current which is derived from the ratio of a newly discovered maximum power to 90% of the array open-circuit voltage under STC. During the scan for a GMPP, the search area becomes narrower if the power is found higher at each progressive step. In practice, however, the irradiance is typically lower than 1000 W/m^2 and when the solar cell temperature is higher than 25˚C, the search area is unnecessary wide. In addition, the scan is needlessly performed despite uniform irradiance since their algorithm lacks inspection of irradiance condition, and thus wastes tracking time. The linear relationship between the irradiance and the array short-circuit current can lead to partial-shading detection (Ahmed & Salam, 2017), which relies on the difference between irradiance values calculated from the module MPP current and from the array current at 80% of the array open-circuit voltage. However, numerous data collection is required for setting the criterion, and relocation of the operating point to the two aforesaid points for each irradiance condition inspection increases the tracking time.

Since the unnecessary scan under uniform irradiance caused by the GMPPT algorithms with search area restriction described above wastes the tracking time and can be considered as needless loss of the array output power, the partial shading detection technique can help the controller to avoid the dispensable scan and therefore reduce the array power losses. However, research on the incorporation of the partial shading algorithm into an MPPT approach has been very limited.

2. Proposed MPPT Method

The proposed MPPT technique incorporated the IncCond algorithm to avoid the steady-state oscillation of the array operating point. It included a new approach to detect the partial shading, and an improvement in search area restriction for GMPPT under partial shading situations. A search of GMPP usually takes much more time in comparison with a uniform irradiance case since a voltage scan up to the array open-circuit voltage is needed. Partial-shading detection can cause the GMPP scan to be used only if it is needed.

2.1 Partial-Shading Detection

Hereby, two partial-shading detection criteria were derived from the two approximately linear relationships, namely between the MPP current (I_{mpp}) and the short-circuit current (I_{sc}), and between the MPP voltage (V_{mpp}) and the open-circuit voltage (V_{oc}) of the PV array:

$$I_{mpp} \cong k_i \cdot I_{sc}\,, \tag{1}$$

$$V_{mpp} \cong k_v \cdot V_{oc}\,, \tag{2}$$

where k_i and k_v are constants. Typical current-voltage characteristic curves of a PV array under different incident irradiance conditions, on which small circles represent MPPs, are shown in Fig. 2. While the incident irradiance is uniform, only one MPP exists on the curve, as represented by the far-right curve. When the partial shading on the array happens, multiple MPPs appear on those curves, and the number of MPPs on each curve depends on shading patterns. On each curve of uneven irradiance cases, there is one MPP which gives the highest current produced by unshaded modules and this current value related to Eq. (1). Therefore, defined as the first detection criterion, the partial shading can be detected as soon as a measured MPP current is lower than the value obtained from Eq. (1).

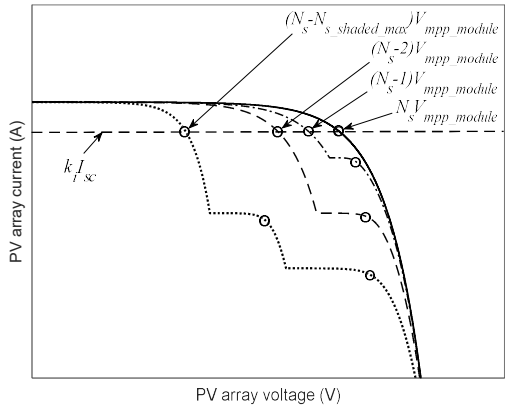

Figure 2 Current-voltage curves of a PV array under various partial shading conditions

In addition, the second detection criterion was based on the relationship between two conductance values of the array, namely the ratio of current to voltage at MPP (G_{mpp}) and the ratio of short-circuit current to open-circuit voltage (G_{ref}). Dividing Eq. (1) by Eq. (2) gives

$$\frac{I_{mpp}}{V_{mpp}} \cong \frac{k_i \cdot I_{sc}}{k_v \cdot V_{oc}}.$$

The above relationship can be written as

$$G_{mpp} \cong \frac{k_i}{k_v} \cdot G_{ref} \cong k_G \cdot G_{ref}. \quad (3)$$

where k_G is a constant and equals k_i/k_v. Equation (3) shows that G_{mpp} is directly proportional to G_{ref}. Moreover, the array MPP voltage under uniform irradiance is approximately equals the product of the module MPP voltage (V_{mpp_module}) and the module number in each string (N_s). As Fig. 2 shows, the MPP conductance of the unshaded array ($G_{mpp\_unshaded}$) can be obtained as

$$G_{mpp\_unshaded} = \frac{I_{mpp}}{N_s V_{mpp\_module}}. \quad (4)$$

According to Fig. 2, the array voltage at an MPP with highest current on each curve in partial shading cases approximately equals the product of the module MPP voltage and the difference between N_s and the maximum number of shaded modules in a string ($N_{s\_shaded\_max}$) compared with any other strings of the array. Therefore, the array conductance at this MPP (G_{mpp_shaded}) can be written as

$$G_{mpp\_shaded} = \frac{I_{mpp}}{(N_s - N_{s\_shaded\_max}) \cdot V_{mpp\_module}}.$$

Calculation of G_{mpp_shaded} can be formulated further as follows.

$$G_{mpp\_shaded} = \frac{I_{mpp}}{(N_s - N_{s\_shaded\_max}) \cdot V_{mpp\_module}} \times \frac{N_s}{N_s} = \frac{N_s}{(N_s - N_{s\_shaded\_max})} \times \frac{I_{mpp}}{N_s V_{mpp\_module}}.$$

Combining the above equation with Eq. (4) gives

$$G_{mpp\_shaded} = \frac{N_s}{(N_s - N_{s\_shaded\_max})} \times G_{mpp\_unshaded}. \quad (5)$$

Equation (5) shows that G_{mpp_shaded} is always higher than $G_{mpp\_unshaded}$ in each weather condition. As a result, the two partial-shading detection criteria can be summarized as follows.

First detection criterion: $I_{mpp} < k_{i\_min} \cdot I_{sc}$.

Second detection criterion: $G_{mpp} > k_G \cdot G_{ref}$.

If just either of these two criteria is satisfied, the array is assumed to be partially shaded. On the other hand, the incident irradiance is assumed to be equally distributed on the array if both criteria are untrue. In addition, the minimum value of k_i (k_{i_min}) is required in order that the first detection criterion is unmet in case of uniform irradiance. To determine k_{i_min} and k_G, details of MPP location were gathered from 450 PV module manufacturers in the database of MATLAB/Simulink. Current and voltage values of the MPPs under various weather conditions with evenly distributed irradiance are presented in Fig. 3, and their related k_i and k_v are shown in Fig. 4.

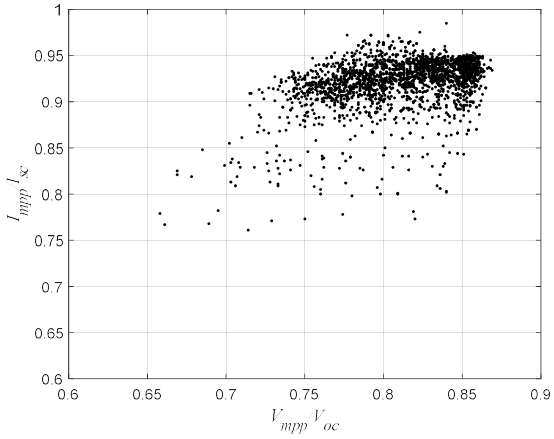

Figure 3 MPPs of 450 PV modules in various weather

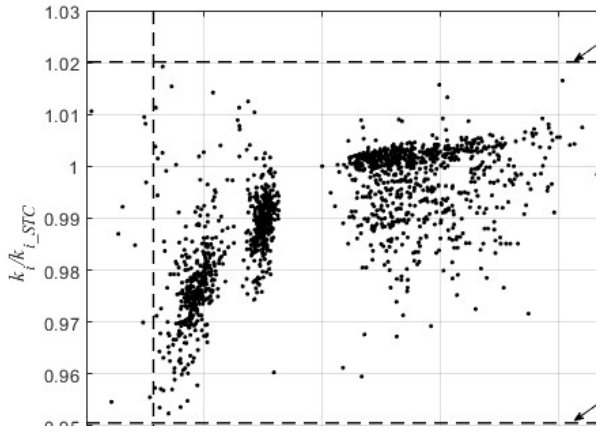

Figure 4 MPP current and voltage constants of 450 PV modules in various weather

Hence, k_{i_min} is specified to be 95% of k_i under STC (k_{i_STC}), and the minimum value of k_v (k_{v_min}) is selected to be 93% of k_v under STC (k_{v_STC}). Consequently, k_{i_min} and k_G for the partial-shading detection criteria are determined as follows.

$$k_{i\_min} = 0.95 k_{i\_STC}. \tag{6}$$

$$k_G = \frac{k_{i\_min}}{k_{v\_min}} = \frac{0.95 k_{i\_STC}}{0.93 k_{v\_STC}}. \tag{7}$$

2.2 Search Area Restriction

After the partial shading was detected, a search for GMPP location was initiated and the search area was limited. The search area restriction developed in this research was an improvement on the algorithm of Ramana et al. (2019). The ratio of newly discovered maximum power (P_{max}) to the product of k_i and the array short-circuit current under the present weather condition determined the minimum voltage (V_{min}), defined as the left boundary of the search area, under which P_{max} were never exceeded. Furthermore, the maximum value of k_i (k_{i_max}) was required in order that all MPPs existing under partial shading were included in the search area. According to Fig. 4, k_{i_max} was specified to be

$$k_{i\_max} = 1.02 k_{i\_STC}. \tag{8}$$

Thus, the left boundary of the search area was derived from

$$V_{min} = \frac{P_{max}}{k_{i\_max} I_{sc}}. \tag{9}$$

In addition, the right boundary of the search area was defined as the minimum current (I_{min}), which was derived from the ratio of P_{max} to 90% of the array open-circuit voltage under the present weather condition. Hence, the right boundary of the search area was calculated from

$$I_{min} = \frac{P_{max}}{0.9 V_{oc}}. \tag{10}$$

As the operating point was shifted during the scan for GMPPT and the array power higher than the latest P_{max} was detected, the values of P_{max}, V_{min} and I_{min} were updated and the voltage value at that point was recorded. The proposed concept of GMPPT within a search area can be described by using Fig. 5. As an example, the array was partially shaded, and the array operating point was currently at the point "P_A" while the system controller realized only the current and voltage values at the present operating point without knowledge of the power-voltage curve relative to the partial shading condition. Using Eqs. (9) and (10), the left boundary $V_{min,A}$ and the right boundary $I_{min,A}$ of the search area were determined. Hereby, the search algorithm started the scan by moving the operating point to the right, and hence higher power of the array was detected. According to Eqs. (9) and (10), the calculated values of V_{min} and I_{min} were higher, thus the left and right boundaries were updated. Accordingly, the search area became narrower until the point "P_B" was reached. Since the array power appeared lower on the right of P_B, the boundaries were unchanged. After the updated right boundary was reached and the scan continued in the opposite direction, the array power was still lower than P_B until the operating point was shifted through the point "P_D", beyond which the array power was higher than P_B, and the boundaries were then updated. The values of V_{min} and I_{min} were higher, and thus the search area became narrower until the point "P_E" was met. Since the array power appeared lower while moving the operating point to the left of P_E, the boundaries were unchanged, and hence the updated search area was determined by $V_{min,E}$ and $I_{min,E}$. The scan stopped after reaching the updated left boundary, and the GMPP location was consequently identified by the recorded voltage at which

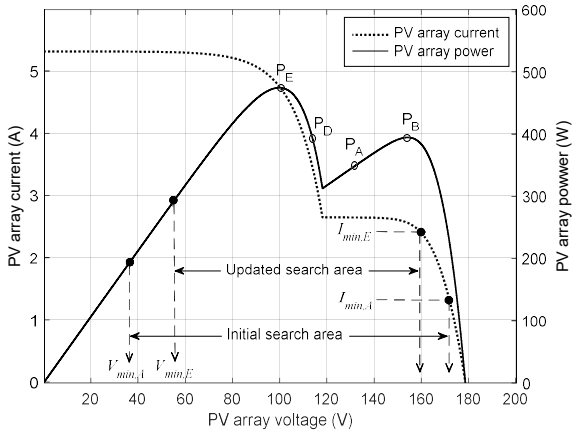

Figure 5 Search area restriction

P_{max} was given. The scan result was obtained identically even though the scan started with the operating point moved to the left first.

2.3 MPPT Algorithm

The proposed technique of MPPT started with a search for a closest MPP, then inspected the irradiance condition on the array, and finally performed GMPPT if the array was partially shaded, as described in Fig. 6. The values of k_{i_min} and k_G of the array were determined. The search for an MPP on the array power-voltage curve was based on the IncCond method with step-size variation presented by Lousuwankun & Jantharamin (2018), in which the determination of the desired step size depended on the change in array power and current, and can be expressed as

$$\Delta V_{pv}^{*} = \frac{\left|\Delta P_{pv}\right|}{V_{pv}\left|\frac{\Delta I_{pv}}{\Delta V_{pv,\max}}\right| + I_{pv}} \cdot \qquad (11)$$

ΔV_{pv}^{*} is the magnitude of desired array voltage variation and refers to the desired step size. ΔP_{pv} and ΔI_{pv} are the changes in array power and current respectively. $\Delta V_{pv,max}$ is the maximum magnitude of array voltage change, which is defined as the maximum step size.

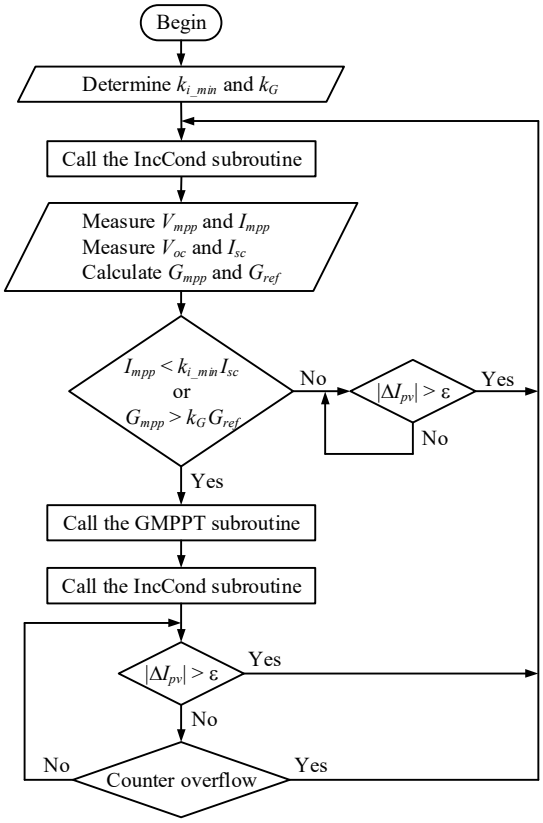

Figure 6 The proposed MPPT algorithm

After the first MPP was found, the irradiance condition on the array was examined. The voltage and current at this MPP, the open-circuit voltage and the short-circuit current of the array were measured. The two partial-shading detection criteria were inspected. If the incident solar intensity was uniform, the array operating point was kept at the present MPP until a change in array current was detected. On the other hand, if the partial shading on the array was detected, the GMPPT with the search area restriction was carried out. Then, the IncCond scheme was called again to locate the exact GMPP finely and the array operating point was kept there until a change in array current was noticed. However, the partial shading pattern on the array could change in such a way that the GMPP was shifted without a noticeable change in array current. Thus, a timer was set additionally after the GMPP was reached. Even if the array current fluctuation was undetected, the MPPT started over again after this certain amount of time elapsed to avoid the array operating point being separated from the GMPP for long.

The aforesaid GMPPT algorithm is described in Fig. 7. After the partial shading was detected, the scan for the GMPP started. The initial left- and right boundaries of the search area were determined by using Eqs. (9) and (10) respectively. Then, the array operating point was moved to the right and the array power value was observed. If the array power at each progressive step was higher than P_{max}, the array power and voltage values of that step were recorded. Hence, P_{max} and both sides of the search area were revised. After the updated right boundary was reached, the necessity of scan to the left boundary was examined. If the voltage at the updated left boundary was higher than the initial operating point voltage, the scan to the left boundary was needless. Thus, the scan was over, and the operating point was then moved to the GMPP related to the latest value of P_{max}. If the voltage at the updated left boundary was however lower than the starting-point voltage, the scan to the left boundary was still necessary. To avoid retracing the route of search, the operating point was moved to its initial position before the scan to the left was carried on. Again, if the array power at each progressive step was higher than P_{max}, the array power and voltage values of that step were recorded. P_{max} and both sides of the search area were therefore revised. Hence, the scan was complete after the updated left boundary was reached, and the operating point was then moved to the GMPP related to the latest value of P_{max}.

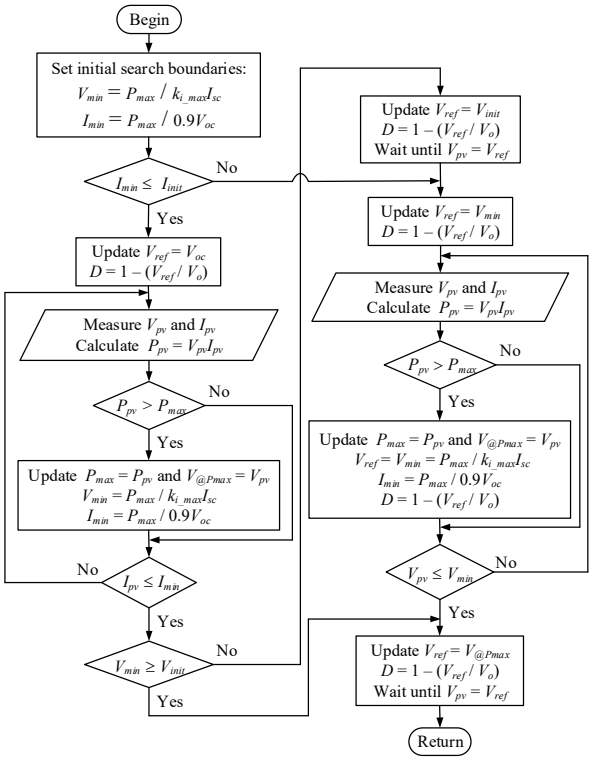

Figure 7 GMPPT algorithm of the proposed technique

2.4 PV System Using a Boost Converter for MPPT

PV array power maximization is typically realized by means of a power converter. A DC boost converter was hereby selected for tracking the MPP, and hence located between the array and a battery bank which served as load of the system as indicated in Fig. 8. The switches S_1 and S_2 contributed to momentary measurement of the array open-circuit voltage and short-circuit current. In a system normal operation, S_1 was open and S_2 was close, the capacitor C_1 was consequently situated over the array terminal, and thus its voltage dictated the array voltage. The performance of the boost converter depended upon switching. The switch duty cycle influenced the voltage of the capacitor C_1 and hence the PV voltage. The characteristic of battery bank was described by a series connection model of a resistor R_b representing the battery internal losses and a capacitor C_b explaining the battery bank capacity. As required, S_1 was first turned off, and thus the voltage en open-circuit voltage value to the controller, S_2 was then turned on, so the current sensor gave the array short-circuit current value to the controller while C_1 acted as a sole voltage source of the circuit. After the temporary measurement, S_2 was turned off and then S_1 was turned on, so C_1 was connected across the array terminal again.

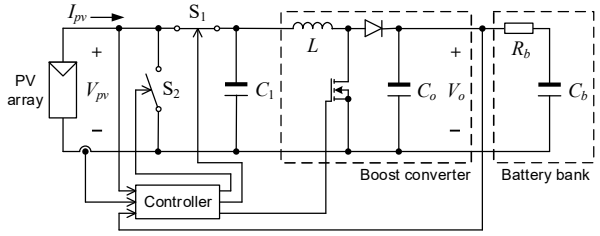

Figure 8 PV system circuit diagram for MPPT

Regarding Fig. 8, chosen parameters of the boost converter and the battery bank were as follows: C_1 = 4700 μF, L = 1 mH, C_o = 1000 μF, switching frequency = 20 kHz; R_b = 0.5 Ω, and C_b = 47 F. In this simulation, the PV array consisted of 2 parallel strings of modules, each of which was formed from 10 modules connected in series. Under STC, the array produced the short-circuit current of 6.66 A, the open-circuit voltage of 181 V and the maximum power of 851 W at 143 V. The array also gives k_{i_STC} of 0.89 and k_{v_STC} of 0.79. Thus,

$$k_{i\_min} = 0.95 k_{i\_STC} = 0.95 \times 0.89 = 0.84,$$

$$k_{i\_max} = 1.02 k_{i\_STC} = 1.02 \times 0.89 = 0.91,$$

and $$k_G = \frac{0.95 k_{i\_STC}}{0.93 k_{v\_STC}} = \frac{0.95 \times 0.89}{0.93 \times 0.79} = 1.15 .$$

3. SIMULATION RESULTS

The PV array was exposed to three environmental conditions consecutively, namely two partial shading conditions and one uniform irradiance situation respectively, as shown in Fig. 9. Under the first condition, the solar cell temperature was 25˚C, six modules of the array were exposed to 500 W/m^2, eight modules were partially shaded to 400 W/m^2, and six modules were incompletely shaded to 200 W/m^2. Then, the array experienced the second condition, under which four modules were exposed to 500 W/m^2, and sixteen modules were partially shaded to 400 W/m^2 while the solar cell temperature remained 25˚C. Finally, the third condition referred to the situation in which the equally distributed irradiance of 400 W/m^2 was incident on the array and the solar cell temperature rose to 27˚C. The array power-voltage characteristic curves related to each irradiance condition are indicated in Fig. 10. Even though higher cell temperature causes the array power to drop and the location of MPPs on the array power-voltage curve to be shifted to the left, a change in the cell temperature has no influence on the tracking performance of the purposed algorithm. Therefore, the cell temperature effect was not emphasized in this simulation.

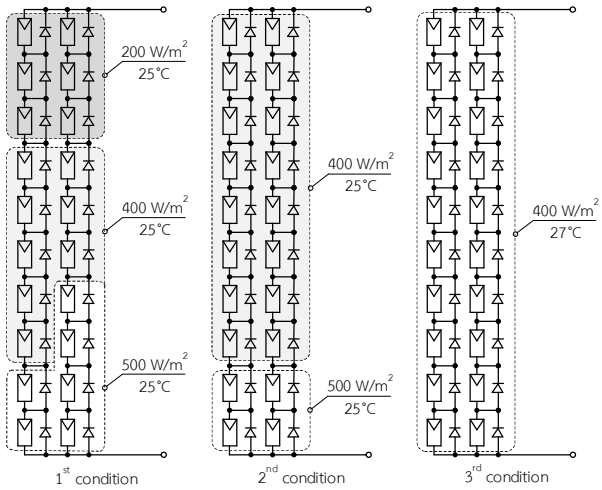

Figure 9 Irradiance conditions on the PV array

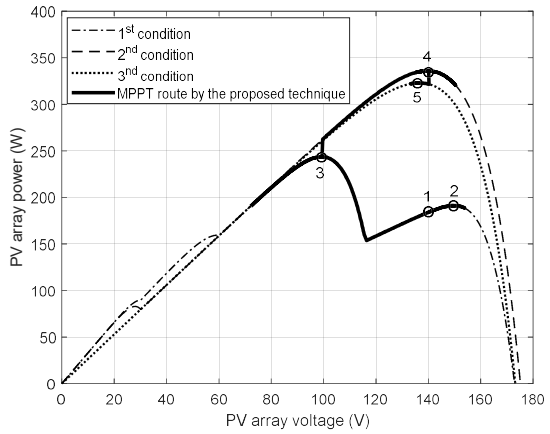

Figure 10 Operating point movement during MPPT

Regarding the width of search area and the true-MPP tracking time, the simulation results of the proposed technique were compared with those obtained from the algorithms previously published by Furtado et al. (2018) and Ramana et al. (2019). The traditional P&O algorithm was also implemented in the simulation for the MPPT performance comparison. The PV array voltage variation during the MPPT is shown in Fig. 11, and the related PV array power fluctuation is illustrated in Fig. 12. At first, the array experienced the first weather condition, under which a partial shading happened as described in Fig. 9. The initial duty cycle of the boost converter caused the operating point to be at 'Point 1' in Fig. 10. The MPPT was commenced after 0.1 s elapsed. The P&O algorithm caused the operating point to be stuck at the LMPP at 'Point 2', at which the array delivered 191.2 W, and thus failed to track the GMPP, at which the array could give 243.5 W. Hence, the P&O algorithm resulted in 21.5% loss of array power. However, the proposed technique and the other two algorithms were able to move the operating point to the GMPP at 'Point 3' eventually. According to the graphs in Fig. 11, the algorithms of Furtado et al. (2018) and Ramana et al. (2019) provided the search area of 121 V and 102 V, or 70% and 59% of the present array open-circuit voltage (173.2 V), with the tracking time of 0.37 s and 0.22 s respectively. However, the proposed technique gave the search area of 81.7 V, or 47.2% of the present array open-circuit voltage, with the tracking time of 0.26 s. In comparison with the algorithms of Furtado et al. (2018) and Ramana et al. (2019), the proposed technique contributed therefore to the search area narrowed by 32.5% and 20% respectively, with 29.7% higher tracking speed compared with the algorithm of Furtado et al. (2018) and 18.2% longer tracking time compared to the algorithm of Ramana et al. (2019).

After 0.8 s passed, the array encountered another partial shading condition as specified to the second weather condition. The operating point was then moved to the present GMPP at 'Point 4'. the algorithms of Furtado et al. (2018) and Ramana et al. (2019) gave the search area of 104 V and 109.5 V, or 59.4% and 62.5% of the present array open-circuit voltage (175.2 V), with the tracking time of 0.41 s and 0.3 s respectively. Nonetheless, the proposed method gave the search area of 50.8 V, or 29% of the present array open-circuit voltage, with the tracking time of 0.2 s. In comparison with the algorithms of Furtado et al. (2018) and Ramana et al. (2019), the proposed method contributed therefore to the search area narrowed by 51.1% and 53.6%, and thus the tracking speed increased by 50% and 32.3% respectively. On the other hand, the P&O technique resulted in the fastest tracking time of 70 ms since the LMPP voltage under the previous weather condition (at 'Point 2') was closest to the present GMPP voltage (at 'Point 4').

After 1.3 s elapsed, the array was exposed to the third weather condition, under which the incident solar radiation was uniform. The operating point was then moved to the present MPP at 'Point 5'. The algorithms of Furtado et al. (2018) and Ramana et al. (2019) provided the search area of 106 V and 98.5 V, or 61.1% and 57% of the present array open-circuit voltage (173.2 V), with the tracking time of 0.33 s and 0.3 s respectively. On the other hand, the proposed approach performed the MPPT without scanning voltage over a search area since no partial shading occurred, and results in the tracking time of 32 ms. While the P&O method spent 62 ms to reach the present MPP, the proposed technique provided faster tracking speed by 48.4%. In comparison with the algorithms of Furtado et al. (2018) and Ramana et al. (2019), the proposed approach contributed therefore to the tracking speed increased by 90.3% and 89.3% respectively. As a result, the operating point movement towards the true MPP related to each irradiance condition, which was caused by the proposed technique, is indicated in Fig. 10.

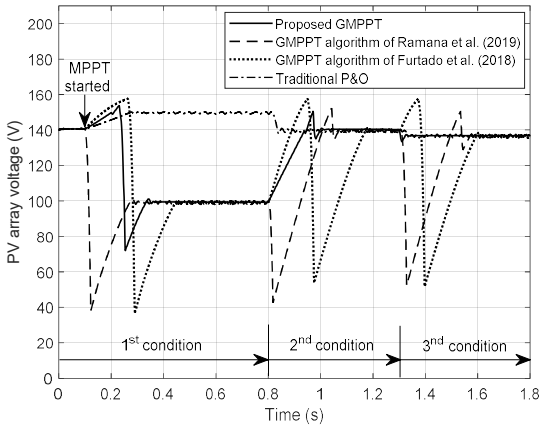

Figure 11 PV array voltage variation during MPPT

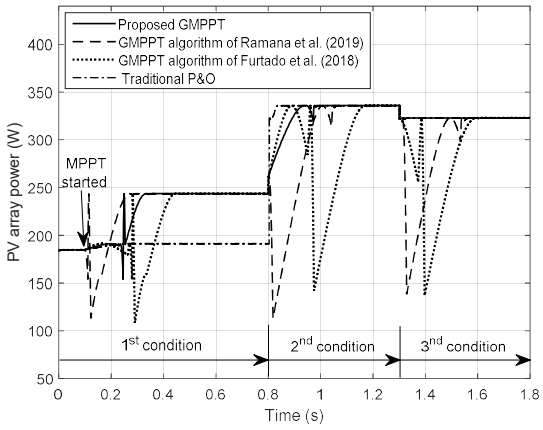

Figure 12 PV array power fluctuation during MPPT

4. DISCUSSIONS

By means of simulation, the width of search area and the speed of MPPT, which resulted from the proposed technique, were compared with those obtained from the algorithms of Furtado et al. (2018) and Ramana et al. (2019). The search area restriction of the proposed MPPT technique was based on the short-circuit current, the open-circuit voltage, and the newly discovered output power of the array under the present weather condition. However, the search area restriction by the algorithms of Furtado et al. (2018) and Ramana et al. (2019) were based on the MPP current and the open-circuit voltage of the array under STC (1000 W/m^2, 25˚C). In addition, the right boundary of the search area created by the algorithm of Furtado et al. (2018) was fixed. Since the simulated irradiance level was lower than 1000 W/m^2, the short-circuit current value used by the proposed technique was lower and therefore resulted in a narrower search area.

The tracking time, which can refer to the tracking speed, is affected by the scan procedure for a GMPP. Regarding the algorithms of Furtado et al. (2018) and Ramana et al. (2019), the operating point was slid to meet one boundary of the search area, and then moved in reverse until it hit the opposite boundary. Hence, backtracking occurred during each scan, and reduced the tracking speed. The proposed technique, however, examined the necessity of scan in reverse after the operating point had met the right boundary. If the scan to the left boundary was needed, the operating point was moved directly to its initial position to avoid going back the same route as demonstrated in case of the first weather condition. If the scan in reverse was unnecessary as shown in case of the second weather condition, the scan was finished, and thus the tracking time was saved. In addition, the traditional P&O algorithm could easily fail to track the GMPP under partial-shading conditions if a LMPP was found first, resulting in loss of array power.

Following the scan throughout the search area, the proposed technique resulted in the operating point being moved directly to the recorded GMPP without a steady-state oscillation due to the IncCond approach with step-size adaptation. The algorithms of Furtado et al. (2018) and Ramana et al. (2019), on the other hand, caused the operating point to oscillate around the MPP due to the P&O scheme. Moreover, they performed the scan even though the incident solar intensity on the array was uniform as presented in case of the third weather condition, thus lost power during the scan and wasted tracking time since a sole MPP was present. The proposed technique, however, searched for the closest MPP and inspected the irradiance condition on the array. Since no partial shading was detected, the operating point was kept at that MPP without performing the unnecessary scan. Based on the step-size variation, the proposed technique was superior to the traditional P&O algorithm in terms of MPP tracking speed.

5. CONCLUSIONS

This paper presented the MPPT approach under partial-shading condition, which was made up of the IncCond technique with step-size variation, the partial-shading detection, and the scan for GMPP with search area restriction. Irradiance condition on the array was investigated, so that the GMPP search over a voltage range is carried out only if the partial shading was detected. Partial-shading detection was based on two criteria, which were analytically devised by using details of MPP location collected from 450 PV module manufacturers in MATLAB/Simulink database. The first criterion involved the MPP current and the short-circuit current. The second criterion relied on the output conductance at the MPP, and the reference conductance derived from the ratio of short-circuit current to open-circuit voltage under the present weather condition. If just either of these two criteria was fulfilled, the irradiance on the array was assumed to be uneven. Then, the array short-circuit current and open-circuit voltage under the present weather condition were also applied for the search area restriction. After the right boundary

of the search area had been met and the scan to the left boundary was obliged, the array operating point was then moved straight to its original location to avert going back the same route before the scan was continued to the left. Compared with the algorithms of Furtado et al. (2018) and Ramana et al. (2019), simulation results under partial-shading conditions showed that the proposed MPPT approach provided a narrower area of GMPP search and higher tracking speed. In case of a uniform irradiance, the proposed technique performed no scan over a search area and therefore saved the tracking time substantially. Future work on this research will focus on validation of the proposed technique, which includes development of an embedded controller and a hardware prototype.

6. ACKNOWLEDGMENT

The authors are grateful to the Faculty of Engineering, Naresuan University for supporting this research financially and also providing research facilities.

7. REFERENCES

Ahmed, J. & Salam, Z. (2017). An Accurate Method for MPPT to Detect the Partial Shading Occurrence in a PV System. *IEEE Transactions on Industrial Informatics*, *13*(5), 2151–2160. https://doi.org/10.1109/TII.2017.2703079

Elserougi, A. A., Diab, M. S., Massoud, A. M., Abdel-Khalik, A. S. & Ahmed, S. (2015). A Switched PV Approach for Extracted Maximum Power Enhancement of PV Arrays During Partial Shading. *IEEE Transactions on Sustainable Energy*, *6*(3), 767–772. https://doi.org/10.1109/APEC.2015.7104786

Furtado, A. M. S., Bradaschia, F., Cavalcanti, M. C. & Limongi, L. R. (2018). A Reduced Voltage Range Global Maximum-power-point tracking Algorithm for Photovoltaic Systems Under Partial Shading Conditions. *IEEE Transactions on Industrial Electronics*, *65*(4), 3252–3262. https://doi.org/10.1109/TIE.2017.2750623

Ghasemi, M. A., Ramyar, A. & Iman-Eini, H. (2018). MPPT Method for PV Systems Under Partially Shaded Conditions by Approximating *I–V* Curve. *IEEE Transactions on Industrial Electronics*, *65*(5), 3966–3975. https://doi.org/10.1109/TIE.2017.2764840

Ji, Y.-H.; Jung, D.-Y.; Kim, J.-G.; Kim, J.-H.; Lee, T.-W.; Won, C.-Y. (2011). A Real Maximum-power-point tracking Method for Mismatching Compensation in PV Array Under Partially Shaded Conditions. *IEEE Transactions on Power Electronics*, *26*(4), 1001–1009. https://doi.org/10.1109/TPEL.2010.2089537

Lousuwankun, P. & Jantharamin, N. (2018). Photovoltaic Module Maximum-Power-Point Tracking with Step-Size Variation. *2018 International Conference on Engineering, Applied Sciences, and Technology*, pp. 1-4, https://doi.org/10.1109/ ICEAST.2018.8434450

Ramana, V. V., Mudlapur, A., Damodaran, R. V., Venkatesaperumal, B. & Mishra, S. (2019). Global Peak Tracking of Photovoltaic Array Under Mismatching Conditions Using Current Control. *IEEE Transactions on Energy Conversion*, *34*(1), 313–320. https://doi.org/10.1109/TEC.2018.2873667

Tey, K. S. & Mekhilef, S. (2014). Modified Incremental Conductance Algorithm for Photovoltaic System Under Partial Shading Conditions and Load Variation. IEEE Transactions on Industrial Electronics, 61(10), 5384–5392. https:// doi.org/10.1109/TIE.2014.2304921

8. BIOGRAPHIES

Peeradech Lousuwankul received the B.Eng. and M.Eng. from Naresuan University in 2017 and 2019 respectively. All degrees are in Electrical Engineering. He studies now towards a research Ph.D. degree in Electrical Engineering at the Faculty of Engineering, Naresuan University in Phitsanulok province, Thailand.

Dr. Niphat Jantharamin received the B.Eng. from King Mongkut's Institute of Technology Ladkrabang (KMITL), Thailand in 1997, the M.Sc. from the University of Kassel, Germany in 2002 and the Ph.D. from the University of Leeds, UK in 2008. All degrees are in Electrical Engineering. He is currently an Associate Professor of Electrical Engineering at Naresuan University, in Phitsanulok province, Thailand. His research interests include Power Electronics, Photovoltaic system technology and efficient energy conversion.

NUEJ
Naresuan University
Engineering Journal

Power Generation Scheduling of Hydropower Plants Using an Artificial Neural Network (ANN)

Souk Lao[1], Suttichai Premrudeepreechacharn[2*] and Kanchit Ngamsanroj[3]

[1] Department of Mechanical, Faculty of Engineering, Chiang Mai University
[2] Department of Electrical Engineering, Faculty of Engineering, Chiang Mai University
[3] Electricity Generating Authority of Thailand (EGAT), Nonthaburi, Thailand

* Corresponding author e-mail: suttic@eng.cmu.ac.th and zouzeng2012@gmail.com

(Received: 27 September 2021, Revised: 26 March 2022, Accepted: 4 April 2022)

Abstract

This paper presents the determination of power generation in hydropower plants using an artificial neural network ANN in the Central-1 region power grid of EDL. The goal aims to reduce the generation cost in terms of the total cost of each power plant to generate the electricity at its lowest point and to maximize the power generation to balance the supply and demand sides. The proposed ANN is applied to solve an optimal generation scheduling, an optimization problem, and an economical dispatching problem. In addition, a quadratic function uses the Lambda iteration method to consider an optimal dispatch problem in a hydropower plant system. Use the ANN tool in MATLAB to solve the power plant generation problem and train it with the back-propagation algorithm considered as 10 power plants in EDL's Central-1 region power grid. The results of the studies show the best-operating costs in comparison between the proposed ANN and the lambda iteration method, which are significantly less than the operating costs of the current system. For the ANN accuracy is measured using the Root Mean Square Error RMSE of the input-output relationship. It shows that the ANN is highly efficient and has an accuracy of better than 0.90.

Keywords: Hydropower Plants, Scheduling, Optimal Power Flow, Artificial Neural Network.

1. INTRODUCTION

Electricite du Laos EDL is a leading company that supplies electricity to the whole country and parts exports to a neighboring country, especially Thailand. According to the company's mission and vision, it is to be the battery of Asia. Owned, operated according to government guidelines. Responsible for the generation and supply of electricity as well as the import and export of electricity at various locations. As almost all electricity generation in the whole country comes mainly from hydropower plants, of which 78 hydropower plants, also 1 thermal, 4 biomass, and 6 solar power plants, the number will continue to increase. For easy handling of electrical systems. Therefore, the network is divided into 4 regions, namely the Northern Region Network, the Central 1 Region Network, the Central 2 Region Network, and the Southern Region Network. An ideal facility for generating electricity is an abundant natural water source. Therefore, the foregoing causes the number of power plants to increase every year. Currently, the power generation system consists of three main sectors: EDL-Generation Public Company EDL-Gen, Domestic Independent Power Producer IPPd, and Exporting Independent Power Producer IPPe. All of them are electricity producers in Laos PDR supplies to EDL and exports to neighboring countries. EDL's grid-connected generation sectors such as EDL-Gen and IPPd go directly to EDL for domestic distribution. And EDL's off-grid generation sector is directly exported to neighboring countries. Figure 1 shows that each year runs from January to April. Some years are from February to May, about 3 months. It shows that the load curve is higher than the production curve, which means that the supply side is lower than the demand side. Due to a dry season, the amount of water in each reservoir begins to decrease, meaning that the inflow is less than the outflow. Water resources are the main factor in power generation. As a result, the power plant cannot cover domestic electricity requirements all year round. Due to seasonal fluctuations to cover the seasonally fluctuating demand in electricity generation, more energy has to be imported from neighboring countries if bottlenecks persist.

Electricity generation will gradually change into reality and management methods will evolve with the increase in population in the country. In addition, technological advances are a key factor behind major changes. In previous work to prove this problem, there are several techniques for simulating the power generation planning of hydropower plants, taking into account the question of optimal load flow and optimal economic operation. These problems can be solved by different methods like unit commitment, Newton-Raphson, and lambda iteration. In addition, the application of machine learning in hydropower plants is

widely used to manage electricity efficiently in terms of forecasts and estimates in various fields.

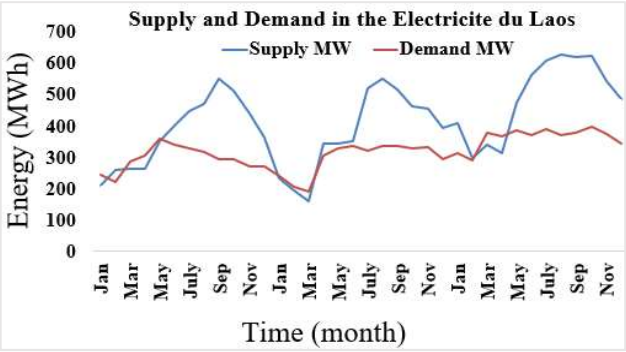

Figure 1 The supply and demand in Electricite du Laos 2016-2018

Table 1 Name, location, and capacity of 10 hydropower plants that are considered

No	Generation Name	Location/ Provinces	Installation Capacity (MW)
1	Nam Ngum1	Vientiane	155
2	Nam Leuk	Xaysomboun	60
3	Nam Mang3	Vientiane	40
4	Nam Lik1-2	Vientiane	100
5	Nam Ngum5	Vientiane	120
6	Nam Ngiep2	Xiengkhouang	180
7	Nam Phai	Xaysomboun	86
8	Nam Chien	Xiengkhouang	104
9	Nam San3A	Xiengkhouang	70
10	Nam San3B	Xiengkhouang	45

Many references describe the literature review as follows: Estoperez and Nagasaka (2006) presented a neural network to plan small hydroelectric power plants to predict electricity generation by forecasting monthly water runoff, Naresh and Sharma (2000) presented a two-phase neural network to do that find optimal planning to maximize hydroelectric power generation of the Bhakra-Beas compound reservoir system, Liang and Hsu (1994) demonstrate how to implement used artificial neural networks for short-term hydroelectric generation planning of a power system, Tufegdzic (1997) Presents the use of neural networks for management and optimization of reservoirs to provide sufficient water for generation, Shadaksharappa (2011) presented a neural network to optimize generation scheduling of thermal power plants and compare the results with the classical method, Dike et al. (2013) presented a solution to the economic dispatch problem using lambda iteration using MATLAB programming and compared the results to genetic algorithms, and Saeed (2019) proposed a neural network to solve the economic burden transfer problem optimize. Based on the Lambda iterative optimization method. These are the relevant theories referenced for this paper and apply an artificial neural network technique for planned power generation for this research.

ANN is one of the proposed machine learning processes, which is a black box model used for various purposes and is a highly effective prediction tool. It is used for forecasts and estimates. It processes records individually and learns by comparing the most arbitrary classifications of records. Error classification begins with entering error data into the network. Then check the exact value. If the result is good, the process ends. Adjust the algorithm again if the result is not good. After every adjustment, it's still not good. Repeat this many times until are satisfied and stop. Especially when predicting flood discharges at downstream stations of unmeasured rivers. Make messages fast and flexible. The complex correlation problem of hydropower nonlinear variables can be overcome by constructing ANN modeling for power plant efficiency predictions based on some data relevant to previous observations of the parameters. For the neural network backpropagation algorithm, this is a very clear and accurate step in model prediction, so many ANN models are more optimized and accurate than various artificial intelligence. To check the accuracy and precision of the hydropower generation model, the input and the output are necessary parameters for testing and validation.

This paper presents 10 power plants in the central-1 region network to be considered as a case study. Such details are shown in Table 1. This research has proposed the abilities of neural networks to predict electricity generation in hydropower plants. The purpose of this paper is to reduce generation costs and maximize power generation to match the supply and demand sides. In particular, to keep electricity imports from neighboring countries as low as possible during the dry season and to ensure that all plants in the country are producing at the highest possible output. This research aimed to study the feasibility of using artificial neural networks in hydroelectric power plants, particularly in the field of power generation and reservoir management. Then use the datasets obtained from the Lambdas data mining steps to feed them into the model to train the last designed architecturally neural network. After that, the neural network generates new prediction results. They are then compared to results obtained using traditional lambdas calculation methods to determine which is better. The results of the comparison show that the side hammer neural network method gives more satisfactory results. This indicates that the designed model can also be applied to hydropower plants generation management.

2. Problem Formulation

2.1 Optimal Power Flow solution.

Optimal Power Flow (OPF) is a program that helps solve electrical system problems, especially in the area of optimal distribution and minimizing power dissipation. Optimal disposition is essential for the electrical system to return the highest production efficiency. Reducing the cost of sending electricity to consumers and maintenance is divided into two parts. The first relates to the minimal

cost of generating electricity, known as economical power distribution, and the other relates to delivering the generated electricity to the load with minimal losses. The allocated economic load determines each power generation plant to reduce the production cost in the system that is fed to the load and focuses on the generation cost of all power plants operating in the system. With the minimal loss, problems can take many paths depending on the current control in the system. There are several optimization methods to solve complex nonlinear problems as shown in Figure 2

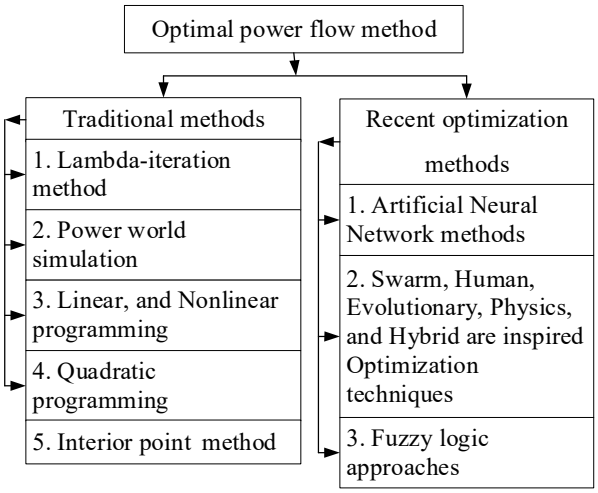

Figure 2 Optimal power flow solution method

2.1.1 Distribution of loads between units in the power plants

When the load increases, power is only supplied to the systems with maximum efficiency. The most efficient facility will supply electricity up to the point of maximum efficiency for that facility. Determination of the economic load distribution between different production units. Distributing the load between two units depends on the increase or decrease of the load on that unit. All costs increase or decrease accordingly. It shows that electricity production is related to costs. Considering the slope of the input-output curves of both units, this will be as shown in Figure 3

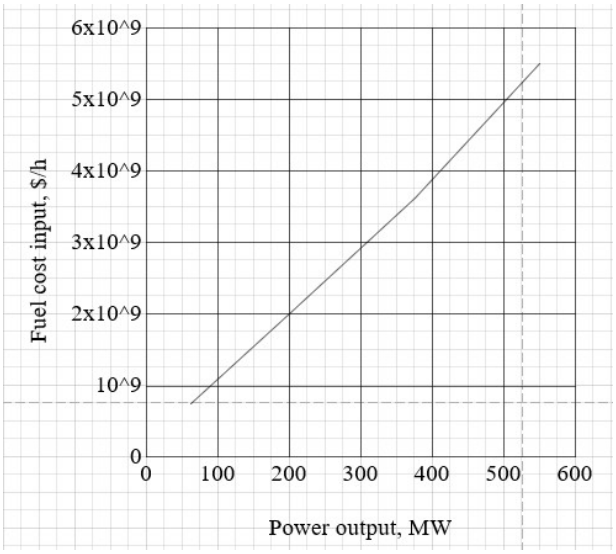

Figure 3 Input-output curve for a generating unit showing fuel cost input versus power, output

If dCi/dPGi is the increased fuel cost in dollars per megawatt-hour and Ci/PGi is the average fuel cost in the same unit, then the unit input-output curve is written as a quadratic function:

$$C_i = a_i + b_i P_{Gi} + c_i P_{Gi}^2 (\$/h) \quad (1)$$

If the unit has an incremental fuel lambda can be defined by:

$$\lambda_i = \frac{dC_i}{dP_{Gi}} = 2c_i P_{Gi} + b_i (\$/MWh) \quad (2)$$

Where a_i, b_i, c_i are the power plant coefficients.

2.1.2 Distribution of loads between the power plants

Loss in power transmission lines must be considered to account for load sharing between power plants. The load needs to be reduced on power plants with low marginal costs and the load needs to be increased on power plants with high marginal costs. It is, therefore, necessary to find a way of keeping these losses as low as possible when sending electrical energy. By planning each crop generation for maximum savings at a given load level.

$$C_T = C_1 + C_2 + \ldots + C_n = \sum_{i=1}^{n} C_i \quad (3)$$

Where Ci is the total cost of generation; C1, C2, and Cn are the cost of generating of each power plaequal
where PG1, PG2, PGn are the power of each power plant and PGT is the total power of the power plant. Which can be written in a new way

$$P_L + P_D - \sum_{i=1}^{n} P_{Gi} = 0 \quad (4)$$

Where PD is the demand and PL is the transmission loss

2.2 Unit Commitment

Future projected a load supply plan knowing the capacity and reserve power to meet potential abnormal operating conditions. For example, consider a thermal unit planning problem where K the generators are 4 units (K = 4), and possible combinations of 15 sets of the theory are obtained as shown in Table 2.

Table 2 Units combined

Unit	1	2	3	4
X1	1	1	1	1
X2	1	1	1	0
X3	1	1	0	1
X4	1	0	1	1
X5	0	1	1	1
X6	0	1	0	1
X7	1	0	0	1
X8	0	0	1	1
X9	1	1	0	0
X10	1	0	1	0
X11	0	1	1	0
X12	1	0	0	0
X13	0	1	0	0
X14	0	0	1	0
X15	0	0	0	1

2.3 Optimal Dispatch Operation

Hydroelectric power generation schedules must follow the Optimal Power Flow (OPF) principle to determine operating costs. According to the principle of system optimization under different load conditions. The power plant must have minimal total production costs. This also results in the lowest overall generation cost. While total power generation still meets demand. If one considers n plants in the network and determines the load side of the power generation, each power plant enters a target function as follows:

Minimize:

$$C_T = C_1 + C_2 + \ldots + C_n = \sum_{i=1}^{n} C_i(P_{Gi}) \quad (5)$$

The actual power generation cost function is expressed as a quadratic function as follows.

$$MinP_{Gi} \sum_{i=1}^{n} C_i(P_{Gi}) = MinP_{Gi} \sum_{i=1}^{n} (a_i + b_i P_{Gi} + c_i P_{Gi}^2) \quad (6)$$

$$P_{GT} = P_{GT} + P_{GT} + \ldots + P_{Gn} = \sum_{i=1}^{n} P_{Gi} \quad (7)$$

$$\sum_{i=1}^{n} P_{Gi} - P_D = 0 \quad (8)$$

Where ai, bi, ci coefficient of plant i
n: is the number of power plant
i: the index of power plants in dispatched

C_i: generation cost of plant i	[$/h]
C_T: total generation cost	[$/h]
P_{Gi}: the power generation of plant i	[MW]
P_T: total power generation	[MW]
P_D: total load demand in the system	[MW]

2.3.1 Power Balance

The power generation of a hydropower station. Should be considered optimal to reduce the cost of power generation and provide higher power generation. Therefore, the power production is equal to the total transmission losses plus the total system load requirement. Which is described as follows:

$$\sum_{i=1}^{n} P_{Gi} = P_{Loss} + P_D \quad (9)$$

Where P_D: Total load demand [MW]
Ploss: Total transmission loss [MW]

2.3.2 Power constraints

The limitation of the power generation optimization problem is that each power plant must be between the minimum and the maximum.

$$P_{Gi(min)} \leq P_{Gi} \leq P_{Gi(max)} \quad (10)$$

Where $P_{Gi(min)}$ is the minimum limit of generation for plant i [MW]
$P_{Gi(max)}$ the maximum limit of generation for plant i [MW]

2.3.3 Lagrange functions

An objective function multiplied by an uncertain multiplier expressed as

$$L = C_T + \lambda\phi \quad (11)$$

Define the Lagrange function

$$L = L(P_{Gi}, \lambda) \quad (12)$$

Substitute equations (6), (5), and (9) into (12).

$$L(P_{Gi}, \lambda) = C_i(P_{Gi}) + \lambda(P_D - \sum_{i=1}^{n} P_{Gi}) \quad (13)$$

Solve equation (14) to get

$$\frac{\partial L(P_{Gi},\lambda)}{\partial P_{Gi}} = \frac{\partial C_i(P_{Gi},\lambda)}{\partial P_{Gi}} - \lambda = 0 \quad (14)$$

$$\frac{\partial L(P_{Gi},\lambda)}{\partial P_{Gi}} = P_D - \sum_{i=1}^{n} P_{Gi} = 0 \quad (15)$$

Solve equation (15) to get

$$\frac{\partial C_i(P_{Gi},\lambda)}{\partial P_{Gi}} = \lambda \quad (16)$$

For i^{th} generating units, the incremental cost becomes

$$\frac{\partial C_i(P_{Gi},\lambda)}{\partial P_{Gi}} = 2a_i P_{Gi} + b_i \quad (17)$$

When equations (17) and (18) are combined, one obtains

$$\lambda = 2a_i P_{Gi} + b_i \quad (18)$$

After arranging an equation (19) will get

$$P_{Gi} = \frac{\lambda - \text{bthe the}_i}{2a_i} \quad (19)$$

Substituting equation (20) into (16) we get

$$P_D = \sum_{i=1}^{n} \frac{\lambda - b_i}{2a_i} \quad (20)$$

Finally got

$$\lambda = \left(\frac{P_D + \sum_{i=1}^{n} \frac{b_i}{2c_i}}{\sum_{i=1}^{n} \frac{1}{2c_i}} \right) \quad (21)$$

2.4 Optimal Dispatch by Lambda Method

Steps to solve the problem with Lambda is to use computer algorithms to calculate complex processes using MATLAB. First, read out system data such as cost functions of each power plant (ai, bi, and ci) and generation boundary conditions. Lambda initial conditions are used to define each asset's power (Pi) based on its incremental cost. Then the load and power generation of the entire power plant is determined. An optimal generation plan is obtained by comparing the tolerance (ε). If they differ, they are recalibrated and reset to the starting point for recalculation. Then the generation cost is simulated using Equation (1).

1. Firstly, start by inputting the number of plants, total demand, power generation limit, coefficient of each power plant, iteration limit, tolerance, and the default setting of λ;
2. Set default lambda
3. Compute P_{Gi} (i=1, 2,…, n) using (20);
4. Check the power generation limit using (11);
5. If $P_{Gi} \geq P_{Gi(max)}$, set $P_{Gi} = P_{Gi(max)}$,
   If $P_{Gi} \leq P_{Gi(min)}$, set $P_{Gi} = P_{Gi(min)}$;
6. Compute ΔP using (9);
7. Compute Δλ(k) using (22);
8. If Δλ(k) ≠ Tolerance. Update the λ
9. Return to step 3
10. If Δλ(k) = Tolerance, stop and display the value of P_{Gi} and λ. Then stop.

Like the flowchart shown in the figure below

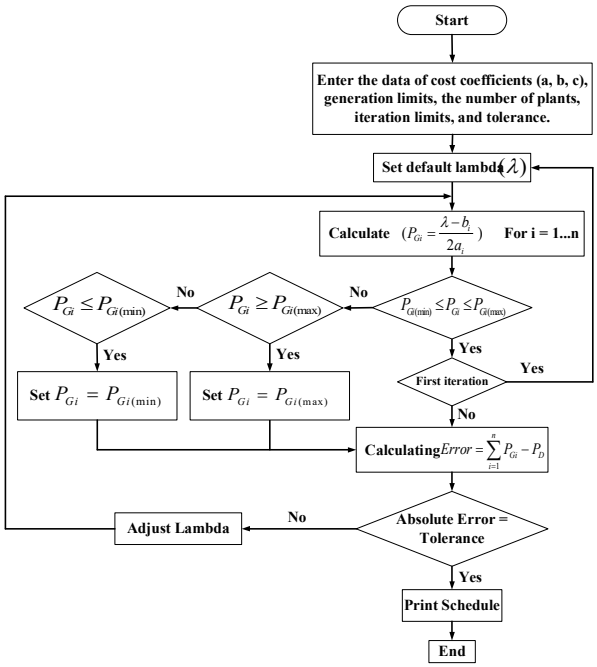

Figure 4 The procedure for calculating the power and cost of each power plant the lambda iteration method

3. ARTIFICIAL NEURAL NETWORK

3.1 Introduction

The concept of information processing by neural networks is the same as that of the human brain. A neural network architecture consists of many interconnected cells that work together through experiential learning through the concept of learning the relationship between cause and effect. The perfect connection of neurons across all layers is the typical architecture. It consists of an input layer that takes external data and transmits it to the network for learning. The layer between the input and output layers is hidden. It can learn things and store the results of different learning methods in the output layer as shown in Figure 5.

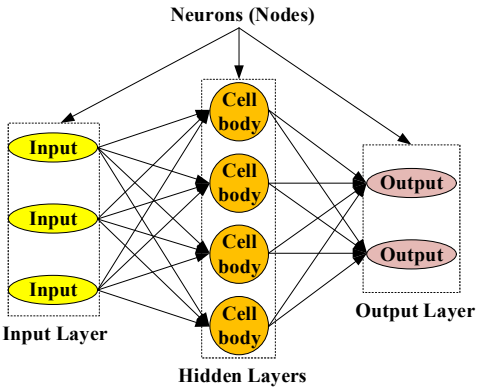

Figure 5 Typical architecture of a neural network

3.2 Neural Networks to Solve Problems

Most problem variables are inputs, weights, and outputs with examples (training data) that identify a problem that can be solved, e.g., Input and output are known. For training purposes, various algorithms can be used to find a set of weight matrices that should match the correct output when applied to any input network. In the learning process, it uses a gradient algorithm for training. It's a simple training algorithm. What is used in the case of supervised training simulation schemes can change the weight of the network, including reducing the error value. Propagation is an extension of the delta gradient learning rule after an error has occurred. The Back-Propagation Neural is one of the error learning algorithms based on the principle of backpropagation. With back-propagation from the output layer to the input layer through a hidden layer. The delta learning rule based on gradients was used to adjust the weights for each error learning. For each weight adjustment, the weights that precede the output layer are adjusted first. Then actually follows the adjustment of the weight on the back of the input layer.

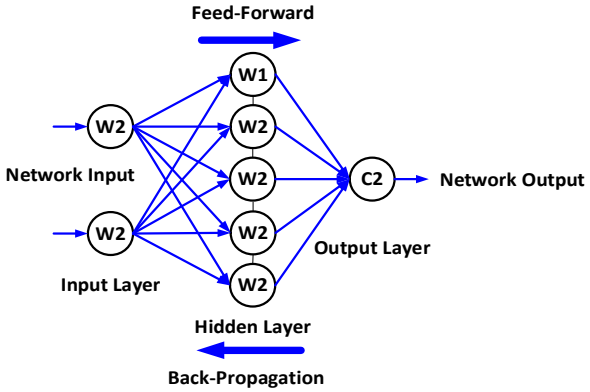

Figure 6 Typical backpropagation architecture of neural networks

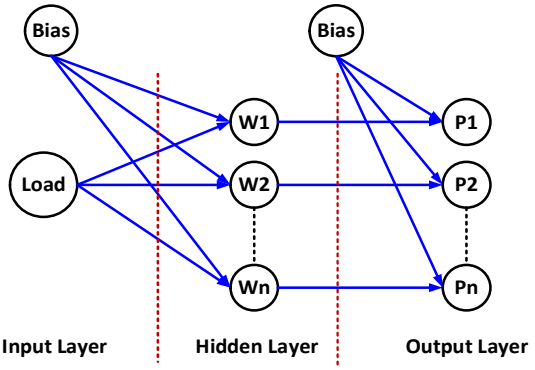

Figure 7 Backpropagation architecture for neural networks to compute power generation

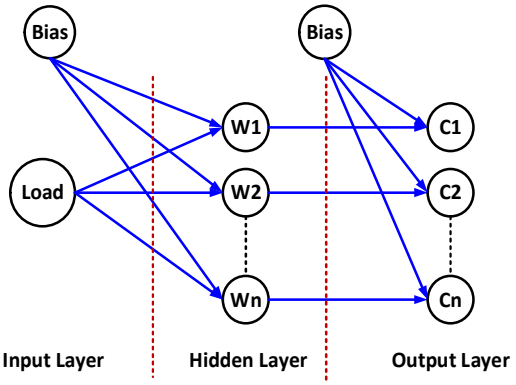

Figure 8 Backpropagation architecture for neural networks to calculate electricity generation costs

Fig. 5 and Fig. 6 are neural network designs for calculating the sum of power generation and the sum of cost generation.

4. Data Collection for Training

4.1 Cost Function Configuration

Figure 4 demonstrates the procedure for determining the variable parameters of the quadratic function of power generation cost function for each power plant. First, the existing power plants in the Central-1 region network of EDL were modeled in the Power World Simulator. The model of the system is then simulated in an optimal power flow. Then power flow and power loss are analyzed. Finally, the cost function of each power plant (ai, bi, ci) is analyzed using the Excel function after simulating the coefficients of the hydropower plants using the Power World Simulation program and the Excel function. The cost function parameters (ai, bi, ci) for each plant are presented in Table 3 and Table 4

Figure 7 and Figure 8 show that there is an input in the input layer that feeds into the networks, resulting in 10 outputs of 32 neutrons. Where both networks use the same input as the load. The output in Figure 7 represents the electricity generation from 10 power plants and Figure 8 represents the costs of generation.

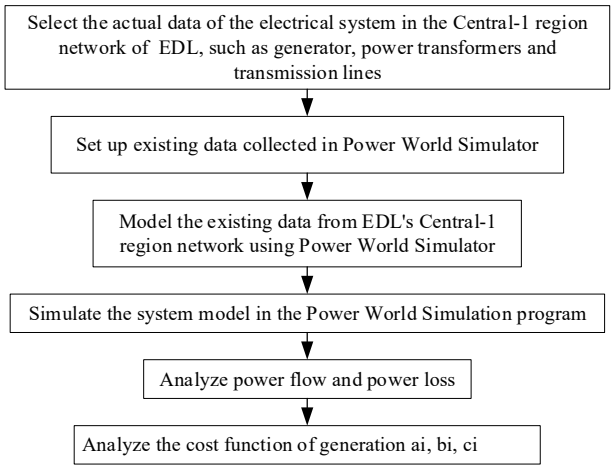

Figure 9 The procedure for calculating coefficients using Power World Simulation Software.

Table 3 Cost coefficients of electricity generation from 10 power plants in the Central Region 1 network

Generation Name	Coefficient of the power generation cost		
	a ($/h)	b ($/MWh)	C ($/MW²h)
Nam Ngum1	441.35	54.1360	0.0086
Nam Leuk	642.60	54.3790	0.0200
Nam Mang3	775.26	52.6390	0.0192
Nam Lik1-2	328.51	48.8930	0.0159
Nam Ngum5	348.51	47.6350	0.0204
Nam Ngiep2	545.86	58.6530	0.0174
Nam Phai	611.33	59.8610	0.0194
Nam Chien	583.34	68.0540	0.0255
Nam San3A	390.14	73.6690	0.0325
Nam San3B	833.84	72.2920	0.0264

Since the cost of production is a condition of this research that must be taken into account. Therefore, the tar values of 10 power plants are defined as shown in Table 5 below.

Table 4 Generation limits of 10 power plants in the Central-1-region network

Generation Name	The Limit of generation	
	Min (MW)	Max (MW)
Nam Ngum1	15	155
Nam Leuk	20	60
Nam Mang3	10	40
Nam Lik1-2	20	100
Nam Ngum5	20	120
Nam Ngiep2	20	180
Nam Phai	15	104
Nam Chien	15	86
Nam San3A	15	70
Nam San3B	10	45

Table 5 Existing tariffs of 10 power plants in the Central-1 region network

No.	Hydro Power Plant	Tariff ($/kWh)
1	Nam Ngum1	0.0533
2	Nam Leuk	0.0533
3	Nam Mang3	0.0533
4	Nam Lik1-2	0.04822
5	Nam Ngum5	0.04729
6	Nam Ngiep2	0.05800
7	Nam Phai	0.05330
8	Nam Chien	0.06800
9	Nam San3A	0.07320
10	Nam San3B	0.07320

4.2 Process of conducting research

First of all, it is necessary to collect the data from power, generation, and transmission systems in the EDL network of the Central-1 region to analyze variables using the Power World Simulator program. Then apply the results to the neural network training. Which details are as follows as Figure 10

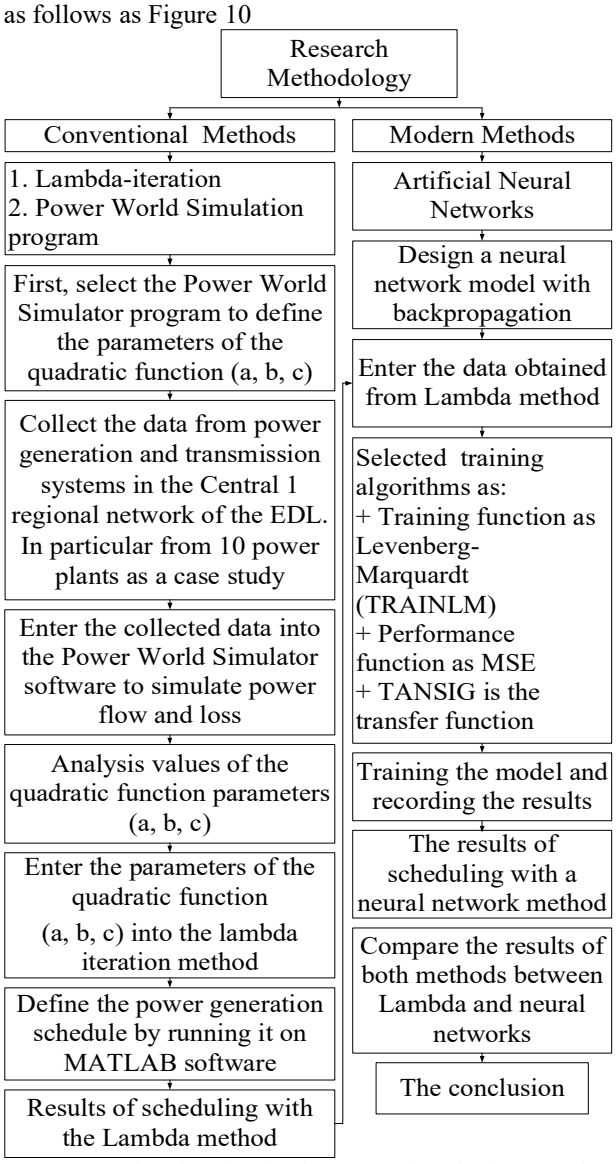

Figure 10 Flow chart showing the process of conducting research

5. SIMULATION RESULTS

Parameters of the quadratic cost function (1) as a, b, c are calculated in the lambda iteration method regardless of transmission line losses and any faults in the power plant. Consider calculating 10 power plants in the Central-1 region network using MATLAB R2018b (9.5.94). First, it is calculated with the lambda method, then the result is calculated in the neural network. Finally, compare the results of both methods with each other as the results are shown in Table 8. This is divided into two training parts. Start the training by entering the data obtained from the Lambda iteration method into the model designed in the MATLAB program and start the model training process. After completing the training process, the result is the power of each power plant PGn (MW). The second part of the training state is the load demand and production cost data. It is obtained from the lambda iterative method. Both are fed into the model in the MATLAB program as input and output data after the training is complete. The result obtained is the cost ($/kWh) as shown in Fig. 5 and Fig. 6. Next comes the explanation of the symbols, e.g., PGn represents the power production of n plants by the Lambda iteration method, and Cost PGn cost represents the production costs of n plants by the neural network method.

The aim of this paper is that the total cost of generation must be as low as possible and the total output must be maximum. The simulation results are as follows. The overall performance with the Lambda Iteration method is lower than that of the Neural Network method (PG < PGn) and the total cost of generation with the Lambda Iteration method is higher than that of the Neural Network method (Cost > Cost PGn) with a load of 160 MW to 960 MW. While the power of generation changes according to the changing load.

The neural network method took 108 seconds to calculate and the lambda iteration method took 528 seconds to calculate. Shows the difference between both methods. This can be summarized as follows: the neural network method is faster than the lambda method. Executed on a single computer by a 64-bit version of MATLAB R2018b. Processor: Intel(R) Core (TM) i5-8300H CPU @ 2.30 GHz; Installed RAM: 8 GB operating system

For back-propagation networks, the training algorithms are selected as the type, Levenberg-Marquardt (TRAINLM) is a training function, MSE is a performance function, and TANSIG is the transfer function. Next, show the detailed parameter settings and the results of running the models

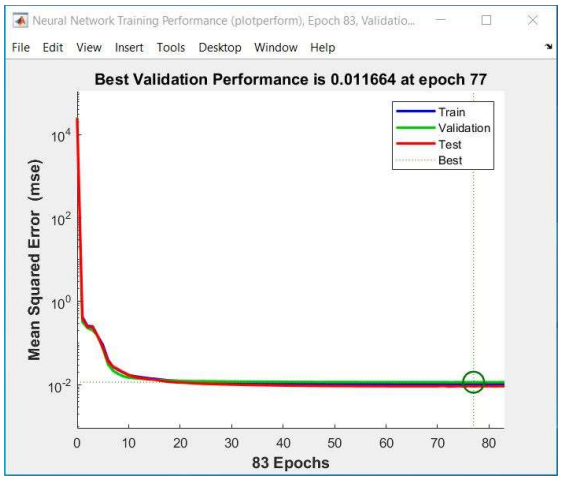

Figure 11 Training performance

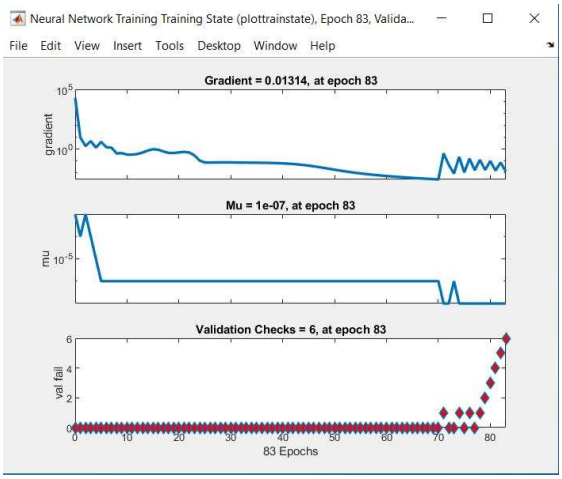

Figure 12 Training state

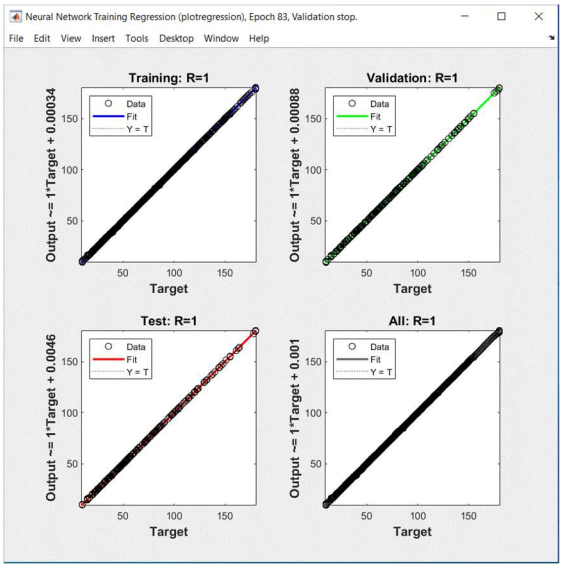

Figure 13 Training regression

For the training process ended at 83 epochs within 108 seconds. The results are shown in Tables 5 and 6.

Table 6 Simulation results of the power generation in neural networks ($P_{G1} - P_{G5}$)

Load	PG1	PG2	PG3	PG4	PG5
160	15.00	20.00	10.00	20.48	20.70
200	15.00	20.00	10.00	27.73	52.22
260	15.00	20.00	10.00	61.31	78.60
300	15.01	20.00	9.97	83.80	96.17
360	14.66	19.96	30.40	100.03	120.05
400	45.04	19.77	40.21	100.00	120.01
600	155.02	60.01	40.00	100.00	120.00
660	155.00	60.00	40.00	100.00	120.00
700	155.00	60.00	40.00	100.00	120.00
760	155.00	60.00	40.00	100.00	120.00
800	155.00	60.00	40.00	100.00	120.00
860	155.00	60.00	40.00	100.00	120.00
900	155.00	60.00	40.00	100.00	120.00

Table 7 Simulation results of the power generation cost in neural networks ($P_{G6} - P_{G10}$)

Load	PG6	PG7	PG8	PG9	PG10
160	20.00	15.00	15.00	15.00	10.00
200	20.00	15.00	15.00	15.00	10.00
260	20.00	15.00	15.00	15.00	10.00
300	20.00	15.00	15.00	15.00	10.00
360	20.00	15.00	15.00	15.00	10.00
400	19.99	15.00	15.00	15.00	10.00
600	61.27	23.69	15.00	15.00	10.00
660	92.81	52.12	15.00	15.00	10.00
700	113.88	71.02	15.00	15.00	10.00
760	145.52	99.40	15.03	15.00	10.00
800	178.99	103.84	17.00	15.00	9.97
860	179.95	103.99	76.30	15.06	9.66
900	180.00	104.00	85.87	15.02	40.26

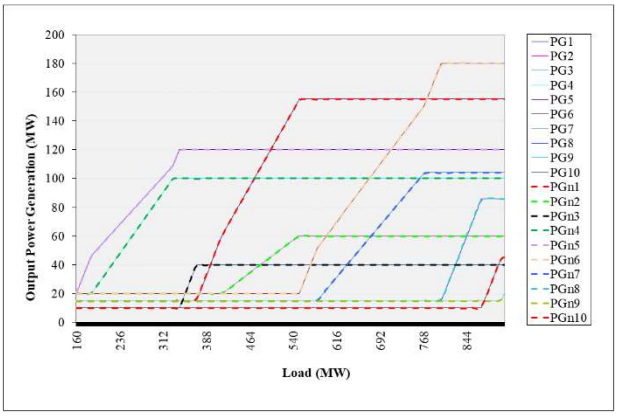

Figure 14 The results of the total power generation using the Lambda iteration method and the neural network for 10 power plants in the Central-1 regional network

The results of both methods can be summarized as shown in Table 8

Table 8 Compare the results calculated by the neural network with the Lambda method calculation

Methods	Total Power Generation (MW)	The total cost of the generation ($/h)	Time (s)
Lambda iteration	448,560	29,664,071.99	528
Neural Network	448,567	29,663,499.09	108
Difference	7.00	-572.90	420

demonstrated the hydroelectric power generation schedule using the neural network method. Both methods deliver different power, so the neural network method can generate one more power generation than the lambda method up to 7 megawatts, saving the capital cost of generation to $572.90/hr. At 420 seconds, the computing time of the neural network is less than lambda iteration.

The results of this study show that the papers refer to are consistent, which is evident in many fields, such as the application of neural networks to forecast electricity demand, forecast electricity supply adequacy, forecast water inflow, forecast precipitation, forecast power plant generation that is used to planning, and is a factor in the decision-making of human who is more positive.

6. Conclusion

This paper presents a guideline for power generation scheduling of 10 power plants in EDL's Central-1-Region network by applying a neural network to train the model based on the data from these power plants using feedforward and backpropagation algorithms running. It was developed to calculate the results according to the neural network architecture designed in MATLAB. The results obtained from the neural network method are compared to the results from the lambda method to determine feasibility. As the results showed, the neural network method provides slightly more satisfactory results than the lambda method, resulting in less computing time and higher productivity due to the neural network method. All work on the theory of optimal dispatch problems, the aim is to find the most suitable methods to minimize production costs and maximize power production. This paper discusses how to use MATLAB's powerful tools to design a model based on the desired architecture and demonstrates the feasibility of using this technique. This applies to optimization tasks in power plants in areas such as storage inflow forecast, storage management, which can also be precipitation forecast, and numerous power generation. The neural network is a simple calculation method and saves calculation time. It can also be used, as a tool to cut off the color of works, which is an alternative that draws a lot of attention.

7. ACKNOWLEDGEMENT

I would like to thank the cooperation project EGAT-CMU for making the master's degree in energy possible. Especially in the technical and academic cooperation projects between EGAT and EDL. Another with EDL Generation Public Company Limited. Which supported this research fund.

8. REFERENCES

Estoperez, N., & Nagasaka, K. (2006). An artificial neural network-based micro-hydro power generation scheduling: considering demand profile and environmental impact. Clean Technologies and Environmental Policy, 8(2), 123-130.

EDL. (2020, October 29). Annual Report 2019. http://www.edl.com.la/file_post.php?id=12

Naresh, R., & Sharma, J. (2000). Hydro system scheduling using the ANN approach. IEEE Transactions on power systems, 15(1), 388-395.Electrical Engineering of Riga Technical University (RTUCON), pp. 1-6. IEEE, 2016.

Sauhats, A., Petrichenko, R., Broka, Z., Baltputnis, K., & Sobolevskis, D. (2016, October). ANN-based forecasting of hydropower reservoir inflow. In 2016 57th International Scientific Conference on Power and Electrical Engineering of Riga Technical University (RTUCON) (pp. 1-6). IEEE.

Dogra, R., Gupta, N., & Saroa, H. (2014, January). Economic load dispatch problem and Matlab programming of different methods. In International conference of advance research and innovation (ICARI-2014).

Arora, I., & Kaur, M. (2016, November). Unit commitment scheduling by employing artificial neural network-based load forecasting. In the 2016 7th India International Conference on Power Electronics (IICPE) (pp. 1-6). IEEE.

Suman, M., Rao, M. V. G., Hanumaiah, A., & Rajesh, K. (2016). Solution of economic load dispatch problem in power system using lambda iteration and backpropagation neural network methods. International Journal on Electrical Engineering and Informatics, 8(2), 347.

Liang, R. H., & Hsu, Y. Y. (1994). Scheduling of hydroelectric generations using artificial neural networks. IEE Proceedings-Generation, Transmission, and Distribution, 141(5), 452-458.

Tufegdzic, N. (1997). Optimal scheduling and dispatch for hydroelectric generation (Doctoral dissertation, University of Tasmania).

Kilinç, I., & Ciğizoğlu, K. (2012). Reservoir management using artificial neural networks. 14th. Reg. Directorate of DSI (State Hydraulic Works), Istanbul, Turkey.

Shadaksharappa, N. M. (2011). Optimum generation scheduling for thermal power plants using artificial neural network. International Journal of Electrical and Computer Engineering, 1(2), 134.

Dike, D. O., Adinfono, M. I., & Ogu, G. (2013). Economic dispatch of generated power using the modified lambda-iteration method. IOSR Journal of Electrical and Electronics Engineering, 7(1), 49-54.

Saeed, I. K. (2019). Artificial Neural Network Based on Optimal Operation of Economic Load Dispatch in Power System. Zanco Journal of Pure and Applied Sciences, 31(4), 94-102.

Imen, L., Mouhamed, B., & Djamel, L. (2013, November). Economic dispatch using classical methods and neural networks. In 2013 8th International Conference on Electrical and Electronics Engineering (ELECO) (pp. 172-176). IEEE.

NUEJ
Naresuan University
Engineering Journal

The Concept of Participatory Urban Management Using Web-based SDSS

Gen Long[1,*] and Sarintip Tantanee[2]

[1]Civil Engineering Department, Faculty of Engineering, Naresuan University 65000 Thailand

[2] Center of Excellence on Energy Technology and Environment, Faculty of Engineering, Naresuan University, Thailand

[*]Corresponding author e-mail: genl63@nu.ac.th

(Received: 31 January 2021, Revised: 7 April 2022, Accepted: 19 April 2022)

Abstract

Decision Support Systems have been popular in the field of information studies, but one of their significant drawbacks is the inability to consider geographical and temporal data. Many decision issues in the real world are spatially related problems, as a result, in recent decades, the Spatial Decision Support System has been a surge in academic interest which integrates Geographic Information Systems with DSS. However, these SDSSs have been seen as centralized, bureaucratic, and top-down techniques implemented by municipal planning offices, authorities, and other stakeholders in urban management. There is a growing demand for participatory urban management that can provide an interactive, open, democratic, communicative, group-based, and informed deliberation process that includes both experts and non-experts. The rapidly evolving Internet has the potential to overcome this limitation, the Web-based SDSS provides the flexibility for working in different places, participants' time convenience, and equal opportunities for participation. The objective of the study is to propose a concept of participatory urban management using Web-based SDSS that is built for all aspects of urban management participants in peacetime, moreover, which can be transformed as a useful disaster response tool when dealing with disasters situation. The result shows the adoption of this system only can optimize and facilitate urban management, but it was also found that participatory urban management and disaster management are somehow linked, and their functions are overlapped, their integration can realize the benefits of cost-saving and flexibility, help to increase the performance of urban governance and improve cities' capacity and resilience to disasters.

Keywords: Decision Support System, Spatial Decision Support System, Web-based Spatial Decision Support System, Participatory Urban Management, Web-based SDSS, Urban Management, Disaster Management

1. Introduction

One of the most difficult challenges of the twenty-first century is urban management. Cities, if efficiently managed, may operate as growth engines, providing residents with more work possibilities, better healthcare, housing, safety, and social development (Avis & R, 2016). The Decision Support System (DSS) is a computerized information system that has been proved as a valuable tool for municipal authorities and organizations at the management, operations, and planning levels, assisting them in making early decisions. However, a key shortcoming of DSS is its inability to consider spatial and temporal data (Sugumaran & Sugumaran, 2007). While Geographic Information System (GIS) has the potential to reduce the restriction of DSS. The GIS-based SDSS is a framework for integrating database management systems to analytical models, graphical presentation and tabular reporting capabilities, and the expertise of decision-makers (Ghavami, 2019). Spatial Decision Support System (SDSS) has been applied to a variety of industries, including agriculture, business, energy, firefighting, land planning, site selection, transportation, water resource management, disaster management (DM), etc. These techniques, on the other hand, have typically been characterized as centralized, bureaucratic, and top-down approaches implemented by municipal planning offices, authorities, and other stakeholders (Figure 1a). They have been criticized for not being able to solve

complicated decision-making problems, engage various stakeholders, or democratize the planning process effectively. Previous research has found that communal geographical decisions are more successful than individual ones, implying that the spatial decision-making paradigm should shift away from traditional ways and toward a holistic, participative, communicative, and collaborative approach (Jelokhani-Niaraki, 2018). Thus, in urban management and planning, the use of collaborative/participatory approaches is recommended, because they can facilitate an interactive, open, democratic, communicative, group-based, and well-informed deliberative process in which experts and non-experts discuss, negotiate, and generate solutions (Figure 1b) (Jelokhani-Niaraki & Malczewski, 2015).

Figure 1 The disadvantages of traditional SDSS (a), and the advantages of WebSDSS (b)

The fast development of computers, the Internet, and especially World Wide Web (WWW) technology has had a significant impact on architecture, landscape architecture, and urban planning education and practice during the past decades. The ability to overcome constrained resources in terms of time, data, and communication is one of the most significant advantages of employing web services in spatial decision-making. Web-based SDSS (WebSDSS) is a Web-based GIS and DSS integration solution that not only allows participants to work in multiple locations and at different times to suit their needs, but also gives equitable possibilities for participation (Jelokhani-Niaraki & Malczewski, 2015). Individual decision-maker's decision time was shortened and the accuracy was increased by using GIS as a component of SDSS (Herold et al., 2005).

At the same time, rapid urbanization and population expansion have exacerbated environmental issues such as resource depletion, global warming, and environmental devastation. Development has increased the occurrence likelihood of natural disasters (Jung & Jung, 2019). Thus, DM should be considered as one of the most important components of urban management. Apart from this perspective, the impact that a disaster occurs in urban areas can be much more severe than in rural areas, due to the high population density and centrally distributed infrastructures. Many disaster losses are predictable to a certain extent, making them manageable to some extent (Abdalla, 2016). Thus, it can be seen that DM plays a significant role in strengthening a city's resilience to both foreseeable and unforeseeable disasters that happen in urban areas.

The Internet can enable the communication of disaster-related information/data and has a tremendous influence and is now being utilized across the DM process. Using the Internet to establish a simple, user-friendly, GIS-based system would allow decision-makers in developing countries to access and adopt data and technologies that they would not otherwise have access to or be competent to use. Access to GIS technology will boost local capacity for DM and minimize dependency on international aid because accessibility is a precondition for utilization (Herold et al., 2005).

Through a comprehensive literature review, by utilizing the advantages of DSS, GIS, and Internet, as well as to realize a better urban management mode, in which DM elements can be considered, the objective of the study is to propose the concept of participatory urban management using Web-based SDSS (PWebSDSS) that is built for involving all aspects of urban management participants in peacetime, moreover, which can be transformed into a useful disaster management tool when dealing with disaster situations. It should be noted that the DM part of the proposed PWebSDSS in this study is

designed for general disaster situations and it is still in the initial conceptual stage, due to the different data needs of different disasters as well as due to different factors in different countries including population distribution, socioeconomic characteristics, and resource bases, the actual detailed components and functions may also differ.

The rest parts of this paper are organized as follows: Section 2 describes the literature review on this topic. Section 3 illustrates the design of the proposed PWebSDSS. Section 4 discusses the value, deficiency, as well as future work of the study. A conclusion is made at the end of this paper.

2. LITERATURE REVIEW

2.1 Development of SDSS

SDSS combines two technologies: decision support system (DSS) and geographic information system (GIS). DSS has several shortcomings, one of which is its inability to process spatial data. GIS, on the other hand, is adept at storing and managing geographical data but falls short in decision-making and collaborative problem-solving issues. SDSS is divided into two streams: geospatial information-based systems and decision support-based systems. Figure 2 depicts a schematic illustration of the SDSS development process.

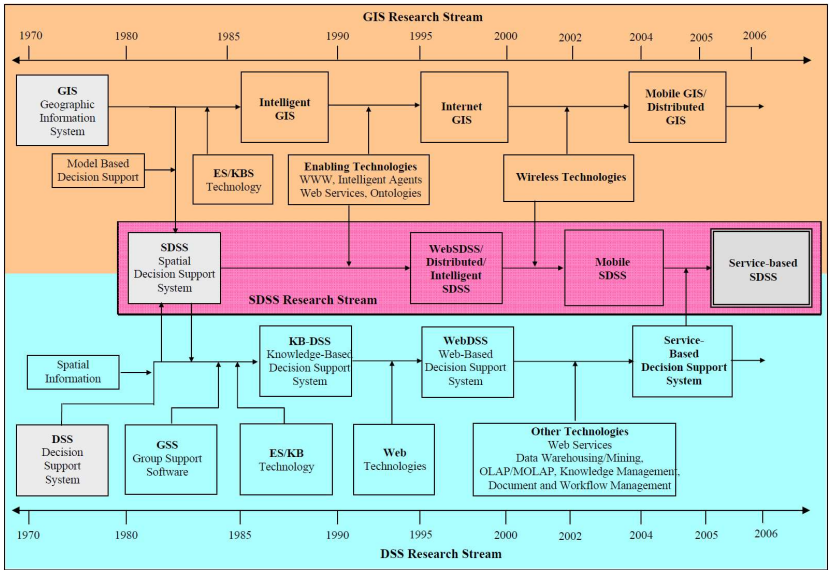

Figure 2 Progression of Spatial Decision Support Systems Development (Sugumaran & Sugumaran, 2007)

2.2 Decision Support System

According to Mohd et al. (2014), a DSS is a collection of tools and processes that work together to manage a certain system. Making decisions in a dynamic and fast-changing environment is difficult because multiple aspects are involved, including the decision-maker, conflicts of interest, the importance of the decision, the various criteria involved in the problem, and so on. It can optimize the decision-making processes in the system. In the face of complicated, uncertain, and contradicting situations, it has been frequently employed (de Lima et al., 2019).

Decision support can be described as the assistance for, substantiation and corroboration of an act or result of the decision. The following requirements should be met by DSSs:

1) Intended for the solution of semi-structured issues

2) Has the ability to combine analytical models with standard data and retrieval functions

3) Accessible and user-friendly for decision-makers with fewer computer skills

4) Adaptable to a variety of decision-making processes (Yatsalo & Sullivan, 2012).

The following are the components of a typical DSS framework:

1) Capabilities in analytical modeling

2) Database management systems

3) Graphical representation

4) Tools for reporting

5) The knowledge of the decision-maker (Oliveira et al., 2012).

2.3 Spatial Decision Support System

SDSS, the same as DSS, is designed to handle semi-structured spatial issues. It is developed from DSS by adding geographical elements. In addition to the aforementioned features of DSSs, SDSSs provide functions and tools for processing and analyzing spatial/geographic data. As a result, SDSS assists decision-making in terms of spatial alternatives analysis by integrating GIS functionalities with DSS tools for stakeholders (Yatsalo & Sullivan, 2012). In certain circumstances, the information is stored in a database like tables, and the linkages between the tables and locations are not visible. GIS allows us to see spatial data by attaching attribute information from tables to a geographic location (Sreekanth et al., 2021). SDSSs are often designed to give a decision-making environment that allows for the flexible analysis of both geographical and attribute components (Mansourian et al., 2011). The SDSS enhanced decision-making and is useful in areas with a significant spatial component, such as planning, monitoring, and assessing delivery, evacuation, intervention coverage, site selection, and accountability (Wangdi et al., 2016). SDSSs have been used in a variety of fields, including flood risk management, seismic catastrophes, infrastructure development, and public education management (de Lima et al., 2019). SDSSs can be used in disaster response to identify the best sites for rescue workers, plan evacuation routes, and assign evacuees to shelters (Nyimbili & Erden, 2017).

A SDSS combines GIS features including geographical data management and cartographic presentation with analytical modeling, a user interface that can be customized, and complicated geographical data structures. It provides the framework for integrating:

1) the ability to model spatially and analytically
2) handling of geographical and non-spatial data
3) domain knowledge
4) spatial display functions
5) Capabilities for reporting (Sugumaran & Sugumaran, 2007).

2.4 Web-based Spatial Decision Support System

Web-based SDSS has been suggested as a useful tool for participatory/collaborative/group spatial planning and decision-making (Jelokhani-Niaraki, 2018). Given the collaborative nature of many decision-making problems, by promoting information/knowledge exchange as well as software and model sharing, a participatory decision-making process is becoming more crucial for resolving conflicts and lowering uncertainty in spatial planning and decision-making (Mansourian et al., 2011). When a large number of people and a diverse group of stakeholders are involved in decision-making, the Internet can be considered as a desirable medium for communication between the public and urban planners (Mansourian et al., 2011). The challenge of transmitting geographical data in real-time has taken on a new dimension with the recent use of web services for various GIS applications (Sreekanth et al., 2021). Web technologies open up new opportunities for using SDSS in a participatory environment, allowing the traditional SDSS to evolve from a closed, place-based (time and location fixed) and synchronous process to an open, asynchronous, dispersed, and active process (Jelokhani-Niaraki, 2018). What the users need to access a WebSDSS is only a web browser that is installed originally on any PCs or mobile devices (e.g., PDA, smartphones). This revolution leads the transformation of decision-making from only individual data browsing, analyzing, and managing, to the group's participation and communication on scientific as well as social decision-making concerns (Mohd et al., 2014).

WebSDSSs have several advantages over stand-alone desktop systems, including platform independence, cost-saving, reduced maintenance complexity, simplicity of use, global data sharing, group discussion assistance, as well as more public accessibility in the decision-making processes (Yatsalo & Sullivan, 2012). Additionally, in the traditional way, citizens and permit applicants must visit the municipality office to submit their applications and track their progress. Therefore, the creation of a WebSDSS can help municipalities in making the transition from traditional urban planning and administration to an online public participatory spatial planning process (Mansourian et al., 2011).

2.5 Urban Management

There is no general definition for the urban management concept, perception of people and political-social demands also differ in different eras (Mahmudi & Saremi, 2015). Urban management is not only the administration of local government but also the management of human settlement activities. It comprises resources management, development, public services, urban growth, and any other partial urban concern (Mattingly, 1995). Urban management as an organizational framework, the governance, urban development, policymaking, projects, plans and

operations, and also citizens' access to services and infrastructure, housing, and employment are concerned (khazaee & Razavian, 2012). To sum up, the general content of urban management is shown in Figure 3.

Figure 3 The general content of urban management

The term "urban management" refers to the process of implementing, coordinating, and evaluating integrated strategies with the guidance of city authorities, whilst also taking private sector objectives and citizen benefit into account, has the main goal of approaching sustainable economic development potential (Mahmudi & Saremi, 2015). In addition, according to Avis and R (2016), urban management:

1) Has a significant impact on the physical and social character of urban areas

2) Has an impact on the quantity and quality of local services as well as delivery efficiency

3) Determines how costs are shared and resources are distributed among various groups

4) Impacts citizens' capacity to engage in decision-making and access local government, impacting local government accountability and responsiveness to community demands.

2.6 Participatory Urban Management

Democratization means an increase in citizen participation in public affairs, citizen participation in urban management is one of the core values of a democracy (Mahmudi & Saremi, 2015). Participation of associated and non-associated citizens in the development, implementation, and/or evaluation of public policy aims to improve democratic governance by reducing citizen distrust of elected officials and providing more effective responses to broader community needs (Falanga, 2020). In urban management, participation can be described as the cooperation between private sectors and municipalities (Mahmudi & Saremi, 2015). Without empowering the municipality to assume full responsibility for planning its jurisdiction in a democratic and responsible framework, as well as coordinating with other authorities, urban planning and management operations will not be effective (Mansourian et al., 2011).

Different areas of expertise and stakeholders with varying levels of knowledge are required for urban planning and management activities. They represent their unique experiences, which results in diverse perspectives on desirable planning outcomes (Mansourian et al., 2011). Participants range from specialists to novices in defining decision knowledge and using spatial decision support tools, with varying levels of competence, experience, subject knowledge, and analytical ability. Due to a lack of expertise and self-doubt, novices' actions are influenced by the presence of others' perspectives within the group. Individual decision-makers need to exchange knowledge for participatory/collaborative urban management to be effective (Jelokhani-Niaraki, 2018).

Urban management should be based on the principles that create the fundament of the structure. These principles can be summed up as follows:

1) Civility in cities and citizen education

2) Consistent citizen polling

3) Norms for informing and directing citizens that are codified

4) Gaining the trust of the public and private sector

5) Assessing and correcting the activities that have already been completed (Mahmudi & Saremi, 2015).

2.7 Disaster Management and Urban Resilience

Disaster management (DM) is a strategy for increasing resilience and, as a result, preventing or mitigating the effects of natural disasters. Thus, DM is characterized as an ongoing process that consists of a series of activities that occur before, during, and after an incident and is divided into four key phases: disaster mitigation, disaster preparation, disaster response, and disaster recovery (Figure 4) (Herold et al., 2005; Horita & Albuquerque, 2013). Although there is growing recognition that these actions greatly overlap, preparedness and mitigation are regarded as pre-disaster activities, while response and recovery are considered during and post-disaster activities, respectively. Some recovery actions may occur at the same time as response efforts (Nyimbili & Erden, 2017).

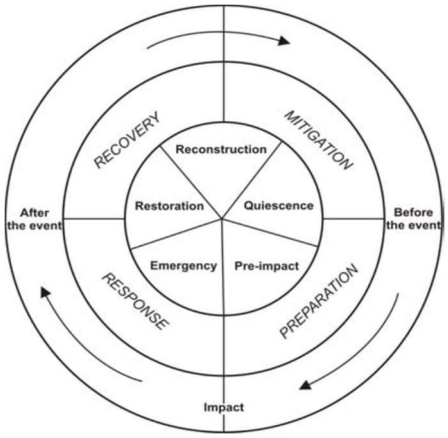

Figure 4 Disaster management cycle (Herold et al., 2005)

DM plays a critical role in enhancing the power of urban resilience, i.e., improving the community's capacity to resist or adapt to extreme events and disasters, as the frequency and magnitude of catastrophic events and disasters increase, which are influenced by climate change (Horita & Albuquerque, 2013).

Assimilation and transmission of real-time information/data to diverse decision-makers are required for effective DM. The usage of GIS and remote sensing technology can greatly assist this process (Herold et al., 2005). To respond quickly to extreme events, emergency managers must make important decisions quickly. It is critical for policymakers to have the proper knowledge at the right time to react, plan, or mitigate disasters (Abdalla, 2016). The goal of disaster response in humanitarian relief chains is to give immediate relief to disaster-affected communities in order to reduce human death and suffering (Barzinpour & Esmaeili, 2013). Many relief measures for disasters from previous studies emphasize the importance of fast response, which basically relies on accessibility to the Internet and communication.

Furthermore, the establishment of a rescue command center, the collecting of information/data about the affected region, the identification of optimal shelter places, the selection of the best evacuation routes, vehicles for evacuation, the delivery of relief items, the installation of medical and fire prevention stations, and emergency construction facilities would all be major responsibilities of DM for urban areas. As a result, DM plans should cover the location of emergency bases and the distribution of relief supplies (Barzinpour & Esmaeili, 2013). DM requires the involvement of various ministries and departments (Madan & Routray, 2016). Apart from the city authorities and organizations, the participation of the public/citizens can have a significant role in this procedure. For example, by adopting the proposed PWebSDSSs, the public/citizens/victims can provide valuable data such as their accurate position coordinates, the casualties and site photos of the disaster area, their rescue and relief material needs, etc. These participatory and proactive means help to improve the DM efficiency as well as reduce the workload of rescue teams. The PWebSDSS can also be useful tools in the DM processes in urban areas. It could include modules for planning, monitoring, and assessing the delivery and coverage of interventions. For example, it can help to build indoor residual spraying and the distribution of long-lasting insecticidal nets to target populations, collecting spatial distribution data of infection cases, vaccinated population, etc.

3. DESIGN OF THE PARTICIPATORY URBAN MANAGEMENT USING WEB-BASED SDSS

Through the above comprehensive literature review in this paper, by analyzing and combining the advantages of DSS, GIS, Internet, participatory management as well as its overlapping nature with disaster management, in this part, we propose a Participatory WebSDSS (PWebSDSS) platform which is designed to establish a participatory method for mobilizing municipal resources and facilities, meeting the requirements of citizens, control and manage the urban area, as well as consider the DM aspects in urban management, then ultimately achieve sustainable urban management. This process and the benefits of the proposed PWebSDSS are shown in Figure 5.

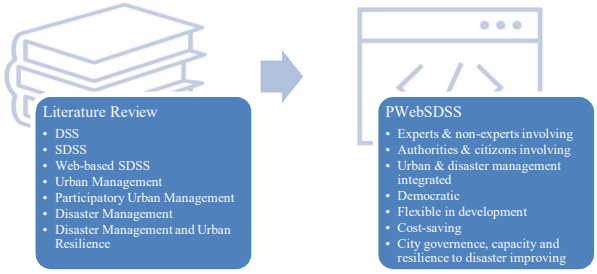

Figure 5 The design process of the proposed PWebSDSS

3.1 Participatory Urban Management Process

In the participatory urban management, for example, a permit applicant like a construction company could query the application process, download and upload the application forms directly from the platform, to save their time and reduce human touch, which shows a necessity, particularly during a disaster situation like Covid-19 pandemic; a citizen could also report the infrastructure failure, pollution area, uncivilized behavior by filling online forms, attaching the spot coordinates (automatically acquired from mobile devices), photos, contact number, and other information to the urban manager. The deployment of the "editing on map" function is an essential characteristic of our system. This enables the development of spatial features (points, polylines, and polygons) on the map, as well as the correlation of specific attributes with these features, and keeping the server-side database up to date. For example, a user could draw on a map or collect an area from mobile phones to establish a distribution center for critical supplies such as medicines, food, and water; or input a point or automatically acquire it from devices, along with a note describing how specific infrastructure, such as a collapsed house, has been affected by the disaster. Allowing users to dynamically update maps with updated data/information can improve the ability to give critical geographical information in a usable way to those who need it most (Herold et al., 2005).

3.2 Disaster Management Process

The system can be updated to bi-functional systems by developing the additional DM sub-system based on the original PWebSDSS. This integration approach has many benefits:

1) The involvement of public participants in their daily life can increase their accessibility, familiarity, interests, and dependence on the platform, accordingly, gaining a large number of local users

2) It can improve the efficiency of both urban management and disaster management role of the platform, due to the shared database that avoids repetitive data collection, the DM process can also feedback to the regular urban management role, to increase the city's capacity and strengthen its resilience

3) It can save costs in both development and maintenance processes, due to their functional overlap and the shared webserver

4) The dynamic transformation makes full use and improves the survivability of the platform, so as not to be idle or abandoned after the disaster relief works end.

In the regular urban management system, the general decision makers' role and their possible achieving means are set as follows:

1) Development and operation plan – online/electronic form, voting system, online/electronic map

2) Resource management – tasks allocation, online/electronic map, the query system

3) Policymaking – online/electronic form, voting system

4) Public service – forum, query system, online/electronic map, navigation system

5) Projects management – supervision system, online/electronic form, online/electronic map, volunteer recruitment

6) Publicity and education – manual, video, message.

Accordingly, the possible roles of the public participants and the activities they may participate in could be:

1) Development and operation plan – submit forms, vote, provide map features

2) Policymaking – submit forms, vote

3) Public service – discussion and suggestions, query, use maps, navigation

4) Projects management – report pollution and violations, view maps, register for volunteer

5) Publicity and education – online learning, receive notifications.

The possible roles of the permit applicants (such as construction companies) and the activities they may participate in could be:

1) Resource management – accept a mission, view maps, query

2) Projects management – self-inspection, submit forms, view maps, coordinate volunteers

3) Public service – complaint, query, use maps, navigation.

According to their working nature, the government departments could be flexible and may be involved in any of the activities, their main role is to partake and execute tasks from the decision-maker or other superiors, or sometimes coordinate between departments.

There are many possibilities for the design of the DM sub-systems, according to the category of the disasters, different disasters have different management modes and relief objectives, accordingly, different functions and data are required.

In the sub-system, the command center is designed instead of the decision-maker as the core role and its possible modules and functions are set as follows:

1) Risk management – risk alarm, online/electronic hazard map, query system, manual, video

2) Relief management – online/electronic form, online/electronic map, volunteer recruitment, supervision system

3) Victim service – query system, online/electronic hazard map, online/electronic form, navigation system.

Accordingly, the possible activities the citizens may participate in could be:

1) Risk management – receive alarms, view hazard maps, query, online learning

2) Relief management – submit forms, use hazards maps, register for volunteer, report risks

3) Victim service – query, use hazard maps, report relief materials requirement, navigation.

Likewise, the main role of government departments is to partake and execute missions from the command center and coordinate between departments and also collaborate with non-government organizations (NGO), which, in the relief works, are mainly responsible for mobilizing donations and volunteers' arrangement jobs.

4. RESULT AND DISCUSSION

The proposed PWebSDSS integrated the DSS, GIS, and Internet (Web) environment, and aims to realize the main goal of sustainable economic development in modern urban management. By adopting the proposed PWebSDSS, the assisting role of the DSS for municipal authorities and organizations in urban management is optimized by introducing GIS, which can solve the drawback that the DSS cannot take spatial-temporal data into account. Meanwhile, the Web technology enabled the possibility of the participatory/collaborative urban management mode, in which both experts & non-experts, authorities & citizens can be involved in realizing a more effective, accurate, and democratic urban management. The proposed PWebSDSS in this study is designed for involving all aspects of urban management participants in peacetime, which can be transformed into a disaster management tool when dealing with a disaster situation.

Because it has been found that the functions of a usual urban management system are overlapping with the components of DM. Apart from the participatory capabilities above, one of the important benefits of the platform is that it has kept the whole development capabilities as other usual webpages, which enables the possibility and the easiness to develop new modules based on the different focus and interests of the decision-makes, By this integration way, the value and efficiency of the urban management process can be improved, the capacity of dealing with disaster situations of the city can be enhanced, and the development cost also can be reduced.

The overall conceptual design of the proposed PWebSDSS for regular urban management and disaster management sub-systems in urban areas can be seen in Figure 6 (a) and Figure 6 (b), respectively. The detailed functional design of the PWebSDSS for regular urban management and the sub-system for DM in urban areas is shown in Figure 7.

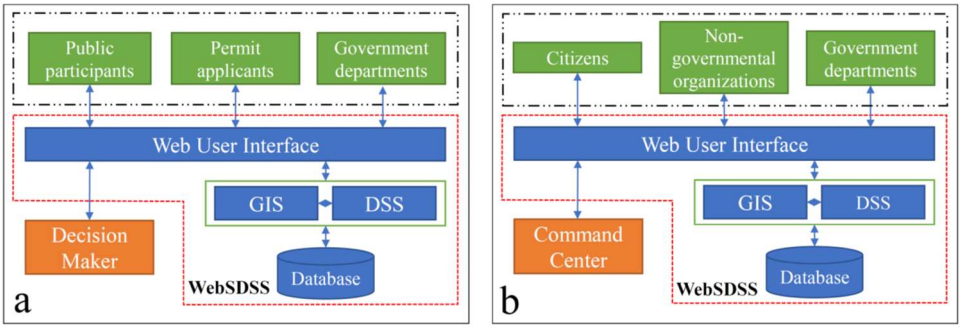

Figure 6 The overall conceptual design of the PWebSDSS for regular urban management (a) and disaster management in urban areas (b)

However, there are also some foreseeable drawbacks of the study. For example, since the system is intended for use by people in developing countries that have a complex political, social, and economic environment, the network facilities may be deficient in some of these areas, or the communication system may go out of operation when a devastating disaster strikes such as tsunami and earthquake. While our platform strongly relies on Internet accessibility, it may be not applicable in some cases. On the other hand, because some people in developing countries may not be able to utilize electronic

products or are unfamiliar with GIS technology, system functionality, and interface design should be given great attention. The interface must be designed in a visually appealing and user-friendly manner, and the functionality should be straightaway. In addition, the government officers from these countries may also be unskilled in using computer programs, a short-term centralism training is also important. The protection of users' privacy and their private data is also an important part that cannot be ignored since the database of the platform could store large amounts of users' information.

Presently, the proposed PWebSDSS is still a concept production that is being summarized and developed from the literature review concerning DSS, SDSS, Urban Management, Disaster Management, and Urban Resilience. The laws and regulations, policies, as well as cultural differences among countries can also determine the practical application effect of the concept. Thus, further studies that focus on practical application are also crucial.

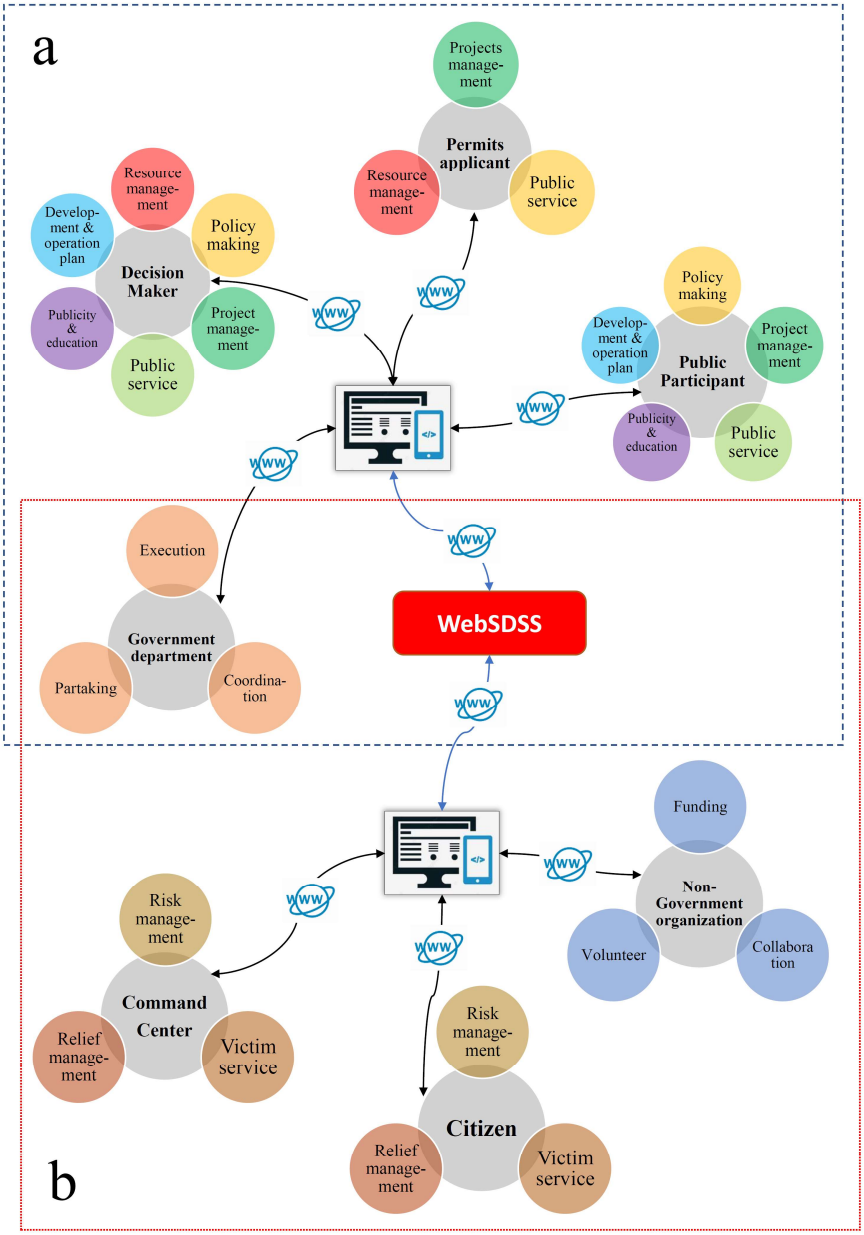

Figure 7 The detailed functional design of PWebSDSS for urban management (a), and the sub-system for disaster management (DM) in urban areas (b)

5. CONCLUSION

Our study reviewed the literature in the field of decision-making analysis and combed the evolution progress from the original non-spatial DSS to the spatial-temporal data supported and Web-based SDSS. Elaborated on each of their roles in the domain and their application area. Analyzed their innate inability and the benefits of each progression. Then we studied the concept of urban management and explored the possibility and the benefits of the participatory/collaborative urban management mode. We also reviewed the concept and content of DM and its relationship with urban management.

It was found that the typical SDSS has been criticized for not being able to solve complicated decision-making problems, engage various stakeholders, or democratize the planning process effectively, while the adoption of the proposed PWebSDSS of the study could optimize and facilitate the management process of urban areas that are rapidly developing, and a growing number of populations are involved, and facilitate an interactive, open, democratic, communicative, group-based, and informed deliberation process.

It was also found that the participatory urban management and the DM that involve proactive participation of citizens are somehow linked, and their functions are overlapped, which enabled their integration possibility. Thus, we believe the proposed PWebSDSS can be used as a regular urban management tool in peacetime and can be updated to a dual system when the DM elements are added. By this integration means, the city governance performance, and its capacity and resilience to disaster can be improved by adopting this concept.

We also believe this integrated participatory urban management platform has but is not limited to the following benefits:

- Experts & non-experts involving
- Authorities & citizens involving
- Urban & disaster management integrated
- Democratic
- Flexible in development
- Cost-saving

6. REFERENCES

Abdalla, R. (2016). Evaluation of spatial analysis application for urban emergency management. *Springerplus*, *5*(1), 2081. https://doi.org/10.1186/s40064-016-3723-y

Avis, & R, W. (2016). *Urban Governance (Topic Guide)*.

Barzinpour, F., & Esmaeili, V. (2013). A multi-objective relief chain location distribution model for urban disaster management. *The International Journal of Advanced Manufacturing Technology*, *70*(5-8), 1291-1302. https://doi.org/10.1007/s00170-013-5379-x

de Lima, L. M. M., de Sa, L. R., Dos Santos Macambira, A. F. U., de Almeida Nogueira, J., de Toledo Vianna, R. P., & de Moraes, R. M. (2019). A new combination rule for Spatial Decision Support Systems for epidemiology. *Int J Health Geogr*, *18*(1), 25. https://doi.org/10.1186/s12942-019-0187-7

Falanga, R. (2020). Participatory Design: Participatory Urban Management. In *Sustainable Cities and Communities* (pp. 1-9). https://doi.org/10.1007/978-3-319-71061-7_7-1

Ghavami, S. M. (2019). Multi-criteria spatial decision support system for identifying strategic roads in disaster situations. *International Journal of Critical Infrastructure Protection*, *24*, 23-36. https://doi.org/10.1016/j.ijcip.2018.10.004

Herold, S., Sawada, M., & Wellar, B. (2005). *Integrating Geographic Information Systems, Spatial Databases and the Internet A Framework for Disaster Management* Proceedings of the 98th Annual Canadian Institute of Geomatics Conference,

Horita, F. E. A., & Albuquerque, J. P. d. (2013). *An Approach to Support Decision-Making in Disaster Management based on Volunteer Geographic Information (VGI) and Spatial Decision Support Systems (SDSS)* Proceedings of the 10th International ISCRAM Conference,

Jelokhani-Niaraki, M. (2018). Knowledge sharing in Web-based collaborative multicriteria spatial decision analysis: An ontology-based multi-agent approach. *Computers, Environment and Urban Systems*, *72*, 104-123. doi.org/10.1016/j.compenvurbsys.2018.05.012

Jelokhani-Niaraki, M., & Malczewski, J. (2015). A group multicriteria spatial decision support system for parking site selection problem: A case study. *Land Use Policy*, *42*, 492-508. https://doi.org/10.1016/j.landusepol.2014.09.003

Jung, E., & Jung, E. J. (2019). Service-oriented architecture of environmental information systems to forecast the impacts of natural disasters in South Korea. *Journal of Enterprise Information Management*, *32*(1), 16-35. https://doi.org/10.1108/jeim-03-2015-0022

khazaee, M., & Razavian, M. T. (2012). The role of urban management in City Spatial Development Case Study Nahavand City. *International Research Journal of Applied and Basic Sciences*, *3*(3).

Madan, A., & Routray, J. K. (2016). *Existing preparedness capacity of disaster management institutions in urban areas: A case study of local institutions in Delhi, India* International Conference on Disaster Management: From Polar Region to the Local Communities,

Mahmudi, A. M., & Saremi, H. r. (2015). The Role of Citizen Participant in Urban Management (Case Study: Aligudarz City). *American Journal of Engineering Research*, *4*(1).

Mansourian, A., Taleai, M., & Fasihi, A. (2011). A web-based spatial decision support system to enhance public participation in urban planning processes. *Journal of Spatial Science*, *56*(2), 269-282. https://doi.org/10.1080/14498596.2011.623347

Mattingly, M. (1995). URBAN MANAGEMENT IN LESS DEVELOPED COUNTRIES. In.

Mohd, M. M., Amin, M. S. M., Kamal, M. R., Wayayok, A., & Yazid, S. A. A. a. M. (2014). *Application of Web Geospatial Decision Support System for Tanjung Karang Rice Precision Irrigation Water Management* Food and Environmental Engineering, Malaysia.

Nyimbili, P. H., & Erden, T. (2017). Spatial decision support systems (SDSS) and software applications for earthquake disaster management with special reference to Turkey. *Natural Hazards*, *90*(3), 1485-1507. https://doi.org/10.1007/s11069-017-3089-7

Oliveira, T. H. M. d., Painho, M., & Henriques, R. (2012). A Spatial Decision Support System for the Portuguese Public Transportation Sector. *ACM SIGSPATIAL IWGS*.

Sreekanth, P. D., Soam, S. K., & Rao, K. V. K. a. N. H. (2021). Spatial decision support system for managing agricultural experimental farms. *Current Science*.

Sugumaran, V., & Sugumaran, R. (2007). Web-based Spatial Decision Support Systems (WebSDSS): Evolution, Architecture, Examples and Challenges. *Communications of the Association for Information Systems*, *19*. https://doi.org/10.17705/1cais.01940

Wangdi, K., Banwell, C., Gatton, M. L., Kelly, G. C., Namgay, R., & Clements, A. C. (2016). Development and evaluation of a spatial decision support system for malaria elimination in Bhutan. *Malar J*, *15*, 180. https://doi.org/10.1186/s12936-016-1235-4

Yatsalo, B., & Sullivan, T. (2012). Environmental risk management with the use of multi-criteria spatial decision support system. *Risk Assessment and Management*.

NUEJ
Naresuan University
Engineering Journal

Spreadsheet Modeling Applied to Food Waste Reduction in Food Supply Chains

Po-ngarm Somkun*, Chanthraphon Konchanthet, Metha Chatsripaiboon, Napatsorn Tangkate and Thoranan Chansangpen
Department of Industrial Engineering, Faculty of Engineering, Naresuan University,
Mueng District, Tapo Subdistrict, Phitsanulok, 65000, Thailand

* Corresponding author e-mail: pongarmr@nu.ac.th

(Received: 6 December 2021, Revised: 26 April 2022, Accepted: 5 May 2022)

Abstract

Food waste is a global issue addressed by the United Nations 2030 Agenda for Sustainable Development to reduce half of the food waste at the retailer and consumer levels. The quantitative approach is required to make correct decisions regarding food waste reduction options in food supply chains. In this study, a spreadsheet modeling method was applied to achieve quantifiable impacts on food waste reduction. A case study of the downstream retail phase of a two-level supply chain of a fresh prepacked food product was used to demonstrate the model application. Information regarding the buying and consuming behaviors of consumers was collected by questionnaires to be used for stochastic analysis of inputs in the spreadsheet model. The results showed that adjusting the packaging size to match a distinct local profile could play a major role in food waste generation with appropriate sizing of retail packages enabling a reduction of up to 127 kgs. per month, or 62%, of food wastage in the supply chain. The tradeoff between the two levels of the supply chain was required to achieve this reduction of food waste. At the consumer level, smaller packaging sizes were preferred to reduce food waste which was more sensitive to the package sizes than the retailer's preference for larger packaging sizes. As well, self-weighing of unpackaged food in quantities required by the customer could reduce food waste by 7 kgs. per month, representing a 10% reduction over the selling-buying method of small pre-packed packages. Overall, good consumer food buying alone could reduce the total food waste by 59% and good consumption practices alone could reduce the total food waste by 66%.

Keywords: Food Waste Reduction, Retail Supply Chain, Spreadsheet Modeling, Selling Method, Consumer Behavior.

1. INTRODUCTION

The Food and Agriculture Organization (FAO) reported that one-third of food was being lost and wasted along the global food supply chain (FAO, 2011). This waste amounted to 1.3 billion tons per year. Food that has been purchased by consumers at the retail level for personal consumption that eventually becomes waste not only has an economic impact on the consumers but also represents significant economic and environmental impacts at every stage of the food supply chain and food life cycle (Nellemann et al., 2009).

Food production and distribution require logistics activities and manpower that consume natural resources such as water and oil. When the food becomes waste, greenhouse gases are produced, and landfill sites for disposal are required with the attendant landfill management cost. Therefore, it is unacceptable if the food is thrown away as waste. The extent of this worldwide issue needs to be addressed by practitioners, researchers, and policymakers not only for these reasons but also from a food security dimension.

The United Nations (2015) has implemented programs on sustainable consumption and production for all countries to achieve a 50% reduction in food waste per capita at both the retail and consumer levels, by 2030. There is an intercorrelation of the two-level supply chain whereby the food waste generation of each of the two stages is interrelated. For example, if the retailer provides only large packaging sizes and introduces sales promotions that attract customers to buy more than they need, there is a greater chance of food waste at the consumer level. Our study investigated these relationships and ensures that food waste is not just pushed from one level to the other level of the supply chain thus avoiding responsibility for food waste.

Our study followed the prevention approaches to food wastage (Papargyropoulou et al., 2014) in proposing some strategic and operational options for the total food waste reduction of the two-level supply chain. Quantitative approaches are applied in our study so that the result could be quantified and the practitioner can see the influence of each option to be able to make the best decisions for their supply chains (de Moraes et al., 2020; Yetkin Özbük and Coşkun, 2020).

This study used a spreadsheet modeling to represent the two-level supply chain of food retailing with consideration of the stochastic consumers' behaviors and the age-based inventory system. The aim was to investigate the impacts of (1) packaging sizes, (2) two selling-buying methods which were small pre-packed

packages versus self-weighing of unpackaged food, and (3) good practice of buying and consuming behaviors of the consumers on the total food waste.

In the organization of this paper, Section 1 introduced the background, importance, scope, and objectives of this study. Section 2 identified research gaps and distinctions of this study from the existing work. Section 3 presents the research methods while the results and discussions are in Section 4. Section 5 provides the conclusions that can be drawn from the study and provides future research opportunities.

2. LITERATURE REVIEW

A hierarchy of favorable approaches for food waste solutions has been introduced for all parties (Papargyropoulou et al., 2014). The "prevention", whose purpose is to prevent or reduce the production of excess food which may become waste, is the most promising approach when compared to other approaches such as "reuse" which is when food that would otherwise be discarded would be provided to people in need, "recycle" is the practice of food waste being used animal feed or being composted, and "recover" is the application of food waste to the production of energy.

Existing research that focused on the preventive methods of food waste reduction of perishables by applying quantitative approaches featured common configurations such as stochastic customer demands, product maximum life, and the inventory of aging products. These studies include Haijema and Minner (2016) who emphasized food waste reduction by comparing the performance of the stock-level dependent inventory replenishment policies of retailers. Other studies that focused on inventory replenishment practices include Janssen et al. (2018a) who investigated the benefit of adjusting replenishment frequency and Janssen et al. (2018b) who considered incorporating retail store closing days into inventory management policy. Another focus has been on dynamic shelf-life management and price discounting for the food that passed its optimal quality (Buisman et al., 2019; Adenso-Díaz et al., 2017).

Although these studies provided successful approaches to the prevention and reduction of food waste, an important aspect of the supply chain was missing: that is the interaction between consumer behavior and retail product supply. Food waste at the retail level is reduced and by various means. The possibility of food waste generation moves from the retailer level to the consumer level when the reduced price, promotions such as buy-one-get-one-free, or too large packaging sizes are implemented at the store. Somkun (2017) looked into this issue and combined the two levels via package size decisions with consumer behaviors as inputs for the spreadsheet model. However, the application of Somkun (2017) is limited to highly perishable products that have a single period shelf life. Somkun (2020) proceeded by allowing the shelf life to be any integer value.

Our study is a progressed work after Somkun (2020) but is distinct from the existing work in many ways. First, the consumer data in this study were grouped by occupation. This was done because, as the descriptive statistics from our data collection showed, the factor suggestively contributed to food waste generation. Gender and age which were analysis factors in the previous study were not considered relevant in our study. This alteration from the existing research generated different buying and consuming behaviors and consequently a different result analysis. Our study also investigated other unique points such as the comparison of food waste generation between selling in fixed packaging sizes and the case of the customer personally weighing and packing their purchases according to their personal preferences. Another unique point in the study is that the influence of consumer behavior, particularly purchasing and buying behaviors, on the scale of reduction of food wastage was examined and quantified.

3. METHODS

This study presents an application of spreadsheet modeling with a case study of a downstream supply chain that consisted of the retailer and consumer levels. We considered a single retail store as the retailer of interest at that level. The store was located in an urban area in provincial Thailand which was characterized as being a convenience store. This store operated an inventory of around 400 stock-keeping units (SKUs) of prepacked fresh food products such as vegetables, fruits, meats, dairy, and bakery. Most of these perishables had a shelf life of between 3 to 7 days. For the consumer level, there were approximately 290,000 locals living in the area of study which was served by 14 other similar stores.

The specific objective of this study was to analyze the influence of packaging sizes of a single type of product on the total food waste from the two supply chain stages. We also investigated the aspect of selling methods such as selling in prepacked packages and weighing as much as the customer desires. The influence of good practice in purchasing and consuming was also investigated. The content in this section is applicable to any one of those prepacked products.

Three main steps were applied in our research methodology as described in Fig. 1.

3.1 Data Collection and Input Analysis

The first step dealt with collecting the data from the case study. The required information for the retailer such as selling methods for different types of products, the product shelf life, and the store's inventory replenishment policy was collected by observation and interview. For the consumer level, we surveyed 400 sample consumers to learn their self-estimated percentages of food wastage of three types of perishables such as vegetables (9.7%), bakery (8.0%), and fresh meat (7.1%) as shown in Table 1. In the initial plan, we wished to categorize the customers by their incomes as it was suggested by FAO

(2011) that the wastage percentage highly depended on household incomes. However, information regarding income is sensitive, even in a survey where the participants remain anonymous, and some people preferred not to expose it. Therefore, occupation was used instead as it could roughly represent the revenue. The occupation groups included government officials, businesses, self-employed, students, and others, which showed quite distinct food waste percentages of 10.2%, 9.6%, 8.2%, 6.8%, and 6.6%, respectively.

The questionnaire responses also provided important inputs for the model; multipliers of the purchasing and consuming behaviors. The consumers were asked to rate their usual performance on the five-point Likert scale from highly disagree, disagree, neutral, agree, to highly agree for each question. There were 8 questions to verify the consumer purchasing behavior: (1) perform stock checking routine, (2) use a shopping list, (3) stick to the shopping list, (4) buy a large amount of food each time to avoid frequent shopping, (5) buy reduced-price food, (6) buy food as seen in the advertisement or at friends' suggestions, (7) buy more by sale promotion and discount or collect points, and (8) like to buy new food that was not previously eaten. Six questions for assessing the consumer consuming behavior included (1) only eat food that is still fresh, freshly cooked, and in perfect condition, (2) discard leftover food after every meal, (3) keep leftover food for subsequent meals, (4) discard fruit and vegetable with flaws, (5) understand the distinction between "Expire date" and "Best before", and (6) make leftovers into new appetizing food. These questions were

based on frequently mentioned factors for food waste in the literature (FAO, 2011; Mondéjar-Jiménez et al., 2016; Parfitt et al., 2010; Richter, 2017; Secondi et al., 2015; Song et al, 2015).

The scores were rearranged and transformed to represent the purchasing and consuming multipliers using the same process employed in Somkun (2020), where the details are published. The interpretation of a 5-score rating answer to each question can be either of positive or negative meaning. Thus, some rating scores were reversed to usable scores which then have the same direction towards food waste reduction. The usable scores were summed up to the total score. In this way, the total score will be meaningful. Each total score is then transformed by dividing by a neutral total score (half of the full score) to obtain the multiplier value as shown in Table 2. The resultant multiplier values of each occupation group were statistically analyzed to identify the probability distribution function using a well-known test called the Goodness-of-Fit test. All multipliers were found to be normally distributed at a 0.01 significant level. The mean and standard deviation of the normal distribution of the purchasing and consuming behaviors multipliers for each occupation group are presented in Table 1. These parameters were used as the stochastic inputs to the spreadsheet model.

3.2 Spreadsheet Modeling of a Two-Level Supply Chain

The second research step was to construct the spreadsheet model. This model was the key method applied in this study owing to its performance in storing and analyzing large volumes of data and the accessibility of statistical and formula verifying tools that facilitated the model construction and verification.

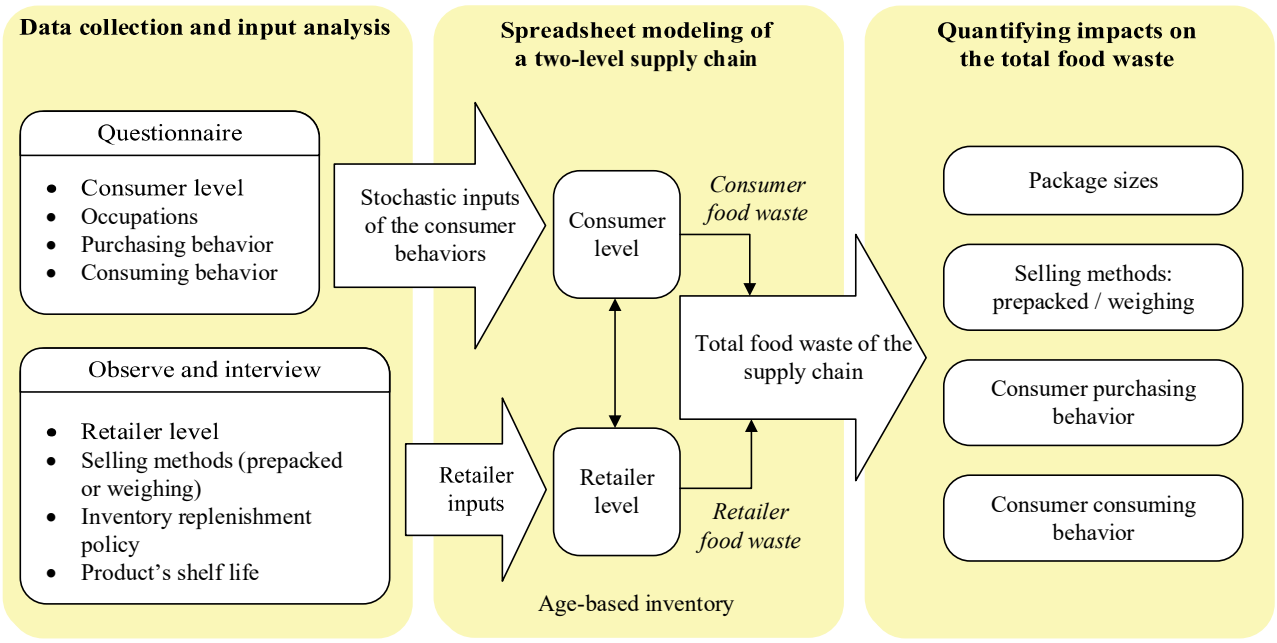

Figure 1 Research methodology

Table 1 Self-estimated percentage of food wastage and behavior multipliers for the model input

Occupations	Number of responses	Self-estimated percentage of food wastage				Behavior multipliers	
		Vegetables	Bakery	Fresh meat	Overall	Purchasing	Consuming
Government official	95	11.5	10.1	9.0	10.2	N(1.066, 0.189)	N(1.153, 0.227)
Business	72	11.6	9.0	8.3	9.6	N(1.043, 0.211)	N(1.220, 0.244)
Self-employed	80	9.7	7.7	7.2	8.2	N(1.034, 0.194)	N(1.276, 0.222)
Students	108	7.8	6.8	5.6	6.8	N(1.164, 0.189)	N(1.130, 0.233)
Others	45	7.7	6.5	5.5	6.6	N(1.052, 0.179)	N(1.224, 0.265)
	Average	9.7	8.0	7.1			

Table 2 Example of score adjustment for a single respondent (Somkun, 2020)

Item	Question number	Direction towards food waste reduction	Example rating scores (* to be reversed)	Usable score	Transform by dividing by half of the full score	Multiplier
Buying behavior	1	+	1*	5	which is 20	Buying multiplier
	2	+	3*	3		
	3	+	4*	2		
	4	–	1	1		
	5	–	5	5		
	6	–	3	3		
	7	–	4	4		
	8	–	5	5		
Full Score =	40		Total score =	28	28 ÷ 20 =	1.40
Consuming behavior	1	–	4*	2	which is 15	Consuming multiplier
	2	–	2*	4		
	3	+	3	3		
	4	–	4*	2		
	5	+	3	3		
	6	+	2	2		
Full Score =	30		Total score =	16	16 ÷ 15 =	1.07

The model represented our two-level supply chain with a single retailer and groups of consumers. We used one sheet of spreadsheet software for the consumer level and arranged the components as shown in Fig. 2. Another sheet is for the retailer level as in Fig.3. Each row contained the value of the variables of each day as this model is a periodic model that the same set of events that happens every day.

The overall consumer demand is the total demand from all consumer groups. For each consumer group, the daily requirement per person is multiplied by the buying multiplier, which is a stochastic component, to generate the need per person in weight unit. Then, it is converted to the number of units required based on the packaging size being considered, and the group demand in weight unit is calculated. The consumer is assumed to buy the product with the longest remaining life first.

Next, the retailer checks whether its inventory is enough for the overall consumer demand. If so, the demands of all consumer groups will be satisfied. Otherwise, the demand of each consumer group will be served as much as its percentage of the overall demand. The product with the longest remaining life will be considered first. When the group demand has not satisfied by the product with the longest remaining life, the next longest remaining life is considered subsequently.

The consuming multiplier, another stochastic component, is used to generate the group consumption need. The consumer is assumed to always eat the freshest food first and eat the next freshest food to fulfill the consumption need. The leftover food is kept until its last day.

The product shelf life was counted from the arrival of the product at the retailer until the end of its life either at the retailer if the product was not purchased by the customer or at the household. The life of the product was assumed to reduce constantly every period and was tracked until it was consumed or discarded. This system is called an age-based inventory where the amount of food with different remaining life is tracked.

Consumer level								
Total food waste of the two-level supply chain	142,997	grams/month						
Food waste at consumer level	125,672	grams/ month	Consumer group	1	Occupation	Government official	Group size	13
Food waste at retailer level	17,325	grams/ month	Buying multiplier pattern	Normal	Mean = 1.066	Stdev. = 0.189		
Package size	225	grams	Consuming multiplier pattern	Normal	Mean = 1.153	Stdev. = 0.227		
Product life	5	days	Daily requirement	200	grams			

Day	Overall consumer demand	Overall 5-day demand	Overall 4-day demand	Overall 3-day demand	Overall 2-day demand	Overall 1-day demand	Buying multiplier	Need per person	Number of units required per person	Group demand	Percentage from overall demand	5-day demand		5-day bought	4-day demand
0															
1	15,975	15,975	-	-	-	-	1.083	217	1	2,925	18.31%	2,925	2,925	2,925	-
2	18,675	18,675	2,700	-	-	-	1.167	233	2	5,850	31.33%	5,850	5,175	5,175	675
3	19,350	19,350	675	675	-	-	0.923	185	1	2,925	15.12%	2,925	2,925	2,925	-
4	14,850	14,850	-	-	-	-	0.777	155	1	2,925	19.70%	2,925	2,925	2,925	-
5	18,675	18,675	3,825	-	-	-	1.209	242	2	5,850	31.33%	5,850	4,725	4,725	1,125
6	19,575	19,575	-	-	-	-	1.079	216	1	2,925	14.94%	2,925	2,925	2,925	-
7	14,850	14,850	-	-	-	-	0.877	175	1	2,925	19.70%	2,925	2,925	2,925	-
8	20,025	20,025	5,175	675	-	-	1.201	240	2	5,850	29.21%	5,850	4,500	4,500	1,350
9	15,975	15,975	-	-	-	-	0.956	191	1	2,925	18.31%	2,925	2,925	2,925	-
10	14,850	14,850	-	-	-	-	0.808	162	1	2,925	19.70%	2,925	2,925	2,925	-
11	14,625	14,625	-	-	-	-	0.884	177	1	2,925	20.00%	2,925	2,925	2,925	-
12	14,850	14,850	-	-	-	-	0.956	191	1	2,925	19.70%	2,925	2,925	2,925	-
13	20,025	20,025	5,175	5,175	3,375	2,250	1.161	232	2	5,850	29.21%	5,850	4,500	4,500	1,350
14	13,725	13,725	-	-	-	-	0.895	179	1	2,925	21.31%	2,925	2,925	2,925	-

(a)

Total food waste for this group (grams/month) = 31,057

2-day demand		2-day bought	1-day demand		1-day bought	Consuming multiplier	Group consumption need	5-day consumed	4-day consumed	3-day consumed	2-day consumed	1-day consumed	4-day stored	3-day stored	2-day stored	1-day stored	Food waste
-	-	-	-	-	-	0.878	2,275	2,275	-	-	-	-	-	-	-	-	-
-	-	-	-	-	-	1.001	2,600	2,600	-	-	-	-	650	-	-	-	-
-	-	-	-	-	-	1.379	3,575	2,925	650	-	-	-	2,575	1,325	-	-	-
-	-	-	-	-	-	0.801	2,080	2,080	-	-	-	-	-	1,925	1,325	-	-
-	-	-	-	-	-	1.625	4,225	4,225	-	-	-	-	845	-	1,925	1,325	1,325
-	-	-	-	-	-	1.399	3,627	2,925	500	202	-	-	500	1,970	-	1,925	1,925
-	-	-	-	-	-	0.934	2,418	2,418	-	-	-	-	-	-	1,768	-	-
-	-	-	-	-	-	0.877	2,275	2,275	-	-	-	-	507	-	-	1,768	1,768
-	-	-	-	-	-	1.108	2,873	2,873	-	-	-	-	2,225	1,857	-	-	-
-	-	-	-	-	-	1.270	3,302	2,925	52	325	-	-	52	2,225	1,857	-	-
-	-	-	-	-	-	1.013	2,626	2,626	-	-	-	-	-	-	1,900	1,857	1,857
-	-	-	-	-	-	1.570	4,069	2,925	299	-	-	845	299	-	-	1,900	1,055
675	450	450	225	225	225	1.088	2,821	2,821	-	-	-	-	-	-	-	-	225
-	-	-	-	-	-	1.226	3,185	2,925	260	-	-	-	1,679	-	675	450	450

(b) continue from (a)

Figure 2 Spreadsheet model for the consumer level

When the product that has one period left before the end of its life is not purchased or consumed, it becomes food waste. Therefore, food waste can occur at both the consumer level and the retailer level. Our analysis utilizes food waste at each of the two levels and the total food waste of this supply chain as the key performance measures. We recommend interested readers to read Somkun (2020) for the mathematical expressions of the relationship of this system.

The Order-Up-To inventory replenishment policy, in which the retailer placed an order periodically (daily) to raise the inventory level of the particular product to the target level, was employed in the model. The formula for the Order-Up-To level (S) in the weight unit is described by:

$$S = (1 + L) \times \bar{D} + z \times \sqrt{(1 + L)} \times s_D, \qquad (1)$$

where L is the lead time between the retailer and the distributor, $\bar{D}$ is the average consumer demand and s_D is the standard deviation of the consumer demand.

The lead time was zero from the interview with the store as the store placed an order at the end of its working hour and the product would be received the next morning, effectively immediately in store opening terms. The $\bar{D}$ and s_D were calculated from a set of the generated overall demand that corresponds to the distribution of the multipliers shown in Table 1. The z term is the inverse of standard normal cumulative distribution or $F^{-1}(prob.)$ function. Input for this function is the cycle service level (CSL). The CSL value shows the probability that the retailer will be able to respond to customer demands by on-hand stocks. The CSL value closer to 100% means a higher stock level and thus a higher customer service level.

3.3 Quantifying Impacts on the Total Food Waste

The final step of this research method was to numerically quantify the impacts of three methods to food waste reduction. We assumed the product shelf life to be 5 days. The Cycle Service Level (CSL) was set to 0.98, which means 98% of the orders in a cycle out of all cycles were satisfied by in-stock inventories.

This investigation included (1) setting a suitable package size and (2) providing an appropriate selling method between the prepacked package and weighing as much as the customer desires. For the consumer stance, (3) the influences of good practice in purchasing and consuming were investigated.

For the first objective, the experiment was designed to test the package size between 50 grams to 350 grams with a 25-gram increment as this range covered the current package size of this product of 200 grams. As of the stochastic nature of the model, the data was collected 300 times for each package size and the average value was used for plotting the graph. The result is presented in Section 4.1.

The best packaging size resulting from the first experiment will be used for setting the experiment in the next section. The scenario is that the store provides a station for the customer to self-weight the require quantity of the food product rather than selling the product in prepacked package size. The spreadsheet model for this scenario allows the customers to buy the exact amount of the food product that they want if the inventory is available. The data was collected 300 times. The result is presented in Section 4.2.

For the last objective, the consumers' buying and consuming behaviors will be investigated to realize how much the consumer can help solve the food waste problem. We assumed that the consumer practiced good buying behavior and therefore agreed to the positive food waste reduction implications of all the questions listed in the questionnaire at the 4th level of the five-point Likert scale where highly disagree is 1, disagree is 2, neutral is 3, agree is 4, and highly agree is 5. This arrangement resulted in a deterministic value of all consumers' buying multipliers while the consuming multiplier still had its stochastic nature. Again, the data was collected 300 times.

The same procedure was applied to the practice of good consuming behavior. Therefore, for this latter case, the consuming multiplier was deterministic while the buying multiplier maintained its stochastic character. The result is presented in Section 4.3.

	A	B	C	D	E	F	G	H	I	J	K	L	M	N	O	P	Q	R	S	T
1	Retailer level																			
2																				
3	Food waste at retailer level			17,325	grams/ month															
4	Inventory replenishment policy			OUT	OUTL =	100	units													
5	Package size		225	grams																
6	Product life		5	days																
7																				
8	**Day**	**Incoming delivery**	**5-day inventory**	**4-day inventory**	**3-day inventory**	**2-day inventory**	**1-day inventory**	**Unmet demand**	**Overall consumer demand**	**5-day sold**	**Group 1**	**Group 2**	**Group 3**	**Group 4**	**Group 5**	**4-day sold**	**Group 1**	**Group 2**	**Group 3**	**Group 4**
9	0	0																		
10	1	22500	22500	0	0	0	0	0	15975	15975	2925	4500	2475	3375	2700	0	0	0	0	0
11	2	15975	15975	6525	0	0	0	0	18675	15975	5175	2025	2250	5850	675	2700	675	225	225	900
12	3	18675	18675	0	3825	0	0	0	19350	18675	2925	4500	2475	6525	2250	0	0	0	0	0
13	4	19350	19350	0	0	3150	0	0	14850	14850	2925	2250	4950	3375	1350	0	0	0	0	0
14	5	14850	14850	4500	0	0	3150	0	18675	14850	4725	1800	2025	5400	900	3825	1125	450	450	1350
15	6	21825	21825	0	675	0	0	0	19575	19575	2925	2250	4950	6750	2700	0	0	0	0	0
16	7	19575	19575	2250	0	675	0	0	14850	14850	2925	2250	4950	3375	1350	0	0	0	0	0
17	8	14850	14850	4725	2250	0	675	0	20025	14850	4500	1800	2025	5175	1350	4500	1350	450	450	1575
18	9	20700	20700	0	225	1575	0	0	15975	15975	2925	4500	2475	3375	2700	0	0	0	0	0
19	10	15975	15975	4725	0	225	1575	0	14850	14850	2925	2250	4950	3375	1350	0	0	0	0	0
20	11	16425	16425	1125	4725	0	225	0	14625	14625	2925	4500	2475	3375	1350	0	0	0	0	0
21	12	14850	14850	1800	1125	4725	0	0	14850	14850	2925	2250	4950	3375	1350	0	0	0	0	0
22	13	14850	14850	0	1800	1125	4725	0	20025	14850	4500	1800	2025	5175	1350	0	0	0	0	0
23	14	22500	22500	0	0	0	0	0	13725	13725	2925	2250	2475	3375	2700	0	0	0	0	0

(a)

	Q	R	S	T	U	V	W	X	Y	Z	AA	AB	AC	AD	AE	AF	AG	AH	AI	AJ	AK	AL	AM	AN
1																								
2																								
3																								
4																								
5																								
6																								
7																								
8	**Group 1**	**Group 2**	**Group 3**	**Group 4**	**Group 5**	**3-day sold**	**Group 1**	**Group 2**	**Group 3**	**Group 4**	**Group 5**	**2-day sold**	**Group 1**	**Group 2**	**Group 3**	**Group 4**	**Group 5**	**1-day sold**	**Group 1**	**Group 2**	**Group 3**	**Group 4**	**Group 5**	**Food waste**
9																								
10	0	0	0	0	0	0	0	0	0	0	0	0	0	0	0	0	0	0	0	0	0	0	0	0
11	675	225	225	900	675	0	0	0	0	0	0	0	0	0	0	0	0	0	0	0	0	0	0	0
12	0	0	0	0	0	675	0	0	0	225	450	0	0	0	0	0	0	0	0	0	0	0	0	0
13	0	0	0	0	0	0	0	0	0	0	0	0	0	0	0	0	0	0	0	0	0	0	0	0
14	1125	450	450	1350	450	0	0	0	0	0	0	0	0	0	0	0	0	0	0	0	0	0	0	3150
15	0	0	0	0	0	0	0	0	0	0	0	0	0	0	0	0	0	0	0	0	0	0	0	0
16	0	0	0	0	0	0	0	0	0	0	0	0	0	0	0	0	0	0	0	0	0	0	0	0
17	1350	450	450	1575	675	675	0	0	0	0	675	0	0	0	0	0	0	0	0	0	0	0	0	675
18	0	0	0	0	0	0	0	0	0	0	0	0	0	0	0	0	0	0	0	0	0	0	0	0
19	0	0	0	0	0	0	0	0	0	0	0	0	0	0	0	0	0	0	0	0	0	0	0	1575
20	0	0	0	0	0	0	0	0	0	0	0	0	0	0	0	0	0	0	0	0	0	0	0	225
21	0	0	0	0	0	0	0	0	0	0	0	0	0	0	0	0	0	0	0	0	0	0	0	0
22	0	0	0	0	0	1800	675	225	225	675	0	1125	450	225	225	225	0	2250	225	0	0	675	1350	2475
23	0	0	0	0	0	0	0	0	0	0	0	0	0	0	0	0	0	0	0	0	0	0	0	0

(b) continue from (a)

Figure 3 Spreadsheet model for the retailer level

4. Results and Discussions

4.1 Influence of Package Sizes on Food Wastage

The results of the first test on the influence of package size of the prepacked food product is depicted in Fig. 4. In general, the smallest size of 50 grams generated the least total food waste. This package size was best for the consumer as it generated the minimum surplus food. This was in opposition to the retailer experience as the smallest size produced the highest food waste at the retail level when compared to other package sizes. This clearly showed the tradeoff situation between this two-level supply chain.

The 200-gram package size, which was the size provided at the store, generated the lowest store level's food waste of 16 kgs. per month but the amount of food waste was relatively high at 157 kgs. per month for the consumer level. It was noticeable that the retailer received less impact from the package sizes where the range between the best and the worst cases was 36 kgs per month of food wastage. The range was 160 kgs per month for the consumer level which showed that the consumer level was much more sensitive to the package size setting. For the supply chain view, the range was 127 kgs per month. This emphasized the importance of the size determination for a distinct community profile.

The relationship between the amount of food waste between the two levels was nonlinear. Although the smallest package size performed the best practice for that two-level supply chain, a smaller package size did not always generate a lower amount of food waste. From Fig. 4, for the package size between 225 to 275 grams, a larger package size produced less food waste. This result showed the benefit of the model in predicting the quantified impact of package size adjusting. The management could then decide the most appropriate package size that helped balance the food waste generation and costs of the implementation.

Another aspect widely debated is that the smaller packing sizes could lead to more packaging waste. Williams and Wikström (2011) suggested that, for some types of food, the total environmental impact could still reduce when trying to reduce food waste increases packing waste. Organic or degradable packaging could also be another option to solve this issue. Other options seen in most open markets are simply arranging food products in a pile or placing the food on a plate just to show the amount of a sale unit. The customers can take the food product directly to their bags. In this way, no packaging is required but the protection provided by a package is lost.

4.2 Influence of the Selling-Buying Method on Food Wastage

Following the result from Section 4.1, the smallest package size introduced the lowest amount of total food waste. The result showed that the weighing scenario could reduce the total food waste of this supply chain from 77 kg. per month to 70 kg. per month as presented in Fig.5. This 7 kg. per month accounted for a 10% reduction when compared to selling-buying by small prepacked packages of 50 grams. The consumers gained more benefit from the weighing scenario as their food wastage could drop 16 kgs. per month from 25 kgs to 9 kgs., which was a 64% reduction. This was unsurprising because the customers bought food in only the amount that they need. Thus, much less surplus food was bought and lessened the chance of food waste generation. The factor for the consumer food waste leaned towards their consuming behavior in this case. However, by implementing the weighing scenario, the retailer could generate 15% more food wastage, which increased from 52 to 61 kgs. per month.

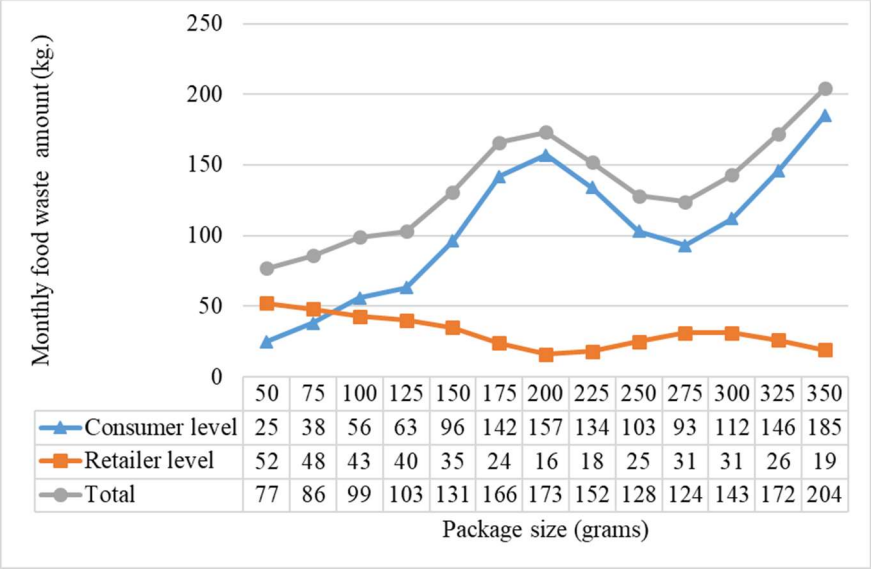

	50	75	100	125	150	175	200	225	250	275	300	325	350
Consumer level	25	38	56	63	96	142	157	134	103	93	112	146	185
Retailer level	52	48	43	40	35	24	16	18	25	31	31	26	19
Total	77	86	99	103	131	166	173	152	128	124	143	172	204

Figure 4 The amount of food waste at the two-level supply chain for different prepacked package sizes

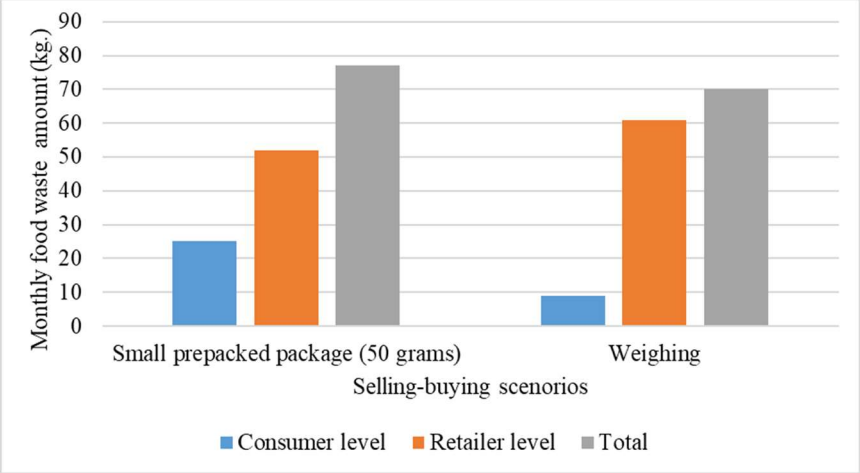

Figure 5 Comparing food waste generation between selling in prepacked package and weighing

This increase in food waste could be higher in real operations. As the retailer generally provides food such as fresh meat, fruits, or vegetables on an open platter for the customers to scoop, pick or select by themselves, the food might be spoiled, bruised, or contaminated as it does not have packaging for protection and eventually more food will be discarded. This deterioration in quality is especially true for food that requires temperature control.

The weighing and prepacked selling scheme could also be provided simultaneously by appropriate types of products at various store settings for customers with different levels of convenience preference. Although this adjustment in selling methods could cost more for the retailer, the pressure from the sustainable development goals (United Nations, 2015) that are currently applied would request all players to act.

4.3 Influence of the Consumer Behavior on Food Wastage

The comparison between the current buying and consuming behaviors of the consumer and these two scenarios showed a significant reduction in the total supply chain food waste as depicted in Fig. 6.

The reduction of 59% of the total food waste from 173 kgs. per month down to 71 could be achieved by the practice of good buying behavior. Considering the consumer level, the reduction was very large where the food waste was reduced to less than 1 kg. per month. The retailer however produced 54% more food waste due to the low customer demand resulting from the better buying behavior.

For the scenario that the consumer practiced good consuming behavior, the reduction of the total food waste was 114 kgs per month or 66%. This food waste reduction happened only at the consumer level. The retailer level's food waste was maintained at the same value (16 kgs.).

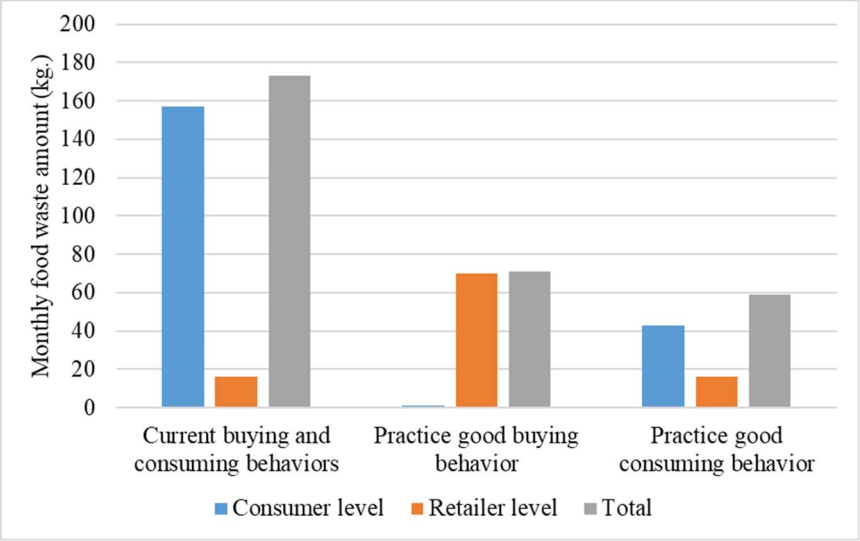

Figure 6 Influence of the consumer's behaviors on the amount of food waste

The result emphasized the importance of consumer involvement to achieve food waste reduction. Good practice of buying behaviors (such as constantly checking food stock at home, using a shopping list and buying as listed, and ignoring sale promotions and advertisements) could adjust the demand volume and the amount of food brought into a household to the appropriate level and resulted in lower household food wastage. Furthermore, good practice of consuming behaviors (such as keeping and re-cook leftovers, being more flexible about the appearance and freshness of food, and understanding date labels) could reduce food discarding.

5. CONCLUSION

This study proposed spreadsheet modeling for decision-making regarding food waste reduction. The model represented a downstream supply chain of a prepacked food product that had a single retail store at the retail level and 5 groups of consumers at the consumer level. The stochastic input data of the buying and consuming behaviors of the consumers were analyzed from a case study of an urban community.

The results suggest that package sizes highly influenced the reduction of the supply chain's total food waste. The consumer level was more sensitive to the package size than the retailer level. The model is a useful tool for the management to decide on a proper package size that helps reduce food wastage for a dissimilar population profile of each area.

Furthermore, the result indicates that allowing the customers to personally weigh the amount of food according to their needs could reduce the total food waste under the assumption that no food was spoiled by the customer selection process.

The consumers' buying and general consuming behaviors also played a major role in food waste reduction. The result showed that the total food waste of the supply chain could be reduced when the consumers applied good buying and consuming behaviors such as routine checking food stock at home, using a shopping list, keeping leftovers for next consumption, and understanding the best-before date labels, for example.

The limitations of this study could be further considered in new research studies. This study is limited to a two-level supply chain to focus on a downstream supply chain. However, the scope could be extended to other supply chain players in the various scenarios in which the product is being packaged, such as the distribution center or the factory, to complete the downstream chain.

A future study could also investigate the selling-buying method of weighing and packing the amount that the customer desires in a more realistic setting. The assumption that no food was spoiled during the customer selection process should be exempted to understand the real benefit of this selling-buying approach.

6. ACKNOWLEDGMENT

This work was supported by the Faculty of Engineering, Naresuan University [grant numbers R2564E006]. Also, the authors acknowledge Mr Roy I. Morien of the Nareusan University Graduate School for his efforts in editing the English grammar, syntax and general expression in this paper.

7. REFERENCES

Adenso-Díaz, B., Lozano, S., & Palacio, A. (2017). Effects of dynamic pricing of perishable products on revenue and waste. *Applied Mathematical Modelling.* 45, 148–164. https://doi.org/10.1016/j.apm.2016.12.024.

Buisman, M. E., Haijema, R., & Bloemhof-Ruwaard, J. M. (2019). Discounting and dynamic shelf life to reduce fresh food waste at retailers. International Journal of Production Economics, 209, 274–284. https://doi.org/10.1016/j.ijpe.2017.07.016.

de Moraes, C.C., de Oliveira Costa, F.H., Roberta Pereira, C., da Silva, A.L., & Delai, I. (2020). Retail food waste: mapping causes and reduction practices. *Journal of Cleaner Production*. 256, 120124. https://doi.org/10.1016/j.jclepro.2020.120124.

FAO. (2011). *Global food losses and food waste – Extent, causes and prevention*, Rome.

Haijema, R., & Minner, S. (2016). Stock-level dependent ordering of perishables: A comparison of hybrid base-stock and constant order policies. *International Journal of Production Economics*. 181, Part A, 215–225. https://doi.org/10.1016/j.ijpe.2015.10.013.

Janssen, L., Diabat, A., Sauer, J., & Herrmann, F. (2018a). A stochastic micro-periodic age-based inventory replenishment policy for perishable goods. Transportation Research Part E: Logistics and Transportation Review, 118, 445–465. https://doi.org/10.1016/j.tre.2018.08.009.

Janssen, L., Sauer, J., Claus, T., & Nehls, U. (2018b). Development and simulation analysis of a new perishable inventory model with a closing days constraint under non-stationary stochastic demand. Computers and Industrial Engineering, 118, 9–22. https://doi.org/10.1016/j.cie.2018.02.016.

Mondéjar-Jiménez, J.-A., Ferrari, G., Secondi, L., & Principato, L. (2016). From the table to waste: An exploratory study on behaviour towards food waste of Spanish and Italian youths. *Journal of Cleaner Production*, 138, 8–18. https://doi.org/10.1016/j.jclepro.2016.06.018.

Nellemann, C., MacDevette, M., Manders, T., Eickhout, B., Svihus, B., Prins, A. G., & Kaltenborn, B. P. (2009). *The Environmental Food Crisis – The Environment's Role in Averting Future Food Crises*. A UNEP Rapid Response Assessment, United Nations Environment Programme, GRID-Arendal, 29 – 32. www.grida.no. ISBN: 978-82-7701-054-0.

Papargyropoulou, E., Lozano, R., Steinberger, J. K., Wright, N., & Ujang, Z. (2014). The food waste hierarchy as a framework for the management of food surplus and food waste. *Journal of Cleaner Production*. 76, 106–115. https://doi.org/10.1016/j.jclepro.2014.04.020.

Parfitt, J., Barthel, M., & Macnaughton, S. (2010). Food waste within food supply chains: quantification and potential for change to 2050. *Philosophical Transactions of the Royal Society B*, 365, 3065–3081. https://doi.org/10.1098/rstb.2010.0126.

Richter, B. (2017). Knowledge and perception of food waste among German consumers. *Journal of Cleaner Production*, 166, 641–648. https://doi.org/10.1016/j.jclepro.2017.08.009.

Secondi, L., Principato, L., & Laureti, T. (2015). Household food waste behaviour in EU-27 countries: A multilevel analysis. *Food Policy*, 56, 25–40. https://doi.org/10.1016/j.foodpol.2015.07.007.

Somkun, P., (2017). Stochastic mathematical model for food waste reduction in a two-level supply chain for highly perishable products. *International Journal of Supply Chain Management*, 6, 1, 165–171.

Somkun, P. N. (2020). Mathematical modeling approach applied to food waste reduction at retailer and consumer levels in food supply chain. In *Food Industry Wastes: Assessment and Recuperation of Commodities*, 409–429. Elsevier. https://doi.org/10.1016/B978-0-12-817121-9.00019-X

Song, G., Li, M., Semakula, H. M., & Zhang, S. (2015). Food consumption and waste and the embedded carbon, water and ecological footprints of households in China. *Science of the Total Environment*, 529, 191–197. https://doi.org/10.1016/j.scitotenv.2015.05.068.

United Nations. (2015). *Sustainable development goals. 17 goals to transform our world*. https://www.un.org/sustainabledevelopment/sustainable-consumption-production/. (accessed 15 June 2021).

Williams, H., & Wikström, F. (2011). Environmental impact of packaging and food losses in a life cycle perspective: a comparative analysis of five food items. *Journal of Cleaner Production*. 19, 1, 43–48. https://doi.org/10.1016/j.jclepro.2010.08.008.

Yetkin Özbük, R.M., & Coşkun, A. (2020). Factors affecting food waste at the downstream entities of the supply chain: A critical review. *Journal of Cleaner Production*. 244, 118628. https://doi.org/10.1016/j.jclepro.2019.118628.

8. BIOGRAPHIES

Po-ngarm Somkun is a lecturer at the Department of Industrial Engineering, Faculty of Engineering, Naresuan University. Her current research topics involve food waste reduction in the supply chain via mathematical and spreadsheet modeling. Other research interest includes lateral transshipment in a distribution network.

Chanthraphon Konchanthet graduated with a bachelor's degree in Industrial Engineering from Naresuan University.

Metha Chatsripaiboon graduated with a bachelor's degree in Industrial Engineering from Naresuan University.

Napatsorn Tangkate graduated with a bachelor's degree in Industrial Engineering from Naresuan University.

Thoranan Chansangpen graduated with a bachelor's degree in Industrial Engineering from Naresuan University.

NUEJ
Naresuan University
Engineering Journal

Capacitor placement in Power Distribution Networks using Particle Swarm Optimization: Case Study Savannakhet Province

Phavixa Vongvilasack [1], Sutthichai Premrudeepreechacharn [1,*] and Kanchit Ngamsanroaj[2]

[1] Department of Electrical Engineering, Faculty of Engineering, Chiangmai University, Chiangmai 50200, Thailand
[2] Electricity Generating Authority of Thailand (EGAT), Nonthaburi, Thailand

* Corresponding author e-mail: suttic@eng.cmu.ac.th

(Received: 21 September 2021, Revised: 27 April 2022, Accepted: 5 May 2022)

Abstract

This research presents the optimal capacitor placement on medium voltage (MV) distribution system with distributed generator (DG) connection applied particle swarm optimization (PSO) algorithm. This paper proposes the simulated collaboration between DIgSILENT PowerFactory and MATLAB software which are developed to solve the problem of capacitor placement in the power distribution system, which purpose to reduce the power losses and minimize the expense of the installation shunt capacitor. To obtain the optimal capacitor placement, the process is carried out by searching the probable candidate location given by the loss sensitivity factor (LSF) for reducing the search space of problem, and the optimal size would be determined with the proposed PSO algorithm. The study is taken into account the daily load variation to specify type of capacitor bank, and the case study is also considered with/without of distributed generator (DG) connected to the distribution grid. The PSO algorithm is validated the effectiveness as against the other algorithms reported on the literature under the IEEE 33-bus test system that conducts in the developed tool. The real power distribution system of Electricite du Lao (EDL) in Savannakhet province is also investigated. The study results demonstrate that the proposed methodology can provide the optimal location and capacity, which can reduce power losses and improve the bus voltage magnitude. The PSO algorithm can be achieved the satisfied annual net saving after capacitor placement as compared with genetic algorithm (GA).

Keywords: Capacitor Placement, Power Distribution System, Distributed Generator (DG), Active Power Loss Reduction, Particle Swarm Optimization (PSO).

1. INTRODUCTION

Presently, many countries worldwide have developed technology to support electric power for enhancement each system become high efficiency. Due to electricity demand growth and aged components have been increased each year, by these issues will be leading to a high loss of revenue and the system will become non-stable. Power loss is a weak point of the power system which affect to electricity response and economic development. For instance, World Bank Group (2018) was carried out the results of an international survey on T&D energy losses in 2018, most of the electricity loss appears in the power distribution network and the portion occurs 13% of the electricity generation. These highly consumed reactive power is the significant effect to the power distribution system losses that leads to decreasing the capability for supply the electric power as much as possible. Some of these losses can be reduced by reactive power compensation as installing shunt capacitors (capacitor banks). Also, this approach provides several advantages as well as improved power factor, improving the voltage level and obvious saving for supplying the electric power, this will lead to increase the existing capacity of the power system. Generally, the optimal capacitor placement in the power distribution system has to determine the quantity, capacity, type, and location of capacitor banks, which are particular importance to gain the maximum economic benefits without constraints violation.

Ever since, the optimum capacitor allocation is a complexity optimization problem, in the past there are many different optimization techniques are commonly solved the problem. According to Ng et al. (2000) classified the techniques of installation shunt capacitor in four kinds as analytical, numerical programming, heuristics, and artificial intelligence. As known on previous works extensively used analytical methods to explain the capacitor placement optimization problem as presented by Cook (1961). However, these methods were built based on their usually assumption operating conditions and giving the uncertainty result. Cho and Chen (1997) described the current analytical methods as more accurate and useful in the practical distribution system. The numerical programming techniques had implemented to solve the problem consist of a nonlinear optimization problem presented by Baran and Wu (1989).

The mixed integer non-linear programming (MINLP) method introduced for the optimum capacitor location for reduction the electric loss cost and minimization the capital cost of capacitors as shown in the research of Nojavan et al. (2014) and Baran and Wu (1989). These techniques also had some inconvenient for solving problem as higher computation time. From viewpoint of optimization problem, Aman et al. (2014) explained the optimal capacitor placement that is rather complicated cause of their high multi structure and size, nonlinear and discontinuous. These problem attributes make a challenging for solving via applying standardize optimization methods of Ng et al. (2000).

Recently, the various computation methods have been developed as well as metaheuristics approaches that can solve many problems on the power system. Singh and Rao (2012) presented particle swarm optimization (PSO) algorithm based-on artificial intelligent. This application also used for the capacitor placement problem, the objectives aimed to maximize cost saving by reduction the power loss and the reactive compensator costs. The research demonstrated that PSO had greater solution and giving the better voltage profile. In the same way, Shuaib et al. (2015) presented gravitational search algorithm (GSA), which purposed to maximize net saving by providing reduction active power losses and operation capacitors costs by considering capacity and location that most suitable to allocation in the distribution system. Díaz et al. (2018) presented a swarm approach known as locust search algorithm, they showed the effectiveness of the algorithm to determine the amount, location, and capacity of shunt capacitor for minimalizing the total capital cost, that purposes to reduce energy losses and improve the voltage profile in the radial distribution systems. Then, Jafari et al. (2020) presented a two-layer hybrid using a few combinations heuristic algorithm for the optimum place and operating times of switched capacitors, and the results indicated that had more effect on the distribution feeder with voltage-dependent loads and more advantages over other optimization algorithms. However, most of the mentioned research focused on developing the optimization algorithms and investigated in the test system. In contrast to the real system, which is the large scale of the power distribution system, that might not lead to the most optimal solution due to some restriction of the different algorithms.

In this paper, the developed tool for solving the optimal capacitor placement problem for the real power distribution system is presented. To clarify, the number, size, type, and location of capacitor banks is taken into account for meet along the profile characteristic of load demand. This research adopts LSF to decrease search space of the capacitor bank solutions. The PSO algorithm is implemented due to its advantages and uncomplexity of the optimization process. According to the proposed consideration of capacitor banks allocation, the experimental is simulated in DIgSILENT PowerFactory and applies the proposed algorithm via MATLAB, which collaborates by the communication the data interchange between two software. Therefore, the study results demonstrate that the proposed tool can be determined the optimal capacitor placement which aims to minimize the total cost of power losses and capital cost of capacitors which are related to the acquired revenue on annual net savings. Additionally, the proposed approach can contribute to implementation with the real distribution system, which can specifically solve the optimization problem for power system. As Shaheen and El-Sehiemy (2020) presented the installed capacitor banks can consider for the coordinated volt/var control due to the integration of DG to manage the reactive power application for the modern distribution grid.

The remaining of the research is ordered as follow: in section 2 discusses concept of power loss calculation and Loss Sensitivity Factor (LSF); In section 3 details the proposed objective optimization process for capacitor placement using (PSO) algorithm; Section 4 presents the study results and discussion of the capacitor placement; The conclusion is summarized in section 5.

2. ANALYSIS OF POWER LOSS IN THE POWER DISTRIBUTION SYSTEM

This section describes a method of power loss calculation, which analyzes by compensating the reactive power into the nodes rather than drawing from the grid. To find the selection bus for placing shunt capacitors apply Loss Sensitivity Factor.

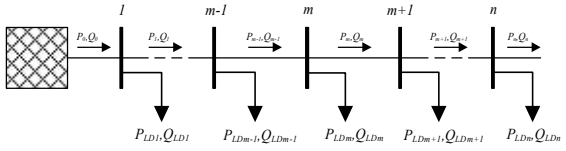

Figure 1 Schematic of radial distribution system diagram

2.1 Power loss calculation

The calculation power loss had been developed to simplified method by Su and Tsai (1996). A set of basic line flow equations is provided as a choice for computing the power line flow analysis based on this method, which completely avoids the iteration process. From Figure 1 demonstrates all connection points connected to the node *m* the power at node *m* can be determined the equations as follows:

$$P_m = P_{m+1} + P_{LDm} + \left(\frac{P_m^2 + Q_m^2}{|V_m|^2}\right) R_{m,m+1}$$
$$\cong P_{m+1} + P_{LDm} + \left(\left(P_{m+1} + P_{Lm}\right)^2 + \left(Q_{m+1} + Q_{Lm}\right)^2\right) R_{m,m+1} \quad (1)$$

$$Q_m = Q_{m+1} + Q_{LDm} + \left(\frac{P_m^2 + Q_m^2}{|V_m|^2}\right) X_{m,m+1}$$
$$\cong Q_{m+1} + Q_{LDm} + \left(\left(P_{m+1} + P_{Lm}\right)^2 + \left(Q_{m+1} + Q_{Lm}\right)^2\right) X_{m,m+1} \quad (2)$$

$$|V_{m+1}|^2 = |V_m|^2 - 2\left(\left(R_{m,m+1} \times P_{LDm}\right) + \left(X_{m,m+1} \times Q_{LDm}\right)\right) + \left(\frac{P_m^2 + Q_m^2}{|V_m|^2}\right) \quad (3)$$

Where: P_m is the active power sent out from bus m, Q_m means the reactive power released from bus m, P_{LDm} denotes the active power load at bus m, Q_{LDm} is a required load of reactive power at bus m, and where $R_{m,m+1}$ is the resistance between bus m and $m+1$ and $X_{m,m+1}$ means the reactance between bus m and $m+1$. Moreover, $|V_m|$ is the voltage level at bus m.

2.2 Loss sensitivity factor

To conduct for power loss reduction there are much research had used Loss sensitivity factor. Due to this technique is useful for estimation which bus has highly probability to install shunt capacitors. The Loss sensitivity factor is commonly applied for evaluation the applicant buses. Prakash and Sydulu (2006) presented a technique that mostly assists to reduce of the exploration area for the optimization work, it can be formulated as follows:

$$\frac{\partial P_{Loss}}{\partial Q_{m-1,m}} = \frac{2 \times Q_{m-1,m}}{|V_m|^2} \times R_{m-1,m} \quad (4)$$

$$\frac{\partial Q_{Loss}}{\partial Q_{m-1,m}} = \frac{2 \times Q_{m-1,m}}{|V_m|^2} \times X_{m-1,m} \quad (5)$$

This LSF implementation lists to arrange capacitor positions in descending order from their indicators. The greater indicator value is the most possibility for capacitor placement.

3. CAPACITOR PLACEMENT USING PSO ALGORITHM

In this research, the purpose of the capacitor allocation issue is to enhance the power distribution system via reducing power losses and sustained the bus voltages under the permissible limit. The objective function is described as below.

3.1 Objective function

To accomplish the reactive power compensation optimization problem, the quantity, place, type, and capacity of shunt capacitors are considered. It can be described as the equation below:

$$min\, F = C_e \times \sum P_{Loss} \times t + \sum_{i=1}^{N_c} (C_{cr} \times Q_c) + C_{cI} \times N_c \quad (6)$$

where: C_e is the price of electricity, t is the time period, C_{cr} is cost per unit of capacitor bank, Q_c is rating of capacitor bank, C_{cI} is cost of capacitor installation, and N_c is the quantity of capacitors to install.

From the objective function above, the proposed approach must be subjected the constraints including the grid voltage and total released of reactive power by capacitor banks as follows:

$$V_{min} < V_j < V_{max} \quad (7)$$

$$\sum Q_C \leq \sum Q_{C,max} \quad (8)$$

Where: Q_C is reactive power compensated to the power line, $Q_{C,max}$ is the maximum allowable compensation reactive power into the network, and $Vmin$, $Vmax$ are the lowest and highest voltage limit at network bus j.

3.2 Particle swarm optimization algorithm

Refer to the purpose and restriction conditions in the proposed optimization algorithm, this research adopts swarm intelligence approach, which is the particle swarm optimization algorithm and widely applied in this field works. The mathematic details of the PSO algorithm describes as below:

$$\begin{cases} V_i^{t+1} = \omega V_i^t + c_1 \cdot r_1 \cdot \left(P_{bi}^t - Q_{ci}^t\right) + c_2 \cdot r_2 \cdot \left(G_{bi}^t - Q_{ci}^t\right) \\ Q_{ci}^{t+1} = X_i^t + \left(V_i^{t+1} \times C\right) \end{cases} \quad (9)$$

Where: c_1 and c_2 are the acceleration factors, V_i means velocity of individual i in repetition t, Q_c is reactive power compensated of individual i in iteration t, P_{bi} is individual best of the i^{th} loop, G_{bi} is global best of all populations, r_1 and r_2 are random variables in the extent of [0,1], and ω is the weight of inertia.

Singh and Yadagiri (2009) described the perception of time-varying inertial weight (TVIM), when initial exploration started with large inertia weight factor and its value would be slowly decreased from the exploring procedure as well. It is expressed as:

$$\omega = (\omega_{max} - \omega_{min}) \times \frac{iter_{max} - iter}{iter_{max}} + \omega_{min} \quad (10)$$

Where: ω_{max} and ω_{min} are the max and min weight of inertia value, $iter_{max}$ is the maximum number setting of iteration, and it defines as $\omega_{max} = 0.9$ and $\omega_{min} = 0.4$.

Moondee and Srirattanawichaikul (2019) introduced the constriction factor to upgrade the convergence of the proposed algorithm.

$$C = \frac{2}{\left|2 - \phi - \sqrt{\phi^2 - 4}\right|} \text{ where } 4.1 \leq \phi \leq 4.2 \quad (11)$$

When the factor C reduces, a convergence turns into gradual due to the variety population is decreased. To have a fast convergence, this paper determines $C = 0.352$.

3.3 Solving process

This work focuses on designing the developed tool by DIgSILENT PowerFactory and MATLAB as shown in

Figure 2 that applies the proposed algorithm, which implements to find the optimal capacitor placement in terms of minimization cost function containing power losses and capacitor installation. As shown, DIgSILENT PowerFactory is applied for built a distribution network modeling and analyzed power flow. The optimization process carries out with MATLAB software because it can develop to provide very flexible research for implementing the algorithms. The two software exchange information data and communicated with CSV file and there is an excel file called Flag that is applied to avoid the conflicted working of both software. Based on this approach, the developed tool is examined in the real distribution feeder of Savannakhet, and the proposed algorithm is verified the effectiveness which compares

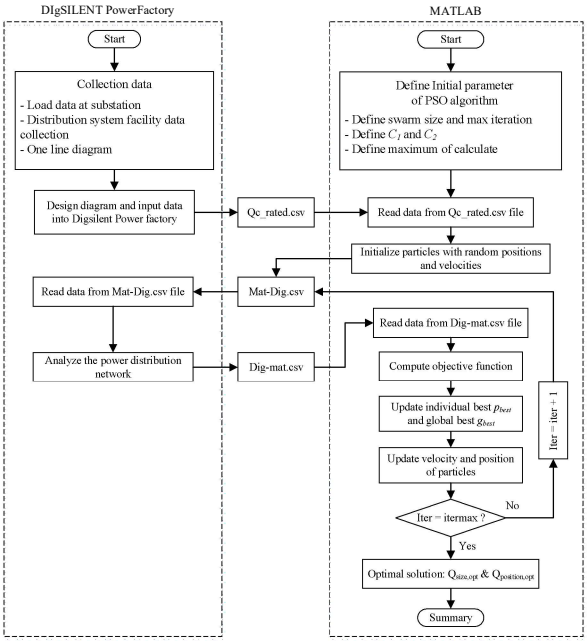

Figure 2 The process of the proposed approach by adopting particle swarm optimization algorithm

with genetic algorithm (GA). The proposed process describes as below:

Step 1: Model the distribution network, input data into DIgSILENT, and send the standard reactive power compensator size to MATLAB.

Step 2: Input PSO parameters include population sizes, weight of inertia, acceleration coefficients, maximum number of iterations.

Step 3: Initialize particle parameters with random the position and velocity.

Step 4: Send the random variables through Mat2Dig.csv file to DIgSILENT.

Step 5: Read the random variables and perform power flow analysis.

Step 6: Send the power flow results of each variable through Dig2Mat.csv file to MATLAB.

Step 7: Read the power flow results and evaluate the optimal values according to an objective function equation (8) and within the restricted conditions.

Step 8: Compare particles objective functions and update $P_{best,i}$ for each particle during the cycle and $G_{best,i}$ through all the particles.

Step 9: Following equation (11) is taking for updating velocity and position

Step 10: Repeat the loop until the maximum iteration.

Step 11: Report the optimal place of capacitor banks.

4. CASE STUDY AND DISCUSSION

In this section, the proposed technique to locate capacitor banks in power distribution system was explained above. The network model was simulated in DIgSILENT PowerFactory. MATLAB was implemented to perform optimization algorithm for achieving the optimum placed and sized of capacitors solution. The results of the study were presented and discussed.

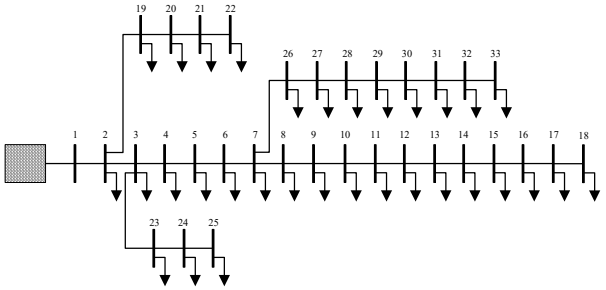

Figure 3 The schematic of IEEE 33-bus test system

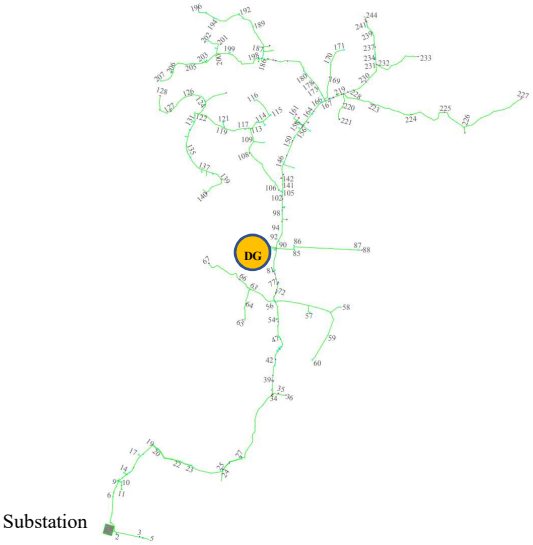

Figure 4 The topology of distribution feeder of Savannakhet province

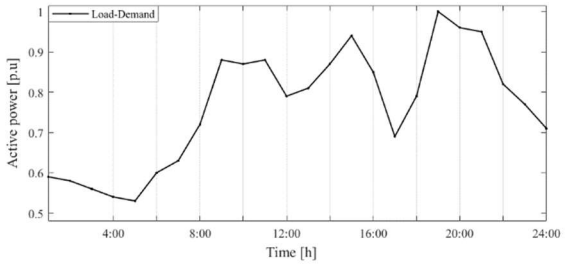

Figure 5 Daily load demand of Savannakhet distribution feeder

Table 1 Parameter of Savannakhet's power distribution feeder and sizes of capacitor bank for placement

Name	Unit	Variable
Peak load	MW	4.50
Power factor		0.85
Rate of distributed generator (DG)	MW	2.50
Capacitor size	kVAR / Unit	150 300 450 600 750 900 1050 1200

To achievement the objective and maximize profit there are some parameters that would be considered to calculate investment criteria including the capital cost of capacitor and distributed generator (DG) operation cost, which assumed as table below:

Table 2 Parameter cost for investment calculation

Descriptions	Price
Fixed capacitor ($/kVAR)	7
Switched capacitor ($/kVAR)	25
Installation capacitor bank ($/Unit)	750
The electricity price ($/kWh)	0.0937
Distributed generator (DG) operation cost ($/kWh)	0.06

4.1 Comparison results for the IEEE 33-Bus radial distribution network

Figure 3 illustrates the schematic of the test system, it comprises 33 buses and 32 lines, the first bus considers the substation bus which is retrieved from Díaz et al. (2018). The total active and reactive power demand connected to the system is 3.72 MW and 2.3 MVAR, respectively. The specification of capacitor bank includes the limit size and different capital cost which is applied from Jafari et al. (2020). Also, the consideration criteria include the constant load model and the objective function regarded only cost of loss and cost of capacitors. The proposed method conducts the simulation in the developed tool.

Table 3 shows the comparison results between the proposed PSO algorithm and some of the other algorithm for the optimal capacitor placement on IEEE 33-bus distribution network. The approach in literature consists of gravitational search algorithm (GSA), locust search algorithm (LS), and Hybrid algorithm (GA-GA), which has been brought up to consider in order to validate the effectiveness of the proposed PSO algorithm. As a result, before reactive power compensation, the power loss of the system is about 210.97 kW, and the annual cost is 35,443 $. Corresponding to the minimization problem the proposed approach can be determined the capacitor placement, which has been chosen allocation at bus 8, 14, 23, and 30, that determines the size as 300, 300, 300 and 1,050 kVAR, respectively. The reactive power compensation served by capacitors can be decreased the total power loss to 131.45 kW, which produces the net savings of about 12,804 $ or 36.16% compared with the uncompensated case. From Table 3, it can be seen that the PSO algorithm is greater effective than the other approach, including the proposed GA. Therefore, this approach would be applied to study the capacitor placement problem with the real power distribution system of Savannakhet in the next subsection.

4.2 Practical distribution system of Savannakhet modelling

To present the capacitor placement in the power distribution network, the network model in Figure 4 is used to examine the proposed method. The network model and load profile were received from the real 22 kV distribution feeder of Savannakhet province. The feeder comprises 244-bus and supplied to the rural area including a several type of consumers such as residential, industrial, and economic, etc. The distribution network parameter was listed in Table 1, defining that the peak load demand is 4.5 MW and power factor (PF) equals 0.85. It should be noted that the distributed generator (DG) rating 2.5 MW is taking into account in cases of with/without DG connected to the feeder and operate at unity power factor (PF). In addition, the standard size of capacitor banks for allocation were also defined. The load demand profile was obtained from real distribution feeder, it is shown in Figure 5.

4.3. Case study and Results

According to the network data and the permissible voltage of distribution system must be under ±5% of nominal voltage at 22kV as applying the capacitor bank for compensation the reactive power as described above. To obtain the condition of fixed and switched type of capacitor, this study applies 24 hours load data time day for model load variation in the distribution network in Figure 5. The case study divides in two cases, i.e., capacitor banks allocation without DG dispatched and capacitor placement with DG connected.

Table 3 The comparison of the different algorithm results for the IEEE 33-bus radial distribution network

	Base case	GSA	LS	Hybrid (GA-GA)	Proposed GA	Proposed PSO
Peak Loss [kW]	210.97	134.50	136.10	135.87	138.59	131.45
Reduction [%]	-	36.25	35.49	35.60	34.31	37.69
Optimum location	-	26, 13, 15	5, 8,11, 6, 24, 26, 30, 32	13, 29, 25	10, 30, 32	8, 14, 25, 30
Optimum size [kVAR]	-	350, 450, 800	150, 150,150,150, 450, 150,750, 150	350, 1200, 350	750, 300, 600	300, 300, 300, 1050
Total capacity of capacitor [kVAR]	-	1,600	2,100	1,900	1,650	1,950
Total cost of capacitor [$]	-	457	771	449	444	554
Cost Energy Loss [$/year]	35,443	22,596	22,865	22,826	23,283	22,085
Total annual cost [$/year]	35,443	23,053	23,636	23,275	23,727	22,639
Net Saving [$/year]	-	12,390	11,807	12,168	11,716	12,804
Net Saving [%]	-	34.96	33.31	34.33	33.06	36.16

4.3.1 The candidate bus by LSF

Firstly, the candidate bus for allocation reactive compensator devices were applied loss sensitivity factor (LSF), this analysis helps to decrease the exploration of the optimization problem. Corresponding to LSF performed the 15 buses in descending order which are possibility to install capacitors including {142, 159, 189, 132, 90, 122, 198, 24, 94, 220, 35, 114, 56, 241and 1}. Following the standard size of capacitor in Table 1, the optimal size would be determined by the optimization algorithms that indicates in the next sub-section.

4.3.2 Case installing OCP without DG connected

Table 4 presents the results of the distribution system before and after allocated the reactive power compensator in case of DG disconnected. The simulation results were validated comparing with genetic algorithm (GA). This table clarifies that the capacity of reactive power compensator of a total 3,900 kVAR is required in the GA method compared to 3,750 kVAR in the PSO algorithm. However, the power losses are least in the case of PSO algorithm, and it provides a reduction power loss at all load levels against base case 540.97 kW, 303.83 kW and 94.43 kW become 359.22kW, 226.72 kW and 128.60 kW, respectively. The proposed PSO algorithm shows better effectiveness than the genetic algorithm (GA) in terms of loss reduction and voltage improvement.

Figure 6 shows the simulation results of power losses reduction during daily period, which compared between base case, GA and proposed PSO algorithm. According to base case before compensation, it can be observed that the shunt capacitors can be reduced significantly power losses. Also, the power losses reduction is decreased slightly low in light load period, but it can reduce more during peak load demand especially in case of the proposed PSO method.

Figure 7 demonstrates the voltage profile of the distribution feeder at light load and peak load time, which is indicates the comparison between the uncompensated and the compensated reactive power by capacitor banks with the optimization algorithm. It can be observed that the bus voltage of base case is lower than the voltage permission limitation of all load level period and the worst bus voltage during peak load which is 0.80 p.u at bus 207. The capacitor placement with the proposed process can regulate the voltage profile during light load to peak load period that can be maintained under grid code and the worst bus voltage was 0.95 p.u at bus 244. Furthermore, the improved voltage profile of GA method is better than the PSO algorithm due to the high injected reactive power from capacitor banks.

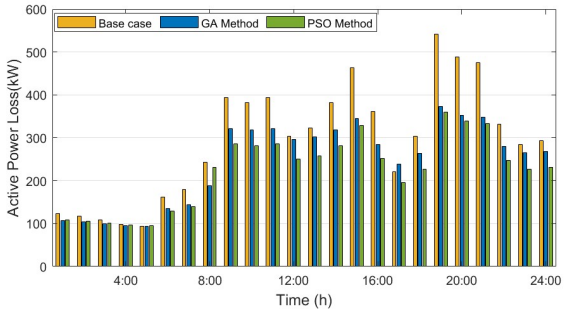

Figure 6 The comparison power losses in case without DG connected

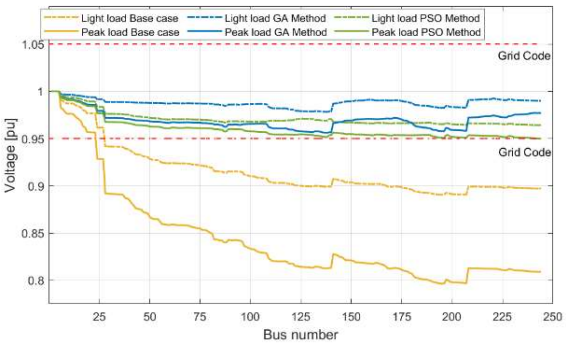

Figure 7 The comparison improved voltage profile of the power distribution system in case without DG connected

Table 4 The performance of power distribution feeder after compensated reactive power on each load level without DG connected

	Load level	S_{HV} (kVA)	Q_{HV} (kVAR)	Optimal capacitor placement			Ploss (kW)	Bus/ V_{max} (p.u)	Bus/ V_{min} (p.u)
				Location	Size (kVAR)	Total capacity (kVAR)			
Base case	Peak (1 p.u)	6,245	3,570	-	-	-	540.97	1.00/1	0.80/207
	Normal (0.75 p.u)	4,559	2,508	-	-	-	284.08	1.00/1	0.85/196
	Light (0.55 p.u)	3,450	1,854	-	-	-	161.33	1.00/1	0.89/196
Proposed GA	Peak (1 p.u)	4,972	-410.75	[56 122 159 220 241]	[450 450 900 1050 1050]	3,900	372.68	1.00/1	0.96/140
	Normal (0.75 p.u)	3,933	-1,034.50	[122 159 220 241]	[450 900 1050 1050]	3,450	265.70	1.02/241	0.99/36
	Light (0.55 p.u)	2,937	-551.73	[56 159 220]	[450 900 1050]	2,400	135.28	1.00/1	0.98/140
Proposed PSO	Peak (1 p.u)	4,946	-192.39	[90 94 132 189 198]	[900 450 900 900 600]	3,750	359.67	1.00/1	0.95/244
	Normal (0.75 p.u)	3,769	-316.25	[94 132 189 198]	[450 900 900 600]	2,850	226.72	1.00/1	0.97/244
	Light (0.55 p.u)	2,880	94.58	[132 189]	[900 900]	1,800	128.60	1.00/1	0.96/244

Table 5 The performance of power distribution feeder after compensated reactive power on each load level when distributed generator (DG) connected

	Load level	S_{HV} (kVA)	Q_{HV} (kVAR)	Optimal capacitor placement			Ploss (kW)	Bus/ V_{max} (p.u)	Bus/ V_{min} (p.u)
				Location	Size (kVAR)	Total capacity (kVAR)			
Base case	Peak (1 p.u)	3,757	2,978	-	-	-	208.75	1.00/1	0.86/196
	Normal (0.75 p.u)	2,454	2,181	-	-	-	96.20	1.00/1	0.91/196
	Light (0.55 p.u)	1,691	1,664	-	-	-	53.43	1.00/1	0.94/196
Proposed GA	Peak (1 p.u)	2,180	170	[35 142 198 220]	[450 900 450 900]	2,700	91.76	1.00/1	0.97/140
	Normal (0.75 p.u)	1,102	-203	[142 198 220]	[900 450 900]	2,250	54.32	1.01/208	0.99/140
	Light (0.55 p.u)	378	-244	[142 220]	[900 900]	1,800	38.16	1.02/208	1.00/1
Proposed PSO	Peak (1 p.u)	2,171	161	[90 94 189 198]	[900 900 450 450]	2,700	83.42	1.00/1	0.96/140
	Normal (0.75 p.u)	1,083	-192	[90 94 189]	[900 900 450]	2,250	36.93	1.01/90	0.99/207
	Light (0.55 p.u)	371	-247	[94 189 198]	[900 450 450]	1,800	26.90	1.02/94	1.00/1

4.3.3 Case installing OCP with DG connected

This case study considers the distributed generator (DG) synchronized to the power distribution and applied the optimization algorithms to allocate capacitor banks. In the same way as the previous case study, the proposed PSO algorithm has investigated the effectiveness compared with the genetic algorithm as shown in Table 5. The obtained results give that each method suggests installing the capacitor bank with the same capacity of 2,700 kVAR but the proposed algorithm performs better than GA, where the power losses at each load level period from peak load to light load can highly reduce that is 83.42 kW, 36.93 kW and 26.90 kW, respectively.

Figure 8 demonstrates a significant reduction in power loss, it can be observed that the PSO algorithm is highly capable of reducing power loss up to twice as compared to the base case. The reason is that the distributed generator and shunt capacitor placed along the feeder can respond the power near the load, which is helpful to assist substation to reduce drawing the power from the power grid and improving efficiency of power distribution system.

Figure 9 shows the voltage profile of the real distribution feeder with a distributed generator connected. As the base case that is only DG connected, it can be seen that cannot improve bus voltage within grid code, because of the topology of the distribution feeder that the load is far from the substation. Contrast, the reactive power compensation using proposed optimization algorithm provided the optimal location and size of shunt capacitor which can regulate the voltage profile maintained under permission limits.

4.2.4 Results and discussion

This study is implemented a real power distribution system to find out the optimal reactive power compensation, which purpose to evaluate the proposed PSO algorithm that compares effectiveness with the widely referred optimization technique as genetic algorithm (GA). Refer to Table 2 listed the capital cost for installing capacitor and the reduction power loss and total annual cost were obtained and listed in Table 6. In the case without DG connected, under uncompensated

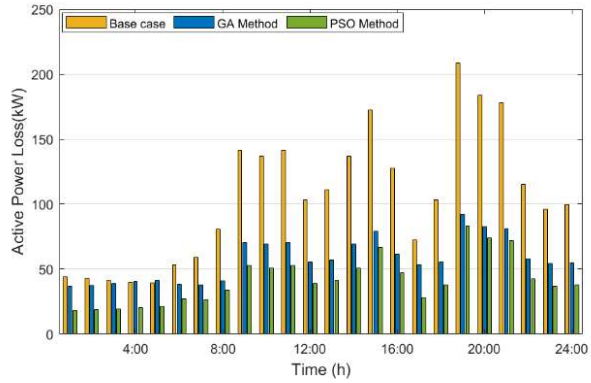

Figure 8 The comparison power losses in case DG connected

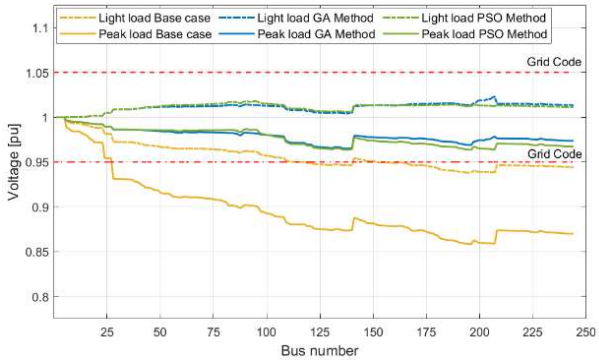

Figure 9 The comparison improved voltage profile of the power distribution system in case DG connected

reactive power the distribution system active loss was 540.97 kW, and a total annual cost was 241,799 $. The PSO algorithm provided the optimal capacity of the capacitor bank that reduced real power losses by 359.2 kW or 33.60% as compared to the base case, which leads to saving the cost of 7,350 $ per year of 3.04%. Moreover, in case DG connected the simulation result shows the base case carried power losses of 208.75 kW and the total annual cost in this case includes the annual cost of energy loss and the operation cost of DG which was approximately 175,039 $ per year. The proposed PSO algorithm shows the outcome that gave the greater net saving compared the genetic algorithm (GA) by reducing

Table 6 The comparison of experiment results for capacitor placement in the real distribution network 244-bus

		Case DG disconnected			Case DG connected		
		Base case	**GA Method**	**PSO Method**	**Base case**	**GA Method**	**PSO Method**
Peak Loss [kW]		540.97	377.36	359.22	208.75	91.761	83.421
Reduction [%]		-	30.24	33.60	-	56.04	60.04
Cost Energy Loss [$/year]		241,799	172,922	170,099	86,533	47,081	34,179
Optimum location of capacitor bank	**Fixed**	-	[159 220]	[132 189]	-	[142 220]	[94 189]
	Switched	-	[56 122 241]	[90 94 198]	-	[35 198]	[90 198]
Optimum size of capacitor bank [kVAR]	**Fixed**	-	[900 1050]	[900 900]	-	[900 900]	[900 450]
	Switched	-	[450 450 1050]	[900 450 600]	-	[450 450]	[900 450]
Total quantity of capacitor		-	5	5	-	4	4
Total capacity of capacitor [kVAR]		-	3,900	3,750	-	2,700	2,700
Total cost of capacitor [$]		-	65,400	64,350	-	36,600	46,200
Total cost of DG operation [$/year]		-	-	-	88,506	88,506	88,506
Total annual cost [$/year]		241,799	238,322	234,449	175,039	172,187	168,885
Net Saving [$/year]		-	3,477	7,350	-	2,852	6,155
Net Saving [%]		-	1.44	3.04	-	1.63	3.52

power losses and supporting the annual cost saving 6,155 $ or 3.52% as against the case of uncompensated reactive power as shown in Table 5. As a result, when DG connected to the distribution grid with capacitor operate simultaneously, it can be seen the potential of the distribution feeder improvement that can reduce power during on-peak, reduce line losses, and regulate voltage profile under allowable limitations. Even though the net saving of each case study was slightly low due to the capital cost of the capacitor bank being expensive, which relates to the number, capacity, and type of capacitor that would be required to support reactive power demand along the feeder. However, the reactive power compensation method provides the satisfied in terms of the power loss reduction and voltage profile. As well, the developed tool can be also accomplished implement the practical distribution system for conducting an installation capacitor following the planner.

5. CONCLUSION

This research presented the optimal capacitor placement in the power distribution system with DG connected to the Savannakhet area using the particle swarm optimization (PSO) algorithm. The developed tool implemented MATLAB software and DIgSILENT PowerFactory which purpose to verify the presented optimization algorithm. This tool has been examined with the real distribution system of Savannakhet province. The proposed algorithm was applied to determine the optimal capacitor allocation which the purpose to reduce power losses and minimize the installation cost of the capacitor. The loss sensitivity factor is adopted to decrease the dimension of the optimal results of the capacitor. Overall, the presented process has obtained the optimal location and size of the capacitor bank following the case study. The PSO algorithm has been provided most efficient in terms of the reduced power loss by up to 30% and it promoted increasing the annual net saving. The proposed PSO algorithm shows greater capabilities over the genetic algorithm (GA). This impact of the study will be implemented to improve the presented power system problem. Furthermore, the proposed optimization approach can develop the capability of the capacitor to study the coordinated volt/var control of the grid modernization application in the future.

6. ACKNOWLEDGEMENT

This research was sponsored by Electricity Generating Authority of Thailand (EGAT) and Electricity du Laos (EDL) under the project of academic collaboration. Furthermore, the author would like to be grateful to the Faculty of Engineering, Chiangmai University.

7. REFERENCES

Abul'Wafa, A. R. (2013). Optimal capacitor allocation in radial distribution systems for loss reduction: A two stage method. *Electric Power Systems Research*, *95*, 168-174.

Aman, M. M., Jasmon, G. B., Bakar, A. H. A., Mokhlis, H., & Karimi, M. (2014). Optimum shunt capacitor placement in distribution system—A review and comparative study. *Renewable and Sustainable Energy Reviews*, *30*, 429-439.

Baran, M. E., & Wu, F. F. (1989). Optimal capacitor placement on radial distribution systems. *IEEE Transactions on power Delivery*, *4*(1), 725-734.

Baran, M., & Wu, F. F. (1989). Optimal sizing of capacitors placed on a radial distribution system. *IEEE Transactions on power Delivery*, *4*(1), 735-743.

Cho, M. Y., & Chen, Y. W. (1997). Fixed/switched type shunt capacitor planning of distribution systems by considering customer load patterns and simplified feeder model. *IEE Proceedings-Generation, Transmission and Distribution*, *144*(6), 533-540. https://digital-library.theiet.org/content/journals/10.1049/ip-gtd_19971387.

Cook, R. F. (1961). Optimizing the application of shunt capacitors for reactive-volt-ampere control and loss reduction. *Transactions of the American Institute of Electrical Engineers. Part III: Power Apparatus and Systems*, *80*(3), 430-441.

Díaz, P., Pérez-Cisneros, M., Cuevas, E., Camarena, O., Martinez, F. A. F., & González, A. (2018). A swarm approach for improving voltage profiles and reduce power loss on electrical distribution networks. *IEEE Access*, 6, 49498-49512.

Hung, D. Q., Mithulananthan, N., & Bansal, R. C. (2015). A combined practical approach for distribution system loss reduction. *International Journal of Ambient Energy*, *36*(3), 123-131.

Jafari, A., Ganjehlou, H. G., Khalili, T., Mohammadi-Ivatloo, B., Bidram, A., & Siano, P. (2020). A two-loop hybrid method for optimal placement and scheduling of switched capacitors in distribution networks. *IEEE Access*, *8*, 38892-38906.

Moondee, W., & Srirattanawichaikul, W. (2019, October). Reactive Power Management of MV Distribution Grid with Inverter-based PV Distributed Generations using PSO Algorithm. *In IECON 2019-45th Annual Conference of the IEEE Industrial Electronics Society* (pp. 2239-2244). IEEE.

Ng, H. N., Salama, M. M. A., & Chikhani, A. Y. (2000). Classification of capacitor allocation techniques. *IEEE Transactions on power delivery*, *15*(1), 387-392.

Nojavan, S., Jalali, M., & Zare, K. (2014). Optimal allocation of capacitors in radial/mesh distribution systems using mixed integer nonlinear programming approach. *Electric Power Systems Research*, *107*, 119-124.

Prakash, K., & Sydulu, M. (2006, October). A novel approach for optimal location and sizing of capacitors on radial distribution systems using loss sensitivity factors and/spl alpha/-coefficients. *In 2006 IEEE PES Power Systems Conference and Exposition* (pp. 1910-1913). IEEE.

Shuaib, Y. M., Kalavathi, M. S., & Rajan, C. C. A. (2015). Optimal capacitor placement in radial distribution system using gravitational search algorithm. *International Journal of Electrical Power & Energy Systems*, *64*, 384-397.

Singh, S. N., & Yadagiri, J. (2009, November). Application of advanced particle swarm optimization techniques to wind-thermal coordination. *In 2009 15th International Conference on Intelligent System Applications to Power Systems* (pp. 1-6). IEEE.

Singh, S. P., & Rao, A. R. (2012). Optimal allocation of capacitors in distribution systems using particle swarm optimization. *International Journal of Electrical Power & Energy Systems*, *43*(1), 1267-1275.

Su, C. T., & Tsai, C. C. (1996, December). A new fuzzy-reasoning approach to optimum capacitor allocation for primary distribution systems. *In Proceedings of the IEEE International Conference on Industrial Technology (ICIT'96)* (pp. 237-241). IEEE.

World Bank Group. (2018). Electric power transmission and distribution losses (% of output). Retrieved from: https://data.worldbank.org/indicator/EG.ELC.LOSS.ZS.

Shaheen, A. M., & El-Sehiemy, R. A. (2020). Optimal coordinated allocation of distributed generation units/capacitor banks/voltage regulators by EGWA. IEEE Systems Journal, 15(1), 257-264.

NUEJ
Naresuan University
Engineering Journal

Ground-Level Ozone Pollution in Upper Northern, Thailand : An ArcGIS-Based Approach

Supawan Srirattana

Department of Civil Engineering, Faculty of Engineering, Naresuan University, Phitsanulok, Thailand

Corresponding author e-mail: supawansri@nu.ac.th

(Received: 15 February 2022, Revised: 9 May 2022, Accepted: 20 May 2022)

Abstract

Ground-level ozone in the air we breathe even relatively low levels can cause health effects. Thus, it is important to analyze the spatial-temporal ozone concentrations. The IDW interpolation technique by ArcMap 10.5® software was used to simulate and access ground-level ozone data in areas where without ambient air quality monitoring stations in 8 provinces (Chiang Rai, Chiang Mai, Phrae, Nan, Phayao, Lampang, Lamphun, and Mae Hong Son) during the year 2017 – 2019. The ground-level zone input data were obtained from the pollution control department, Thailand. The Mean Error (ME) and Root Mean Squared Error (RMSE) were used to find the most suitable power for IDW interpolation. The IDW interpolation with power 3 was represented the best condition. IDW interpolation of monthly maximum 1-hour reveal that orange and red were found as the major of AQI colors in all 8 provinces. Orange was found in every province, while red was only distributed in Chiang Rai and some areas in Chiang Mai during ozone crisis (February to June). For monthly maximum 8-hour, AQI ratings were ranging from green to purple, and most areas were faced with ozone pollution in the red to the purple. Nevertheless, July to January was rarely reached a high level of ozone. Additionally, the IDW interpolation map of Chiang Mai in May 2017 was chosen for discussion as an example to converted data from 2D - spatiotemporal interpolation map to the number of sub-districts in which ozone AQI levels were got to the unhealthy zone.

Keywords: Ground-Level Ozone, ArcGIS, Spatial Interpolation, Inverse Distance Weighted.

1.Introduction

Ozone (O_3), a gas composed of three atoms of oxygen, is one of the six common air pollutants indicated in the Clean Air Act, and its level in ambient air needs to be decreased based on health criteria (US. EPA, 2021). Ozone can be "good" or "bad" for the environment and human health depending on where it is found in the atmosphere (US. EPA, 2021). Good ozone or Stratospheric ozone, which can protect living things from ultraviolet radiation from the sun, is found in the Stratosphere (US. EPA., 2021a). Eq.1 – Eq.4 illustrates the ozone formation in the Stratosphere. Ozone forms readily as incoming ultraviolet (UV) radiation can readily destroy two oxygen atoms of an oxygen molecular into atomic oxygen (a single atom) (National Aeronautics and Space Administration, 2003). Afterward, atomic oxygen can combine with an oxygen molecule to form ozone. Moreover, sunlight can readily split ozone into an oxygen molecule and an individual oxygen atom which is ready to form a new molecule of ozone again. Bad ozone or tropospheric ozone, found in ground-level where humans live, is found in the Troposphere (US. EPA., 2021a). Ground-level Ozone is a destructive air pollutant, because of its effects on a variety of health problems and the environment (US. EPA., 2021a). People with asthma, children, older adults are at greatest risk from breathing air containing ozone especially children because their lungs are still developing (US. EPA., 2021b). Moreover, ground-level ozone in high amounts can cause serious health issues, such as chronic lung disorders like bronchitis and cancer (Stockholm Environment Institute, 2021). In the troposphere near the Earth's surface, ozone is formed by two origins. Eq.5 – Eq.8 illustrates the ozone formation in the Troposphere. Firstly, ozone forms through the splitting of molecules by sunlight as it does in the stratosphere (National Aeronautics and Space Administration, 2003). Secondly, ozone is formed by chemical reactions between oxides of nitrogen (NOx) and volatile organic compounds (VOC) emitted by the burning of fossil fuels, cars, power plants, industrial boilers, refineries, chemical plants, and other sources, as well as some natural sources react in the presence of sunlight (US. EPA, 2021). Burning fossil fuels is also the main driver of climate change. Climate change is a rise in global and local temperatures. Climate change causes temperatures to climb, more ozone pollution is formed because the warmer the air, the faster the chemical reaction that creates ozone (State of Global Air, 2020). Moreover, ozone is also a greenhouse gas and is now 30–70% higher than 100 years ago (State of Global Air, 2020).

Chemistry of Ozone formation in the Stratosphere:

$$O_2 + \text{UV (Sunlight)} \rightarrow O + O \quad (1)$$

$$O + O_2 \rightarrow O_3 \quad (2)$$

$$O_3 + UV\ (Sunlight) \rightarrow O + O_2 \quad (3)$$
$$O + O_3 \rightarrow O_2 + O_2 \quad (4)$$

Chemistry of Ozone formation in the Troposphere:

$$NO_2 + UV\ (Sunlight) \rightarrow NO + O \quad (5)$$
$$NO_2 + VOC + UV\ (Sunlight) \rightarrow O_3\ (and\ other\ products) \quad (6)$$
$$O + O_2 \rightarrow O_3 \quad (7)$$
$$+ O_3 \rightarrow NO_2 + O_2 \quad (8)$$

Thailand has seen ground-level ozone exceeding the Thailand National Ambient Air Quality Standard (TNAAQS) value of 1-hour and 8-hour as 100 and 70 parts per billion (ppb) (Table 1) countrywide over the last 10 years especially during the summer season (Pollution Control Department, 2020). It is normal to detect a higher level of ground-level ozone during the summer as high temperatures and sunlight are the catalysts for an increase in the ground-level ozone (Asian Institute of Technology, 2020; US. EPA, 2021). Thailand has an average temperature of about 30°C with a tropical climate (Viroat Srisurapanon & Chana Wanichapun, 2019). Northern Thailand faces high levels of particulate matter ($PM_{2.5}$ and PM_{10}), VOCs, and ground-level ozone from January to April for more than 10 years, which is the dry season, when wildfires are common and agricultural burning takes place (Pollution Control Department, 2020; Stockholm Environment Institute, 2021). Furthermore, topography and weather conditions like solar radiation, rain, temperature, wind speed, and air pressure play an important role in determining the concentration of pollutants (Stockholm Environment Institute, 2021). For example, on March 10, 2020, at the Chiang Mai provincial government center monitoring station has been observed the level of the maximum 8-hour average value of ozone was as high as 86 ppb, reaching a maximum value at 117 ppb, thus exceeding the TNAAQS (70 ppb) up to 1.67 times (Asian Institute of Technology, 2020; Pollution Control Department, 2020). Ekbordin Winijkul, an Asian Institute of Technology atmospheric scientist whose work focuses on PM 2.5 and other air pollution, has suggested people in northern Thailand should avoid outdoor activities during the summer daytime for reducing high risks or health problems (Asian Institute of Technology, 2020).

Currently, only 14 ambient air quality monitoring stations (AAQMS) in 8 provinces (758 sub-district) across upper northern Thailand can monitor, record, and report ground-level ozone (Pollution Control Department, 2021) as illustrated in Figure 1(a) and 1(b) and Table 2. It should be noted that AAQMS does not cover all areas. The ozone concentration was measured in part per billion (ppb). AAQMS have typically been installed in urban areas where population density is high or industrial areas (Beelen et al., 2009; Bell, 2006). GIS is a computer-based tool for mapping and analyzing the geographic phenomenon that exists and occurs on earth (Mishra et al., 2015). GIS is not only innovative and important component of many projects for public health and epidemiology studies but also plays a vital role in the planning of air quality management (Mishra et al., 2015). GIS has been used to identify risks of exposure to air pollutants at the community level (Hammond et al., 2011; Rytkönen, 2004). For example, mortality rates from toxic air pollutants were calculated using the number of people exposed to pollution at the census area unit level (Mishra et al., 2015). Interpolation technique in GIS is an optional technique to predict the value of attributes at non sites from measurements made at point locations within the same area (Sajjadi et al., 2017) by specifying search distance, closest points, power setting, and barriers (Bartier & Keller, 1996; GISGeography, 2021; Gong et al., 2014; Pinichka et al., 2017a; Rojas-Avellaneda, 2007; Weber & Englund, 1992). Evaluations of interpolation techniques have been determined across environmental disciplines (Simpson & Wu, 2014) such as rainfall (Jeffrey et al., 2001; Willmott et al., 1985), wind velocity (Jarvis & Stuart, 2001), air temperatures (Jarvis & Stuart, 2001), evapotranspiration studies (Willmott, 1982), air pollution exposure (Mishra et al., 2015; Sajjadi et al., 2017), and others. However, evaluations of interpolation involving ozone data is rarely studied and never has a study such as this occurred in the in the upper northern, Thailand.

Therefore, this study has two goals. First, we would like to use a mathematical model via IDW interpolation technique by ArcMap 10.5® software to simulate and access ground-level ozone data in areas where without AAQMS in 8 provinces in upper Northern, Thailand (Chiang Rai, Chiang Mai, Phrae, Nan, Phayao, Lampang, Lamphun, and Mae Hong Son) during the year 2017 – 2019. Second, we converted the IDW interpolation data (2D - Spatiotemporal Interpolation map) to the number of sub-districts in which ozone AQI levels were got to the unhealthy zone.

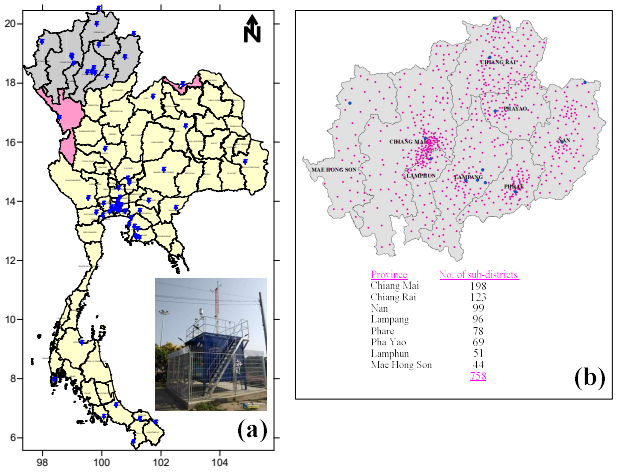

Figure 1 (a)Ambient air quality monitoring stations in Thailand (blue markers), (b) 758 sub-districts (pink markers) in 8 provinces

Table 1 National Ambient Air Quality Standard (NAAQS) for Ozone

Parameter		Value
Thailand	1-hour	100 ppb (200 µg/m^3)
	8-hour	70 ppb (140 µg/m^3)
EPA	1-hour	120 ppb (235 µg/m^3)
	8-hour	70 ppb (140 µg/m^3)
O_3 1 ppb = 2.00 µg/m^3		

2. METHODOLOGY

2.1 Study Area and Input Data

Figure 1(a) shows the positions of 14 AAQMS and study areas in 8 provinces in the north of Thailand. These stations are operated under the supervision of the division of air quality and noise management bureau, pollution control department, Thailand. Measurement of ozone according to the standard method by ultraviolet light metering (Pollution Control Department, 2022). The coordinate longitude and latitude were used for specifying the location of each monitoring station (Table 2). The ground-level zone input data were the monthly averages maximum of 1-hour and 8-hour during 2017–2019 (Table S1 – S6 and Figure S1 – S2 in supporting information (SI)). Moreover, we also use the data from 2 monitoring stations outside the main study area (Tak and Nong Khai province) (Pink area in Figure 1(a)) to obtain more reliable results in the southern part of Mae Hong Son, Chiang Mai, Lamphun, Lampang, Phrae, and in the eastern part of Nan where have no AAQMS. Forasmuch, the IDW interpolation technique is based on the proximity of neighboring stations to the target station (Wuthiwongyothin et al., 2021).

Table 2 Description of ambient air quality monitoring stations (Pollution Control Department, 2021)

No.	Station	ID	Lat.	Long.
1	Chiang Rai	57T	19.90921	99.82334
2	Chiang Rai	73T	20.42738	99.88371
3	Chiang Mai	36T	18.84075	98.96974
4	Chiang Mai	41T	18.79090	98.98813
5	Nan	67T	18.78880	100.77640
6	Nan	75T	19.57592	101.08158
7	Pha Yao	70T	19.20027	99.89285
8	Phare	69T	18.12886	100.16240
9	Mae Hong Son	58T	19.30462	97.97161
10	Lampang	37T	18.27823	99.50649
11	Lampang	38T	18.25074	99.76399
12	Lampang	39T	18.41963	99.72650
13	Lampang	40T	18.28278	99.65912
14	Lamphun	68T	18.56734	99.03862
15	Tak	76T	16.73445	98.56696
16	Nong Kahi	82T	17.87790	102.72861

2.2 Colored Bar of the Ground-level Ozone Risk Map

Risk map colors use color-coded criteria from Air Quality Index (AQI) of the United State. Because Thailand has a benchmark of only 8-hour, but not for 1-hour (Figure 2). The meaning of AQI colors has been described in Figure 3. The AQI uses colors, numbers, and words to tell people about the air quality (AirNow, 2022). The AQI is divided into six categories. Each category corresponds to a different level of health concern. Each category also has a specific color. The color makes it easy for people to quickly determine whether air quality is reaching unhealthy levels in their communities (AirNow, 2021). AQI is a color rating that runs from 0 to 500. The higher the AQI value, the greater the level of air pollution and the greater the health concern. For example, an AQI value of 50 or below represents good air quality, while an AQI value over 300 represents hazardous air quality (AirNow, 2021).

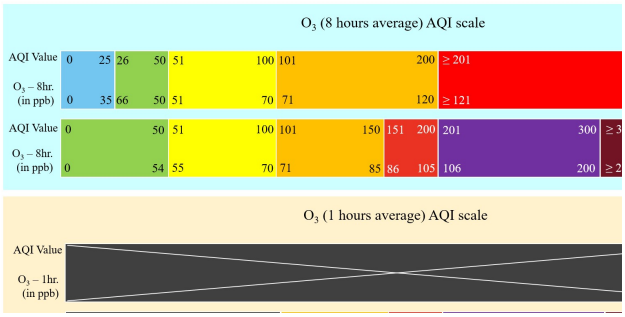

Figure 2 AQI ratings of Thailand and the US

Daily AQI	Color Levels of Concern	Values of Index	Description of Air Quality
Green	Good	0 to 50	Air quality is satisfactory, and air pollution poses little or no risk.
Yellow	Moderate	51 to 100	Air quality is acceptable. However, there may be a risk for some people, particularly those who are unusually sensitive to air pollution.
Orange	Unhealthy for Sensitive Groups	101 to 150	Members of sensitive groups may experience health effects. The general public is less likely to be affected.
Red	Unhealthy	151 to 200	Some members of the general public may experience health effects; members of sensitive groups may experience more serious health effects.
Purple	Very Unhealthy	201 to 300	Health alert: The risk of health effects is increased for everyone.
Maroon	Hazardous	301 and higher	Health warning of emergency conditions: everyone is more likely to be affected.

Figure 3 AQI ratings and Description of US (AirNow, 2021)

2.3 The Evaluation Method for the Accuracy of Spatial Interpolation

The error statistics used in this paper are: Mean Error (ME) and Root Mean Squared Error (RMSE). ME is used for determining the degree of bias in the estimates often referred to as the bias. Since positive and negative estimates counteract each other, the resultant ME tends to be lower than the actual error prompting caution in its use as an indicator of accuracy (Maduako et al., 2017). RMSE provides a measure of the error size, but it is sensitive to outliers as it places a lot of weight on large errors (Maduako et al., 2017). They are defined as follows in Eq.9 – Eq.10 (Royal Irrigation Department, 2018):

$$ME = \frac{1}{n}\sum_{i=1}^{n}(x_i - x) \quad (9)$$

$$RMSE = \sqrt{\frac{1}{n}\sum_{i=1}^{n}(x_i - x)^2} \quad (10)$$

Where n is the number of observations, xi is the observed value at location xi, and x is the interpolated value at location xi (Maduako et al., 2017; Qiao et al., 2018; Royal Irrigation Department, 2018).

2.4 ArcGIS: Spatial Interpolation Using Inverse Distance Weighting (IDW)

The study involved integrating data from in-situ measurements (AAQMS) of ozone concentration into digital map layers to determine the spatial variations. The coordinate longitude and latitude tool helped identify various households in which the data were obtained and processed in excel format for use in GIS software (ESRI, ArcMap 10.5®).

In this study, the generation of spatial objects and their attributes, geospatial analysis (IDW) technique was performed to calculate the value of each cell at locations without AAQMS. IDW interpolation is easy to apply, less time consuming, and requires inexpensive computation than more complicated methos (Wuthiwongyothin et al., 2021). IDW interpolation is one of the best ways to estimate unknown values by specifying search distance, closest points, power setting, and barriers (GISGeography, 2021; Kravchenko & Bullock, 1999; Li et al., 2016; Robichaud & Ménard, 2014) and largely used for creating continuous data when data are collected at discrete locations in a GIS (Akkala et al., 2010). IDW interpolation assuming closer values are more related than further values with its function (GISGeography, 2021). For example, the red points have known concentration values, the other points will be interpolated (Figure 4). Accordingly, if you need to measure the purple point, you can set up your interpolation so that it takes a fixed or variable number of points. Therefore, it uses a fixed number of points of 3 and uses the three closest points. The main factor affecting the accuracy of IDW is the value of the power parameter (Isaaks, 1989). The general formula of the IDW interpolation method is defined as follow in Eg.11 (Eldrandaly & Abu-Zaid, 2015; GISGeography, 2021; Li et al., 2016):

$$Z_p = \frac{\sum_{i=1}^{n}\left(\frac{Z_i}{d_i^p}\right)}{\sum_{i=1}^{n}\left(\frac{1}{d_i^p}\right)} \quad (11)$$

Where Z_p is the interpolated value at the unknown (or unsampled) location (x, y), n is the number of nearest known points surrounding (x, y), Z_i are the observed values at the nearest known points of (x_i, y_i), di are the distances between each (x_i, y_i) and (x, y), p is the specified power which controls the degree of local influence (Eldrandaly & Abu-Zaid, 2015; GISGeography, 2021; Li et al., 2016).

An important considerations that were required prior to the use of IDW interpolation was the power value (Munyati & Sinthumule, 2021). The power parameter can be chosen based on error measurement (e.g., Mean Error (ME) and Root Mean Squared Error (RMSE)), resulting in optimal IDW (Isaaks, 1989). The most reasonable IDW interpolation results are obtained using power parameter values from 0.5 to 3 (Munyati & Sinthumule, 2021). Please note that the method is suitable to evaluate for events that already happened (Li et al., 2016).

2.5 Linking Ozone to Community Level

As is evident from Figure 1(b), the study areas in 8 provinces consist of a total of 758 sub-districts, spread over an area of 85,852.40 square kilometers (Energy Policy and Planning office, 2022). In this section, the IDW interpolation data were converted to the number of sub-districts where at risk of exposure to ground-level ozone. The shapefile data of 758 sub-districts was used to identify the location of the each 758 sub-district obtained from Chontanat Suwan (2022) (Chontanat Suwan, 2022) (pink markers in Figure 1(b)). The shapefile is a geospatial data format for use in geographic information system (GIS) software (United States Census Bureau, 2022). Moreover, we also analyze the population with unhealthy ozone exposure. The current population of 8 provinces in the upper northern is 5,874,503 (Table S7) as of December 31, 2021, based on the Bureau of Registration Administration (BORA), Thailand data (Bureau of Registration Administration, 2021). We assumed the proportions of population located within each grid to have been exposed to the same pollutant concentrations in the grid cells (Pinichka et al., 2017b).

3. RESULTS AND DISCUSSION

3.1 The Accuracy of IDW Spatial Distribution Method

The significant of this section is to find the most suitable power for IDW interpolation. Table 3 illustrates the level of bias in estimation for IDW interpolation with power 1 to 3 (p=1 to p=3). The lower value of ME and RMSE for each interpolation method indicates the optimality of that method (Sajjadi et al., 2017). The results revealed that power 3 (p=3) provided better performance than the power 1 (p=1). Through the comparison of power 1 to power 3, we had known that the level of bias in estimation is lowest for power 3 (p=3) and highest for power 1 (p=1) as indicated by the respective ME and RMSE. A negative result indicates that the prediction has been achieved with a value that is lower than the actual value (Royal Irrigation Department, 2018). On the other hand, A positive result indicates that the prediction has been achieved with a value that is higher than the actual value (Royal Irrigation Department, 2018). The results were the same as in previous studies of Munyati

et al (2021), higher power value puts more weightage on the nearest data points, means that nearby data will have

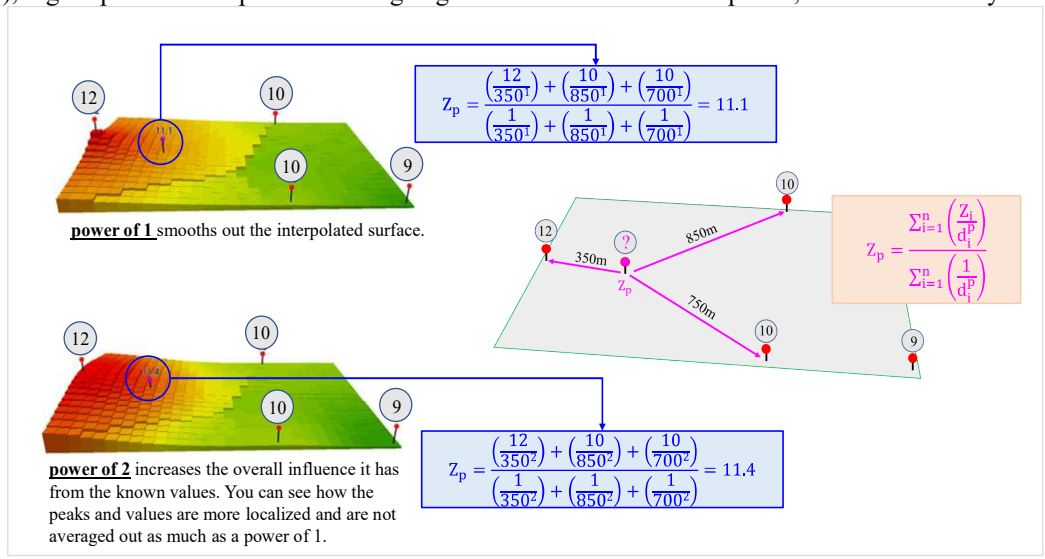

Figure 4 Inverse Distance Weighting (IDW) Interpolation (GISGeography, 2021)

the most influence (Munyati & Sinthumule, 2021). Therefore, IDW with Power 3 (p=3) was utilized in this study to generate all maps of ground-level ozone interpolation in section 3.2.

Table 3 The level of bias in estimation for IDW interpolation with power 1 to 3

Data Set		IDW- Power 1		IDW- Power 2		IDW- Power 3	
		Min. (ppb)	Max. (ppb)	Min. (ppb)	Max. (ppb)	Min. (ppb)	Max. (ppb)
1	Actual: Xi	77	112	77	112	77	112
	Predicted: X	77.8269	110.7949	77.0037	111.9733	77.0000	111.9993
2	Actual: Xi	60	129	60	129	60	129
	Predicted: X	61.1308	128.1412	60.0042	128.9982	60.0000	129.0000
3	Actual: Xi	69	97	69	97	69	97
	Predicted: X	69.9159	96.5726	69.0056	96.9977	69.0000	97.0000
n		3	3	3	3	3	3
ME		-0.9579	0.8304	-0.0045	0.0103	0.0000	0.0002
RMSE		1.6591	1.4384	0.0078	0.0178	0.0000	0.0004

3.2 IDW Interpolation

The using of mathematical model via IDW interpolation technique by ArcMap 10.5® software to simulate and access ground-level ozone data in areas where without AAQMS in 8 provinces in upper Northern, Thailand during the year 2017 – 2019 is the first goal of this paper. Figure 5 and Figure 6 show the generated maps of the monthly maximum of 1-hour and 8-hour during 2017–2019 predicted using IDW interpolation technique of the study area in 8 provinces.

3.2.1 Monthly Maximum 1-hour Average Value of Ozone

As can be seen from Figure 5, the data reveal that orange (unhealthy for sensitive groups; 125 - 164 ppb) and red (unhealthy; 165 - 204 ppb) were found as the major of AQI colors in all 8 provinces. Anywise, ozone was never seen the AQI get to purple and maroon. It can be observed that every province was faced with orange zone, but the red zone was only distributed in Chiang Rai and some areas in Chiang Mai. February to June (summer season) shows more unhealthy zones than other months since temperature is one of the elements which impacts ozone production, increased temperature also means increased ozone (State of Global Air, 2020; US. EPA, 2021). The temperature profile of 8 provinces was shown in Figure S3 in SI (Weather Spark, 2022). Nevertheless, July to January was rarely reached a high level of ozone.

3.2.2 Monthly Maximum 8-hour Average Value of Ozone

In this section, IDW interpolation map of monthly maximum 8-hour average value of ozone will be discussed. The AQI ratings of ozone were ranging from green (good: 0 to 50 ppb), yellow (moderate: 51 to 100 ppb), orange (unhealthy for sensitive groups; 101 - 150 ppb), red (unhealthy; 151 to 200 ppb), and purple (very unhealthy; 201 to 300 ppb), respectively (Figure 6). February to May, almost all areas were faced with ozone pollution in the red to the purple zone over the period of 3 years, like in case of the monthly maximum 1-hour average in section 3.2.1. From the data, during the ozone crisis, people living in Chiang Mai, Lampang, Phare and Mae Hong Son were significantly more health risks from ozone exposure than other provinces due to the AQI get to purple color. Nevertheless, July to January was found relatively high correlation of yellow and green, while the orange zone was found slightly.

In summary, it is apparent that the green zone was found only in 2017 (June to September), the yellow zone was encountered for 4-month in 2017, 7-month in 2018, and 3-month in 2018, the orange zone was suffered for 2-month in 2017 and 2018 and 5-month in 2018, the red zone was detected for 2-month in 2017 and 2018, and 4-month in 2018, and the purple zone was discovered for 2-month in 2017 and 1-month in 2019, respectively.

3.3 Linking Ozone to Community Level

The second goal of this paper is to convert the IDW data (2D - Spatiotemporal Interpolation map) from section 3.2 to the number of sub-districts in which ozone AQI levels were got to the unhealthy zone. However, the data conversion must be converted on a case by case. Thus, the total cases are 576 cases (288 cases for 1-hour and 288 cases for 8-hour (3-year x 12-month x 8-province = 288 cases)). Therefore, this study cannot present the calculations for the entire of 576 cases. Consequently, at this article, Chiang Mai in May 2017 was chosen to debate as an example.

3.3.1 Monthly Maximum 1-hour Average Value of Ozone

In May 2017, 12 sub-districts of Chiang Mai province including 1) Mae Ai, 2) Ron Mae Sao, 3) Son Ton Mue, 4) Wiang, 5) Mon Pin, 6) Mae Ngon, 7) Sansai, 8) Mae Kha, 9) Pong Nam, 10) Pong Tam, 11) Si Dong Yen, and 12) Mae Thalop, respectively (accounting for 7.48% of Chiang Mai's population (133,873 people)) were got in orange zone (unhealthy for sensitive groups). Furthermore, 3 sub-districts including 1) Tha Ton, 2) Mae Na Wang, and 3) Ban Luang (accounting for 1.99% of Chiang Mai's population (35,569 people)) were got in red zone (unhealthy). The details were presented in Figure 7 and Table 4.

3.3.2 Monthly Maximum 8-hour Average Value of Ozone

In May 2017, 15 sub-districts of Chiang Mai province including 1) Pong Nam Ron, 2) Mon Pin, 3) Wiang, 4) San Sai, 5) Mae Kha, 6) Mae Ngon, 7) San Ton Mue, 8) Ban Luang, 9) Mae Ai, 10) Nong Bua, 11) Mae Thalop, 12) Si Dong Yen, 13) San Sai, 14) Pa Nai, and 15) Pa Tum, respectively (accounting for 9.66% of Chiang Mai's population (172,837 people)) were got in orange zone. In addition, 2 sub-districts including Tha Ton and Mae Na Wang (accounting for 1.55% of Chiang Mai's population (27,806 people)) were got in red zone (unhealthy). The details were demonstrated in Figure 8 and Table 5.

4. CONCLUSION

The mathematical model via IDW interpolation technique by ArcMap 10.5® software can used as an alternative method to simulate and access ground-level ozone data in areas were without AAQMS. This technique has been used in other research to forecast alert pollutant levels, assessment of relationships between air pollutant exposure and health outcomes, alternative for epidemiological analyses at the individual-level on the health effects for locations without authentic data (Jung et al., 2016; Mishra et al., 2015), for example. The IDW interpolation with Power 3 (p=3) was represented the best condition of this study via Mean Error (ME) and Root Mean Square Error (RMSE) equations.

The ground-level ozone concentrations in 8 provinces in upper Northern, Thailand (Chiang Rai, Chiang Mai, Phare, Nan, Phayao, Lampang, Lamphun, and Mae Hong Son) during the year 2017 – 2019 were usually high in the summer (February to June) because temperature is one of the elements which impacts ozone production (State of Global Air, 2020; US. EPA, 2014, 2021), while July to January was found at a safe level for both 1-hour and 8-hour. The highest AQI ratings of monthly maximum 1-hour average value of ozone was red (unhealthy; 165 - 204 ppb), while 8-hour average value of ozone was purple (very unhealthy; 201 to 300 ppb). From the data, during the ozone crisis, people should spend more time indoors than outdoors to avoid the health effect from ozone, especially those who are sensitive (US. EPA, 2014). This is because ozone levels are higher outdoors, and physical activity causes faster and deeper breathing, drawing more ozone into the body (US. EPA., 2014).

Lastly, on behalf of the researcher, I sincerely hope that the authorities or government agencies should not ignore the ground-level ozone pollution. Additionally, I hope this article will be helpful for stakeholders or sensitive groups can utilize this information for initial assessment of relationships between ground-level ozone exposure and health outcomes, provide useful basic information for authorities to improve strategy formulation to choose appropriate locations for future AAQMS in Thailand, respectively.

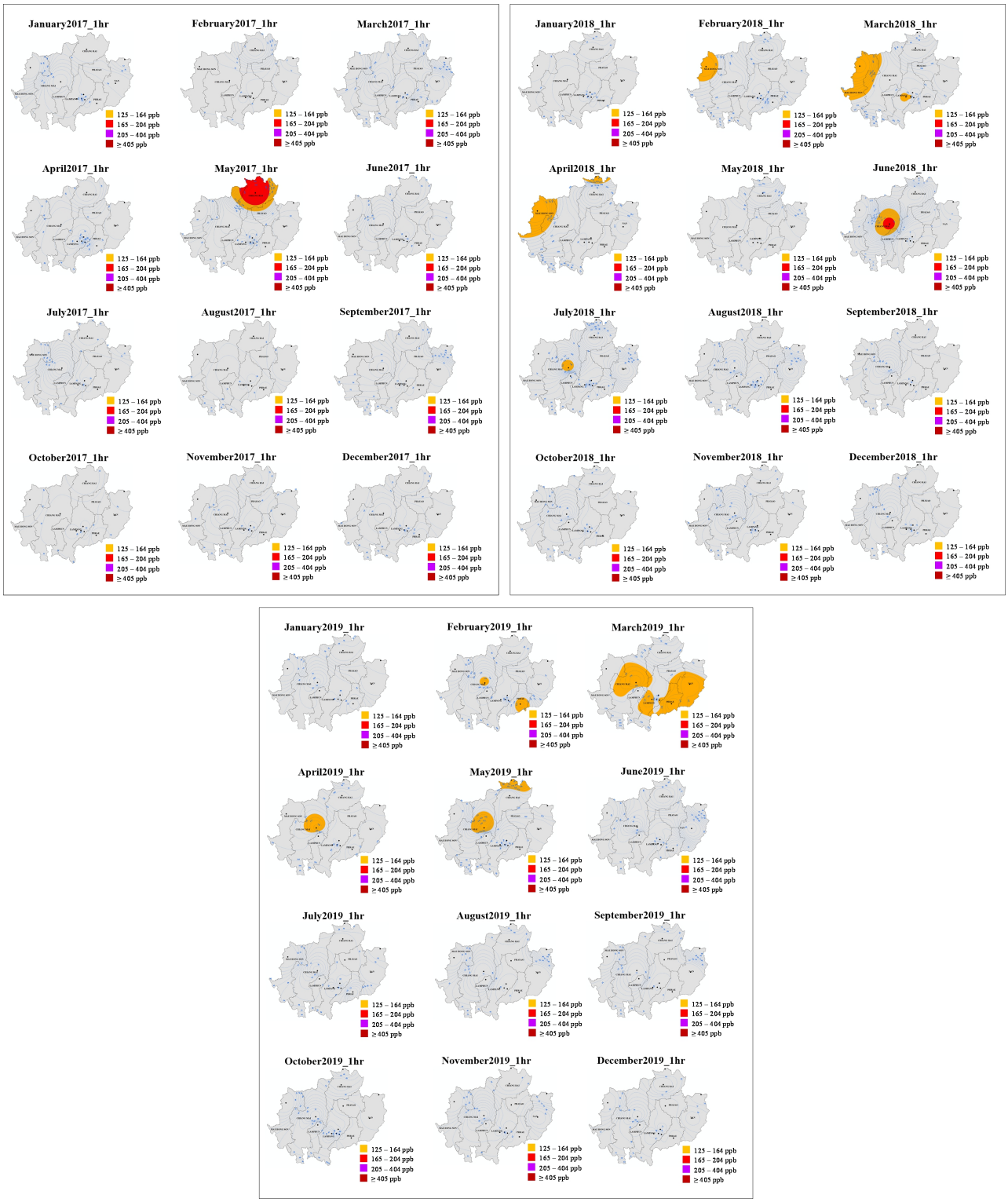

Figure 5 IDW interpolation map of monthly maximum 1-hour average value of ozone in 2017 – 2019

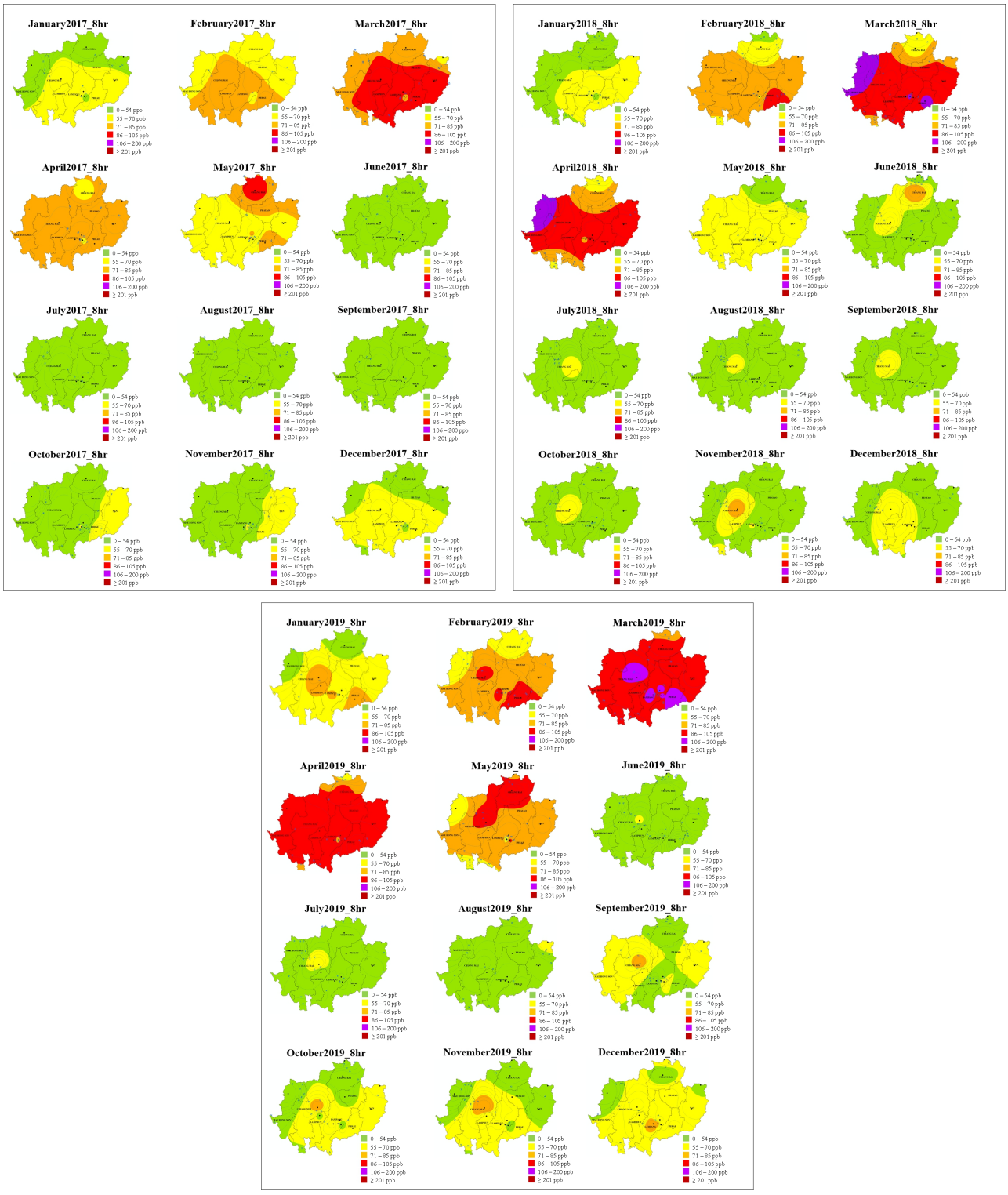

Figure 6 IDW interpolation map of monthly maximum 8-hour average value of ozone in 2017 – 2019

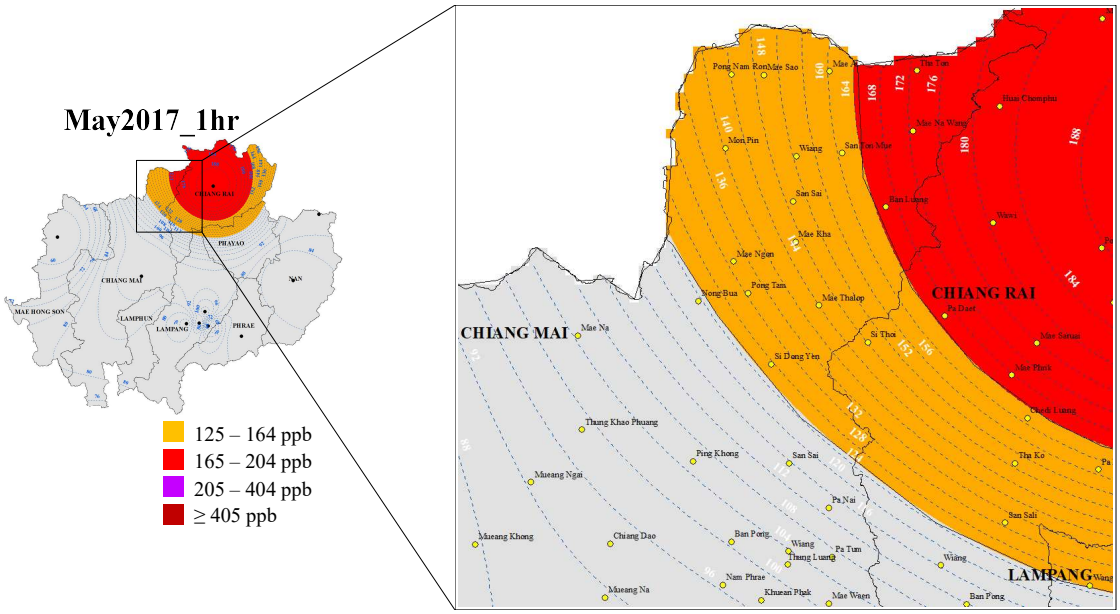

Figure 7 Map of sub-district where exposure to maximum 1-hour average of ozone in orange zone and red zone in Chiang Mai in May 2017

Table 4 The number of population exposure to monthly maximum 1-hour average of ozone in orange zone (unhealthy for sensitive groups) and red zone (unhealthy) in Chiang Mai in May 2017

No.	Sub-district Name	Population (Orange Zone)		
		Male (people)	Female (people)	Total (people)
1	Mae Ai, Mai Ai District	1,834	1,721	3,555
2	Ron Mae Sao, Mai Ai District	6,185	6,301	12,486
3	San Ton Mue, Mai Ai District	7,686	7,522	15,208
4	Wiang, Fang District	9,809	9,808	19,617
5	Mon Pin, Fang District	10,389	10,632	21,021
6	Mae Ngon, Fang District	8,545	8,504	17,049
7	Sansai, Fang District	5,341	5,754	11,095
8	Mae Kha, Fang District	3,710	3,887	7,597
9	Pong Nam, Fang District	3,130	3,156	6,286
10	Pong Tam, Chai Prakan District	52	24	76
11	Si Dong Yen, Chai Prakan District	6,020	5,891	11,911
12	Mae Thalop, Chai Prakan District	3,980	3,992	7,972
Total		66,681	67,192	133,873

No.	Sub-district Name	Population (Red Zone)		
		Male (people)	Female (people)	Total (people)
1	Tha Ton Sub-district, Mai Ai District	3,032	3,196	6,228
2	Mae Na Wang Sub-district, Mai Ai District	10,780	10,798	21,578
3	Ban Luang Sub-district, Mai Ai District	3,898	3,865	7,763
	Total	17,710	17,859	35,569

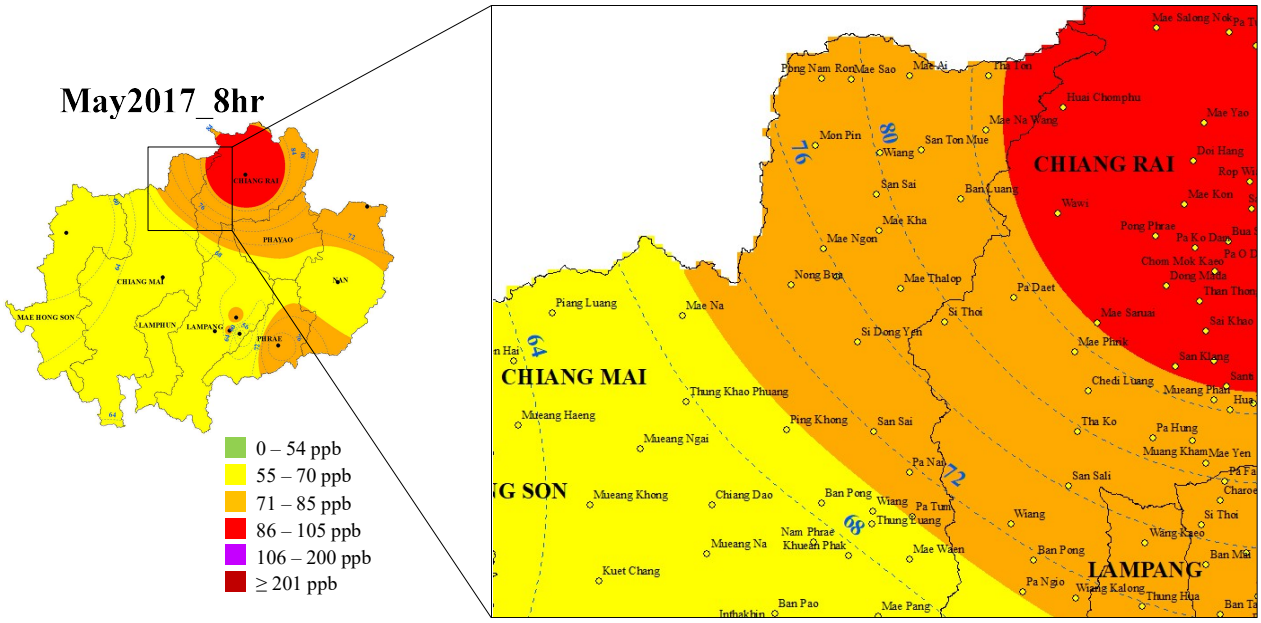

Figure 8 Map of sub-district where exposure to monthly maximum 8-hour average of ozone in orange zone and red zone in Chiang Mai in May 2017

Table 5 The number of population exposure to monthly maximum 8-hour average of ozone in orange zone (unhealthy for sensitive groups) in Chiang Mai in May 2017

No.	Sub-district Name	Population (Orange Zone)		
		Male (people)	Female (people)	Total (people)
1	Pong Nam Ron, Fang District	3,130	3,156	6,286
2	Mon Pin, Fang District	10,389	10,632	21,021
3	Wiang, Fang District	9,809	9,808	19,617
4	San Sai, Fang District	5,341	5,754	11,095
5	Mae Kha, Fang District	3,710	3,887	7,597
6	Mae Ngon, Fang District	8,545	8,504	17,049
7	San Ton Mue, Mai Ai District	7,686	7,522	15,208
8	Ban Luang, Mai Ai District	3,898	3,865	7,763
9	Mae Ai, Mai Ai District	1,834	1,721	3,555
10	Nong Buat, Chai Prakan District	7,571	7,798	15,369
11	Mae Thalop, Chai Prakan District	3,980	3,992	7,972
12	Si Dong Yen, Chai Prakan District	6,020	5,891	11,911
13	San Sai, Phrao District	3,101	3,200	6,301
14	Pa Nai, Phrao District	2,218	2,191	4,409
15	Pa Tum, Phrao District	2,537	2,661	5,198
	Total	85,954	86,883	172,837

No.	Sub-district Name	Population (Red Zone)		
		Male (people)	Female (people)	Total (people)
1	Tha Ton, Mai Ai District	3,032	3,196	6,228
2	Mae Na Wang, Mai Ai District	10,780	10,798	21,578
	Total	13,812	13,994	27,806

5. ACKNOWLEDGMENT

This work was supported by the Faculty of Engineering, Naresuan University [grant numbers R2564E009].

6. REFERENCES

AirNow. (2021). *Air Quality Index (AQI) Basics.* https://www.airnow.gov/aqi/aqi-basics/

AirNow. (2022). *What Is the AQI?* https://www.airnow.gov/education/students/what-is-the-aqi/

Akkala, A., Devabhaktuni, V., & Kumar, A. (2010). Interpolation techniques and associated software for environmental data. *Environmental Progress & Sustainable Energy*, *29*(2), 134-141. https://doi.org/https://doi.org/10.1002/ep.10455

Asian Institute of Technology. (2020). *Hidden Danger! Summer 'Ozone' Spikes.* https://www.ait.ac.th/2020/03/hidden-danger-summer-ozone-spikes-ait-expert-dr-ekbordin-winijku-advises-avoiding-outdoor-activities/

Bartier, P. M., & Keller, C. P. (1996). Multivariate interpolation to incorporate thematic surface data using inverse distance weighting (IDW). *Computers & Geosciences*, *22*(7), 795-799. https://doi.org/https://doi.org/10.1016/0098-3004(96)00021-0

Beelen, R., Hoek, G., Pebesma, E., Vienneau, D., de Hoogh, K., & Briggs, D. J. (2009). Mapping of background air pollution at a fine spatial scale across the European Union. *Sci Total Environ*, *407*(6), 1852-1867. https://doi.org/10.1016/j.scitotenv.2008.11.048

Bell, M. L. (2006). The use of ambient air quality modeling to estimate individual and population exposure for human health research: a case study of ozone in the Northern Georgia Region of the United States. *Environ Int*, *32*(5), 586-593. https://doi.org/10.1016/j.envint.2006.01.005

Bureau of Registration Administration. (2021). *Official statistics registration systems.* https://stat.bora.dopa.go.th/new_stat/webPage/statByYear.php

Chontanat Suwan. (2022). *GIS DATA.* https://csuwan.weebly.com/3604363436233609366036503627362136 04--download.html

Eldrandaly, K. A., & Abu-Zaid, M. S. (2015). Comparison of Six GIS-Based Spatial Interpolation Methods for Estimating Air Temperature in Western Saudi Arabia. *2015*, *18*(1). https://doi.org/38-45

Energy Policy and Planning office. (2022). *The provinces and administrative areas.* http://www.e-report.energy.go.th/area.html

GISGeography. (2021). *Inverse Distance Weighting (IDW) Interpolation.* https://gisgeography.com/inverse-distance-weighting-idw-interpolation/

Gong, G., Mattevada, S., & O'Bryant, S. E. (2014). Comparison of the accuracy of kriging and IDW interpolations in estimating groundwater arsenic concentrations in Texas. *Environ Res*, *130*, 59-69. https://doi.org/10.1016/j.envres.2013.12.005

Hammond, D., Conlon, K., Barzyk, T., Chahine, T., Zartarian, V., & Schultz, B. (2011). Assessment and application of national environmental databases and mapping tools at the local level to two community case studies. *Risk Anal*, *31*(3), 475-487. https://doi.org/10.1111/j.1539-6924.2010.01527.x

Isaaks, E. H. a. S., R.M. (1989). *An Introduction to Applied Geostatistics* (Vol. 1). Oxford University Press N.

Jarvis, C. H., & Stuart, N. (2001). A Comparison among Strategies for Interpolating Maximum and Minimum Daily Air Temperatures. Part II: The Interaction between Number of Guiding Variables and the Type of Interpolation Method. *Journal of Applied Meteorology*, *40*(6), 1075-1084. https://doi.org/10.1175/1520-0450(2001)040<1075:ACASFI>2.0.CO;2

Jeffrey, S., Carter, J., Moodie, K., & Beswick, A. (2001). Using spatial interpolation to construct a comprehensive archive of Australian climate data. *Environmental Modelling & Software*, *16*, 309-330. https://doi.org/10.1016/S1364-8152(01)00008-1

Jung, S.-W., Lee, K., Cho, Y.-S., Choi, J.-H., Yang, W., Kang, T.-S., Park, C., Kim, G.-B., Yu, S.-D., & Son, B.-S. (2016). Association by Spatial Interpolation between Ozone Levels and Lung Function of Residents at an Industrial Complex in South Korea. *International journal of environmental research and public health*, *13*(7), 728. https://doi.org/10.3390/ijerph13070728

Kravchenko, A., & Bullock, D. G. (1999). A Comparative Study of Interpolation Methods for Mapping Soil Properties. *Agronomy Journal*, *91*(3), 393-400. https://doi.org/https://doi.org/10.2134/agronj1999.00021962009100030007x

Li, L., Zhou, X., Kalo, M., & Piltner, R. (2016). Spatiotemporal Interpolation Methods for the Application of Estimating Population Exposure to Fine Particulate Matter in the Contiguous U.S. and a Real-Time Web Application. *International journal of environmental research and public health*, *13*(8). https://doi.org/10.3390/ijerph13080749

Maduako, I., Ebinne, E., Idorenyin, U., & Ndukwu, R. (2017). Accuracy Assessment and Comparative Analysis of IDW, Spline and Kriging in Spatial Interpolation of Landform (Topography): An Experimental Study. *Journal of Geographic Information System*, *09*, 354-371. https://doi.org/10.4236/jgis.2017.93022

Mishra, R., Kumar, A., & Singh, S. (2015). GIS Application in Urban Traffic Air Pollution Exposure Study: A Research Review. *Suan Sunandha Science and Technology Journal*, *2*.

Munyati, C., & Sinthumule, N. I. (2021). Comparative suitability of ordinary kriging and Inverse Distance Weighted interpolation for indicating intactness gradients on threatened savannah woodland and forest stands. *Environmental and Sustainability Indicators*, *12*, 100151. https://doi.org/https://doi.org/10.1016/j.indic.2021.100151

National Aeronautics and Space Administration. (2003). *Chemistry in the Sunlight.* https://earthobservatory.nasa.gov/features/ChemistrySunlight/chemistry_sunlight3.php

Pinichka, C., Makka, N., Sukkumnoed, D., Chariyalertsak, S., Inchai, P., & Bundhamcharoen, K. (2017a). Burden of disease attributed to ambient air pollution in Thailand: A GIS-based approach. *PloS one*, *12*(12), e0189909-e0189909. https://doi.org/10.1371/journal.pone.0189909

Pinichka, C., Makka, N., Sukkumnoed, D., Chariyalertsak, S., Inchai, P., & Bundhamcharoen, K. (2017b). Burden of disease attributed to ambient air pollution in Thailand: A GIS-based approach. *PloS one*, *12*(12), e0189909. https://doi.org/10.1371/journal.pone.0189909

Pollution Control Department. (2020). *Thailand State of Pollution 2020.* http://air4thai.pcd.go.th/webV2/download.php

Pollution Control Department. (2021). *Thailand's air quality and situation reports: Air Quality Map.* http://air4thai.pcd.go.th/webV2/index.php

Pollution Control Department. (2022). *Regional Air Quality and Situation Reports.* http://air4thai.pcd.go.th/webV3/#/Home

Qiao, P., Lei, M., Yang, S., Yang, J., Guo, G., & Zhou, X. (2018). Comparing ordinary kriging and inverse distance weighting for soil as pollution in Beijing. *Environmental Science and Pollution Research*, *25*(16), 15597-15608. https://doi.org/10.1007/s11356-018-1552-y

Robichaud, A., & Ménard, R. (2014). Multi-year objective analyses of warm season ground-level ozone and PM2.5 over North America using real-time observations and Canadian operational air quality models. *Atmos. Chem. Phys.*, *14*(4), 1769-1800. https://doi.org/10.5194/acp-14-1769-2014

Rojas-Avellaneda, D. (2007). Spatial interpolation techniques for stimating levels of pollutant concentrations in the atmosphere. *Revista Mexicana de Física*, *53*(6). https://doi.org/92.60.Sz; 02.50.Tt; 02.50.Sk

Royal Irrigation Department. (2018). *Spatial precipitation analysis from ground rainfall data and satellite imagery together with topographic data: case study in southern Thailand.* http://kmcenter.rid.go.th/kchydhome/km_hydro/tran/1.pdf

Rytkönen, M. J. (2004). Not all maps are equal: GIS and spatial analysis in epidemiology. *Int J Circumpolar Health*, *63*(1), 9-24. https://doi.org/10.3402/ijch.v63i1.17642

Sajjadi, S. A., Zolfaghari, G., Adab, H., Allahabadi, A., & Delsouz, M. (2017). Measurement and modeling of particulate matter concentrations: Applying spatial analysis and regression techniques to assess air quality. *MethodsX*, *4*, 372-390. https://doi.org/https://doi.org/10.1016/j.mex.2017.09.006

Simpson, G., & Wu, Y. H. (2014). Accuracy and Effort of Interpolation and Sampling: Can GIS Help Lower Field Costs? *ISPRS International Journal of Geo-Information*, *3*(4), 1317-1333. https://www.mdpi.com/2220-9964/3/4/1317

State of Global Air. (2020). *Ozone Exposure Ground-level ozone pollution is on the rise, contributing to health problems and climate change.* https://www.stateofglobalair.org/air/ozone#climate-connection

Stockholm Environment Institute. (2021). *Air quality in Thailand Understanding the regulatory context.* https://cdn.sei.org/wp-content/uploads/2021/02/210212c-killeen-archer-air-quality-in-thailand-wp-2101e-final.pdf

United States Census Bureau. (2022). *Cartographic Boundary Files - Shapefile.* https://www.census.gov/geographies/mapping-files/time-series/geo/carto-boundary-file.html

US. EPA. (2014). *Air quality index: A guide to air quality and your health.* https://www.airnow.gov/sites/default/files/2018-04/aqi_brochure_02_14_0.pdf

US. EPA. (2021). *Ground-level Ozone Pollution: Ground-level Ozone Basics.* https://www.epa.gov/ground-level-ozone-pollution/ground-level-ozone-basics#wwh

US. EPA. (2021a). *Ground-level Ozone Pollution.* https://www.epa.gov/ground-level-ozone-pollution

US. EPA. (2021b). *Ground-level Ozone Pollution: Health Effects of Ozone Pollution.* https://www.epa.gov/ground-level-ozone-pollution/health-effects-ozone-pollution

Viroat Srisurapanon, & Chana Wanichapun. (2019). *Environmental Policies in Thailand and their Effects.* https://www.un.org/esa/gite/iandm/viroatpaper.pdf

Weather Spark. (2022). *The Weather Year Round Anywhere on Earth.* https://weatherspark.com/

Weber, D., & Englund, E. (1992). Evaluation and comparison of spatial interpolators. *Mathematical Geology*, *24*(4), 381-391. https://doi.org/10.1007/BF00891270

Willmott, C. J. (1982). Some Comments on the Evaluation of Model Performance. *Bulletin of the American Meteorological Society*, *63*(11), 1309-1313. https://doi.org/10.1175/1520-0477(1982)063<1309:SCOTEO>2.0.CO;2

Willmott, C. J., Ackleson, S. G., Davis, R. E., Feddema, J. J., Klink, K. M., Legates, D. R., O'Donnell, J., & Rowe, C. M. (1985). Statistics for the evaluation and comparison of models. *Journal of Geophysical Research: Oceans*, *90*(C5), 8995-9005. https://doi.org/https://doi.org/10.1029/JC090iC05p08995

Wuthiwongyothin, S., Kalkan, C., & Panyavaraporn, J. (2021). Evaluating Inverse Distance Weighting and Correlation Coefficient Weighting Infilling Methods on Daily Rainfall Time Series. *SNRU Journal of Science and Technology*, *13*(2), 71-79. https://ph01.tci-thaijo.org/index.php/snru_journal/article/view/243635/166054

7. BIOGRAPHIES

Supawan Srirattana

Graduation B.Eng. (Environmental Engineering), and M.Eng. (Environmental Engineering), and Ph.D. (Environmental Engineering) respectively at Naresuan University.

Currently working as a lecturer at the Department of Civil Engineering, Faculty of Engineering, Naresuan University, Phitsanulok, Thailand.